



<https://theses.gla.ac.uk/>

Theses Digitisation:

<https://www.gla.ac.uk/myglasgow/research/enlighten/theses/digitisation/>

This is a digitised version of the original print thesis.

Copyright and moral rights for this work are retained by the author

A copy can be downloaded for personal non-commercial research or study, without prior permission or charge

This work cannot be reproduced or quoted extensively from without first obtaining permission in writing from the author

The content must not be changed in any way or sold commercially in any format or medium without the formal permission of the author

When referring to this work, full bibliographic details including the author, title, awarding institution and date of the thesis must be given

Enlighten: Theses

<https://theses.gla.ac.uk/>
research-enlighten@glasgow.ac.uk



Frontispiece. Pyramids on silver after 20 days heating
at 900°C in air (negative interferogram).

ProQuest Number: 10656377

All rights reserved

INFORMATION TO ALL USERS

The quality of this reproduction is dependent upon the quality of the copy submitted.

In the unlikely event that the author did not send a complete manuscript and there are missing pages, these will be noted. Also, if material had to be removed, a note will indicate the deletion.



ProQuest 10656377

Published by ProQuest LLC (2017). Copyright of the Dissertation is held by the Author.

All rights reserved.

This work is protected against unauthorized copying under Title 17, United States Code
Microform Edition © ProQuest LLC.

ProQuest LLC.
789 East Eisenhower Parkway
P.O. Box 1346
Ann Arbor, MI 48106 – 1346

ABSTRACT

The work presented in this thesis was carried out in the University of Glasgow during the period 1959 to 1962 under the supervision of Dr. N. Myhrum. The experimental measurements and analysis is original work of the author with the exception of the measurements on (110) facets which were undertaken by Dr. Myhrum and the calibration of the liquid microscope by Dr. Myhrum in collaboration of the liquid microscope.

THE THERMAL ETCHING OF SILVER

by

G.E. Rhead

- (1) 'Thermal etching of silver in various atmospheres', Letter to the Editor in J. Appl. Phys. 33 378 (May 1962)
- (2) 'A preliminary report on etching without gas evaporation'
- (3) 'Thermal etching of silver in various atmospheres', G.E. Rhead and N. Myhrum, submitted to J. Appl. Phys. (January 1962) due to be published about August 1962. (This covers most of Chapters 3 and 4)
- (4) 'Surface self-diffusion on atomically smooth metal crystal surfaces', G.E. Rhead and N. Myhrum.

A thesis submitted to the University of Glasgow for the degree of Doctor of Philosophy.

Department of Natural Philosophy, July, 1962.
University of Glasgow

PREFACE

The work presented in this thesis was carried out in the University of Glasgow during the period 1959 to 1962 under the supervision of Dr. H. Mykura. The experimental measurements and analysis is original work of the author with the exception of the measurements on $\{110\}$ facets which were undertaken by Dr. Mykura and the calibration of the Linnick microscope which was done in collaboration.

Part of the work has already been reported:

- (1) 'Thermal etching of silver', G.E. Rhead and H. Mykura
Letter to the Editor in Acta Met. 10 578 (May 1962)
(A preliminary report on faceting without net evaporation)
- (2) 'Thermal etching of silver in various atmospheres',
G.E. Rhead and H. Mykura.
Submitted to Acta Met. January 1962 due to be published about August 1962.
(This covers most of Chapters 3 and 4)
- (3) 'Surface self-diffusion across atomically smooth metal crystal surfaces'. G.E. Rhead and H. Mykura.
Paper given at the Conference on Diffusion and Mass transport in Solids, Institute of Physics and the Physical Society, Reading University, April, 1962.
(A report of the results presented in Chapter 7).

ACKNOWLEDGMENTS

The author wishes to thank Dr. H. Mykura for suggesting a problem which proved both interesting and stimulating and for considerable advice and encouragement in supervising the work. Thanks are also due to Professor P.I. Dee for providing the facilities; to Dr. G.A.P. Wyllie for his interest; to Dr. A.J.W. Moore for a valuable exchange of ideas; to Professor W.W. Mullins, Professor P.G. Shewmon, Dr. Inman, Dr. Tipler, Dr. Gjostein and Dr. Drew for sending copies of their papers prior to publication; to the Director of the National Engineering Laboratory (East Kilbride) for the use of the Linnick interference microscope. The author is particularly indebted to Miss M. Low for her skill in the photography and for the illustrations reproduced here.

1.5 Relevance of the present work

CHAPTER 2. Experimental Techniques

2.1	Specimen preparation	31
2.2	Furnaces	32
2.3	A continuous flow gas system	32
2.4	Determination of crystal orientations	34
2.5	Interference microscopy	37

CHAPTER 3. Thermal Etching of Silver in Air and Oxygen

CONTENTS

3.1	General features of etched structures	39
	List of illustrations	(vi)
3.2	Contact angles	46
	List of tables	(ix)
3.3	Simultaneous development of two facets	46
	Summary	(x)
3.4	Temperature dependence of the contact angles	51
	<u>INTRODUCTION</u>	51
	Effect of enhanced evaporation	51

CHAPTER 1. Surface energy and thermal etching: a review.

CHAPTER 4. Thermal Etching of Silver in

1.1	Surface energy: theoretical considerations	4
1.2	Measurements of surface energy	6
1.3	Variation of surface energy with orientation	10
1.4	Surface energy and adsorption	13
1.5	Surface energy and thermal etching	16
1.6	Mass transfer on surfaces	22
1.7	Previous work on the thermal etching of silver	27
1.8	Relevance of the present work	30
	Twin boundaries in air	67
	Conclusions	69

CHAPTER 2. Experimental Techniques

2.1	Specimen preparation	31
2.2	Furnaces	32
2.3	A continuous flow gas system	32
2.4	Determination of crystal orientations	34
2.5	Interference microscopy	37
2.6	Grain boundary groove profiles	70
2.7	Scratch smoothing experiments	77

<u>CHAPTER 3.</u>	<u>Thermal Etching of Silver in Air and Oxygen</u>	
7.1	with growth by evaporation	
3.1	General features of etched structures	39
3.2	Effect of inhibiting evaporation	40
3.3	Contact angles	42
3.4	Simultaneous development of two facets	46
3.5	Temperature dependence of the contact angles	51
3.6	Effect of enhanced evaporation	53
<u>CHAPTER 4.</u>	<u>General Discussion</u>	
8.1	Low index facets	93
<u>CHAPTER 4.</u>	<u>Thermal Etching of Silver in Various Atmospheres</u>	
8.3	with adsorbed	
4.1	Etching in nitrogen, hydrogen and vacuum	56
4.2	Etching in oxygen:nitrogen mixtures	57
4.3	Adsorption and thermal etching	62
<u>APPENDIX:</u>	<u>Errors in Interference Microscopy</u>	90
<u>CHAPTER 5.</u>	<u>Twin Boundary Grooves</u>	
5.1	Twin boundaries in nitrogen	65
5.2	Twin boundaries in air	67
5.3	Conclusions	69
<u>CHAPTER 6.</u>	<u>Grain Boundary Grooves and Surface Self-diffusion on Silver</u>	
6.1	Rate of grain boundary grooving	72
6.2	Grain boundary groove profiles	76
6.3	Scratch smoothing experiments	77

<u>CHAPTER 7. The Kinetics of Facet Formation</u>		
7.1	Comparison with growth by evaporation and condensation	Following page 79
7.2	Investigations on the rate of growth of facets.	82
Fig. 7.3	Measurements on single facets	85
Fig. 7.4	Nucleation of facets	90
	on oxygen concentration	10
<u>CHAPTER 8. General Discussion</u>		
Fig. 8.1	Low index facets	93
8.2	Adsorption and the Y plot	94
8.3	Diffusion on surfaces with adsorbed layers	95
Fig. 8.4	Future work	96
Fig. 6	Furnace and continuous flow gas system	33
<u>APPENDIX: Errors in Interference Microscopy</u>		98
Fig. 7	Non-orientational crystal orientations	33
Fig. 8	A chart for determining orientations	33
<u>REFERENCES</u>		102
Fig. 9	Optical systems for interference microscopy	36
Fig. 10	Thermally etched surfaces after 10 days in oxygen	39
Fig. 11	Interferogram of facets after 10 days in oxygen	39
Fig. 12	{110} striations continuous across twin boundaries	39
Fig. 13	Interferogram of {100} facets with mainly {111} steps	39

List of illustrations

	Following page:
Fig. 14 Stereographic triangle illustrating secondary and simultaneous primary	46
Frontispiece. Pyramids on silver	46
Fig. 1 Schematic γ plot and the Wulff construction	10
Fig. 2 Surface energy Silver:Oxygen - dependence on oxygen concentration	10
Fig. 3 Equilibrium of intersecting surfaces	16
Fig. 4 Various changes in surface topography produced by a lowering of total surface energy	17
Fig. 5 Dependence of surface profiles on transport mechanism	24
Fig. 6 Furnace and continuous flow gas system	33
Fig. 7 Determination of crystal orientations	35
Fig. 8 A chart for determining orientations	35
Fig. 9 Optical systems for interference microscopy	36
Fig. 10 Thermally etched surfaces after 10 days in oxygen	39
Fig. 11 Interferogram of facets after 10 days in oxygen	39
Fig. 12 $\{110\}$ striations continuous across twin boundaries	39
Fig. 13 Interferogram of (100) facets with mainly $\{111\}$ steps	39

Fig. 14	Stereographic triangle illustrating secondary and simultaneous primary faceting	46
Fig. 15	Interferogram showing simultaneous primary faceting	47
Fig. 16	Schematic representation of Fig. 15	47
Fig. 17	The formation of facets during enhanced evaporation	53
Fig. 18	Interferogram of pyramids formed by enhanced evaporation	54
Fig. 19	Surface after 5 days heating in nitrogen	56
Fig. 20	Evaporation roughening in vacuum	56
Fig. 21	Stereographic projections illustrating etching in 10 p.p.m. and 100 p.p.m. oxygen	58
Fig. 22	Typical area of surface heated for 10 days in 10^{-5} parts oxygen	58
Fig. 23	Variation of the cosine of the contact angles with logarithm of partial pressure of oxygen	61
Fig. 24	Twin boundary grooves in nitrogen and in air; orientations of $\frac{\partial \theta}{\partial \theta}$ values	66
Fig. 25	Absence of twin boundary grooves on complex surfaces	70
Fig. 26	Low angle grain boundary and continuous facets	70

Fig.27	Grain boundary groove width as a function of time. Silver in air at 900°C	73
Fig.28	Temperature dependence of surface self-diffusion on silver in air	73
Fig.29	A grain boundary groove after 4 days in air	76
Fig.30	Multiple scratches after 5 hours in air	76
Fig.31	An isolated (111) facet after 16 hours	83
Fig.32	Discontinuous development of a facet with nucleation of additional facets	83
Fig.33	Plot of $\omega = X^*/(Bt)^{\frac{1}{4}}$ for the two limiting cases of surface diffusion	85
Fig.34	Theoretical standardized facet profiles	87
Fig.35	Standardized facet profiles from measurements of interferograms	87
Fig.36	Plot of $Z''' = A/2m(Bt)^{\frac{1}{2}}$ for $d = \infty$	85
	Calibration of interference microscopes	100

were oxygen on the low index surfaces.

SUMMARY

A review is given of surface energy effects on solid surfaces with particular reference to the formation of facets and to the thermal etching of silver. Recent studies on the kinetics of mass transport on surfaces, the development of grain boundary and twin boundary grooves, the decay of surface undulations and the formation of facets are discussed.

It is found that silver heated in atmospheres containing oxygen develops low index facets ($\{111\}$, $\{100\}$ and $\{110\}$). Measurements were made, using interference microscopy, of the contact angles between the low index surfaces (surface energy γ_L) and complex high index surfaces (surface energy γ_C) on specimens annealed at 900°C .

The theory is discussed for equilibrium between two and between three sets of planar surfaces. The cosine of the contact angles (γ_L/γ_C) is found to increase as the oxygen partial pressure is lowered from about 1 to 10^{-5} atmospheres. This variation, interpreted in terms of the Gibbs adsorption equation, shows that, with a complete monolayer on all surfaces, there is about 4%

An appendix deals with errors in interference microscopy at high wedge angles.

more oxygen on the low index surfaces.

Net evaporation gives rise to the formation of large pyramids with low index faces; evaporation rates from the low index surfaces are extremely low. But net evaporation is not essential for the formation of facets. There is evidence that less oxygen is adsorbed when a surface is in equilibrium with its vapour.

Twin boundary groove angles confirm that the γ plot (surface energy against orientation) has cusps at low index orientations.

Measurements of the rate of grain boundary grooving and the smoothing of scratches on silver in air shows that surface self diffusion is the dominant transport mechanism for distances up to at least 30 microns and the diffusion constant $B = 3.99 \pm 0.36 \times 10^{-19} \text{ cm}^4 \text{ sec}^{-1}$ at 900°C .

The diffusion coefficient is given by $D_s = D_0 \exp \{-Q/kT\}$ where $D_0 \approx 10^6 \text{ cm}^2 \text{ sec}^{-1}$ and $Q = 2.48 \pm 0.12 \text{ ev}$. This high activation energy indicates diffusion in the presence of a chemisorbed layer and not of a pure metal surface.

Facet growth is shown to be predominantly by a surface diffusion mechanism. Measurements on isolated single facets agree with the theory of Mullins. Very fast diffusion occurs across the low index surfaces.

An appendix deals with errors in interference microscopy at high wedge angles.

INTRODUCTION

The importance and diversity of surface phenomena in both pure science and technology are immense. There is however comparatively little quantitative data on such fundamental surface properties as detailed structure, surface energy and atomic migration. The material presented in this thesis is concerned mainly with surface energy effects on solids and the transport of surface atoms at high temperatures. Experimental studies were made of silver surfaces in various atmospheres. 'Pure' surfaces are rare - if not unknown - and part of the object of these experiments was to investigate effects due to the adsorption of gaseous atoms. The experimental results give emphasis to the variation of surface properties with crystalline orientation and particularly to the differences between exact low index, atomically smooth, surfaces and atomically rough surfaces.

Much of the theoretical background to this work originates from classical papers by Smith (1) and by Herring (2)(3) in which the importance of surface free energy and the role it plays in determining equilibrium shapes of surfaces and in atomic migration was pointed out.

Two extreme approaches to surface phenomena are

possible: the macroscopic and the atomistic. From a macroscopic point of view a surface may be simply a boundary - with merely geometrical properties - but on a more sophisticated level with macroscopic properties such as stress and free energy. The atomistic approach attempts to relate surface phenomena to detailed structure, atomic configurations and interactions between a small number of atoms. Both approaches are necessary here; the experimental observations, made by interference microscopy, are on the scale of a few hundred to a few thousand atomic diameters.

The use of interference techniques adds a third dimension to ordinary optical studies of surfaces and makes possible quantitative measurements of surface topography. Most well known in this field is perhaps the work of Tolansky (4) and his co-workers on the structure of diamond surfaces, growth spirals on crystals and other topographical studies. But the multiple-beam interference techniques are limited to quite small wedge angles (not greater than about 5°) and they can only be used to examine the structure of fairly flat surfaces. On the other hand, the interference microscope, although not giving such high resolution of small surface steps is in

many ways more versatile than the multiple-beam interferometer. The ability to resolve wedge angles up to 30° makes the instrument very suitable for measuring relatively large scale changes of topography and the investigations described here point to its usefulness as a tool for research of free energy - for surfaces the surface free energy. In this chapter a review is given of various thermal etching phenomena with particular reference to silver. Since any thermal etching process is 'driven' by a lowering of total surface free energy it is appropriate to discuss first solid surface energies, their measurement, and the factors which influence surface energy.

1.1 Surface energy: theoretical considerations.

The physical concept of a surface is not easy to formulate. Strictly speaking a surface is always an interface between two media and as such it is considered as a separate phase with properties quite different from those of the bulk phases it separates. Herring (3) discusses the rigorous treatment of a surface following the method of Gibbs and shows that many important properties can be described by use of concepts carried over from thermodynamics. Thus surface free energy or for brevity

CHAPTER 1.

SURFACE ENERGY AND THERMAL ETCHING: A REVIEW.

Any spontaneous change in surface topography occurring at high temperature may be termed 'thermal etching'. Like all irreversible processes such changes are accompanied by a lowering of free energy - for surfaces the surface free energy. In this chapter a review is given of various thermal etching phenomena with particular reference to silver. Since any thermal etching process is 'driven' by a lowering of total surface free energy it is appropriate to discuss first solid surface energies, their measurement, and the factors which influence surface energy.

1.1 Surface energy: theoretical considerations.

The physical concept of a surface is not easy to formulate. Strictly speaking a surface is always an interface between two media and as such it is considered as a separate phase with properties quite different from those of the bulk phases it separates. Herring (3) discusses the rigorous treatment of a surface following the method of Gibbs and shows that many important properties can be described by use of concepts carried over from thermodynamics. Thus surface free energy or for brevity

total free energy of an area, i.e. $\int \gamma dA$.

surface energy (designated by γ ergs cm^{-2}) is defined as the surface density of the Helmholtz free energy. This is the work required to create unit area of surface for example by cleavage of the bulk material.

Surface free energy may be written:

$$\gamma = E_{(s)} - TS_{(s)} \quad (1.1)$$

where $E_{(s)}$ is the total surface energy* and $S_{(s)}$ the surface entropy. Theoretical estimates of some total surface energies have been made, notably by Shuttleworth (5) on the basis of atomistic theories. These serve to show that variations of surface energy with crystal orientation are expected.

The literature contains numerous references to surface stress and particularly to the meaningfulness of such a concept. Shuttleworth (6) has discussed the relationship between surface stress and surface energy for solids. The existence of surface stress would imply that the spacing of surface atoms parallel to the surface is not the same as in the bulk material. Without experimental evidence this is difficult to believe although

* 'Total surface energy' strictly means $E_{(s)}$ as defined above. Later the same term will be used to denote the total free energy of an area, i.e. $\int \gamma dA$.

there is evidence of anomalous spacing perpendicular to the surface. On surface energy phenomena there is confusion even at the elementary text book level; correct explanations of liquid capillarity are rarely found.

The view is put forward here that for solids, as well as for liquids, observable phenomena can be interpreted in terms of surface energy without invoking the concept of surface stress and that the term 'surface tension' is an anachronism similar to the 'tubes of force' of 19th century electromagnetism. It can only be used for crystals

and for planes which cleave, moreover the conditions are

1.2 Measurements of surface energy.

Largely because of difficulties of measurement there is a dearth of experimental values for solid surface energies. Inman and Tipler (7) have reviewed progress in this field up to 1962 and have pointed to the lack of data needed for metallurgical problems. Earlier reviews have been given by Udin (8) and by Fisher and Dunn (9).

Prior to 1930 no reliable data were available; the only measurements had been based on the comparison of heats of solution of finely divided particles with the heats of solution of bulk material (10). This method gives a measure of the solid:liquid interfacial energy and

has rather low accuracy ($\pm 50\%$).

The most direct method is the measurement of the work done during reversible cleavage of a crystal. This method was applied by Obreimov (11) to crystals of mica and an improved technique has been used by Gilman (12) for the surface energies of a number of ionic crystals and for Si, Zn, and Fe (3% Si). Gilman's measurements were at low temperatures and give effective energies for the solid:coolant interfaces. The cleavage technique has the disadvantage that it can only be used for crystals and for planes which cleave, moreover the conditions are not strictly reversible and part of the measured work is expended in plastic deformation.

The most fruitful technique devised so far is the wire-pulling or zero creep method. This was first used by Udin, Shaler and Wulff (13) to determine the surface energy of copper in vacuum. Fine metal wires are hung in a furnace and loaded with known weights. At high temperatures the wires tend to elongate under the action of the applied load and to contract due to a minimisation of total surface energy. A determination of the load required just to balance the effective 'surface energy forces' gives a measure of the surface energy. The analysis

has to take into account the 'hoop stresses' due to the grain boundary interfacial energies; Shuttleworth (14) corrected Udin's original treatment to allow for this. The wire pulling method can be used for pure metals and has fair accuracy ($\pm 10\%$). It gives an average value of surface energies over all orientations and for the metal:vapour or metal:gas interface. However the method can only be used at high temperatures where creep occurs due to atomic diffusion.

Table 1. Surface energies of some metals.

<u>Metal</u>	<u>Atmosphere</u>	<u>T°C</u>	<u>γ(ergs cm⁻²)</u>	<u>Reference</u>
Cu	Vacuum	1050	1670	(8)
Cu	Helium	950	1770	(7)
Ag	Helium	870-945	1140	(17)
Ag	Air	932	360	(17)
Au	Helium	1040	1370	(8)
Sn	Vacuum	215	685	(18)
Ni	Argon	1240-1450	1725	(19)
Fe, 3%Si	-	- 259	1360	(12)
Zn	-	- 196	105	(12)
W	Vacuum	2000	2900	(15)

Two additional indirect methods may be mentioned.

Barbour and his collaborators (15) have used pulsed field emission microscopy to measure the surface energy of tungsten. Single crystal field emission cathodes were made with tip radii between 10^{-5} and 10^{-4} cm. At high temperatures migration of atoms from the curved tip occurs since this process is accompanied by a lowering of the total surface energy. The migration rate can be measured from observation of the emission pattern and can be reversed by application of an electric field. A value for the surface energy was found from a determination of the field required to balance the surface energy driven migration. The use of a pulsed emission field, with a low ratio of field on time to total time, permitted the effect of this field to be separated from the bias field.

Blakely and Mykura (16) have shown that it is possible to make an estimate of surface energy by comparison of surface mass transfer rates with volume diffusion measured by radioactive tracer methods. The mass transfer measurements are made by the scratch smoothing technique (section 1.6) over transport distances for which volume diffusion is the dominant mechanism.

Table 1 summarises the most reliable available data for surface energies of metal:gas, metal:vapour, systems.

1.3 Variation of surface energy with orientation

The techniques described above - with the exception of the cleavage method - have been used to measure average surface energies. Very few investigations have been made of the variation of surface energy with orientation. Such a variation is expected and it is convenient to discuss the anisotropy of surface energy in terms of a polar plot - the so called γ plot - in which surface energy is plotted as a radial vector in three dimensions. A

section through a hypothetical γ plot is shown in Fig. 1.

Fig. 1. Schematic γ plot and the Wulff construction.

An argument due to Herring (3) shows that in general there will be cusps in the γ plot in directions corresponding to orientations with low Miller indices: a low index plane is as near as possible atomically smooth and a surface at an orientation slightly removed from the low index orientation will be made up of areas of smooth low index surface with widely spaced steps. These steps will add a certain amount to the surface energy which will increase as the density of steps increases, that is as the surface orientation moves away from the low index position.

Important consequences follow from the shape of the γ plot regarding the equilibrium shapes of surfaces and small particles. The Wulff theorem (3) states that if

Fig. 2. Surface energy Silver: Oxygen—dependence on oxygen concentration (Buttner et al. 1952).

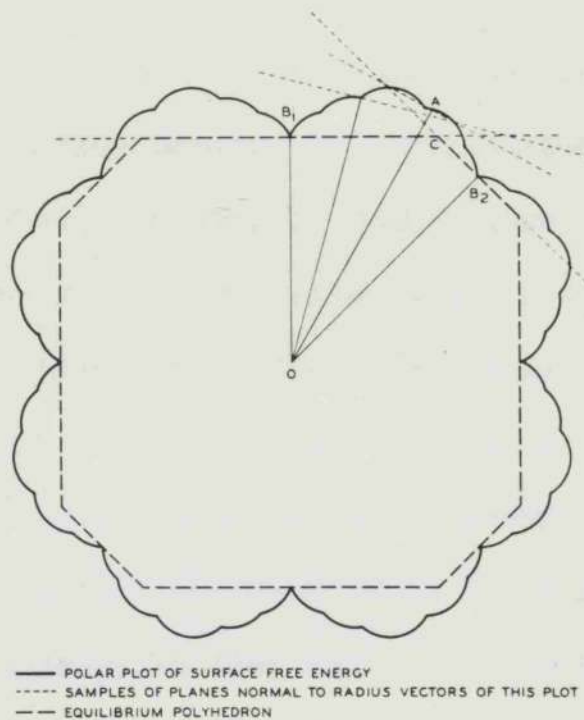


Fig.1. Schematic γ plot and the Wulff construction.

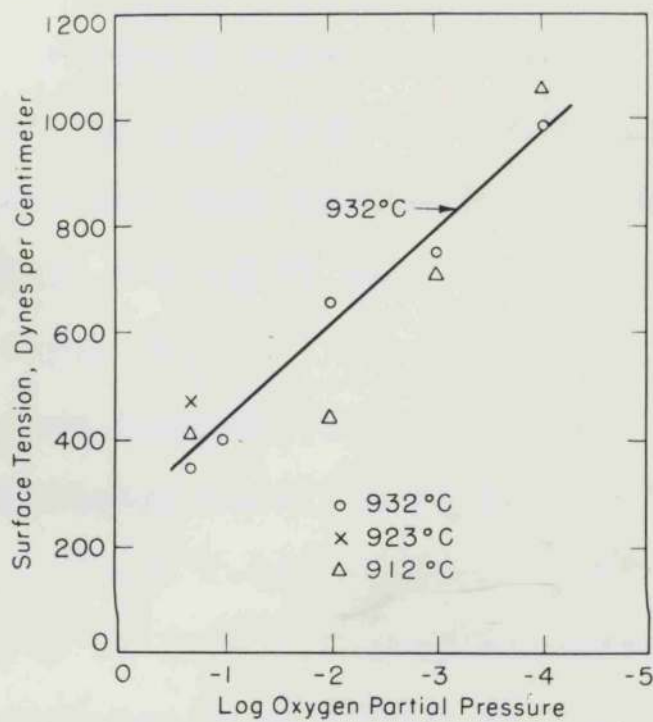


Fig.2. Surface energy Silver: Oxygen—dependence on oxygen concentration (Buttner et al. 1952).

planes are drawn normal to all radius vectors of the γ plot then the equilibrium shape of a crystal will be geometrically similar to the body formed by all points which can be reached from the origin without crossing any of these planes. It follows that for a sharply cusped γ plot the equilibrium shape will consist predominantly of low index surfaces. The Wulff construction predicts only the equilibrium shape and whether this occurs in practice depends very largely on the kinetics of atomic migration.

The first measurement of a γ plot was made by Mykura (20)(21) on vacuum annealed nickel by a method based on the observation of inverted twin boundary grooves by interference microscopy (section 1.5). The surface energy was found to decrease by about 6% between the middle of the stereographic triangle and the (100) orientation and there was a shallower cusp at the (111) orientation. It was concluded that the (100) cusp was mainly due to adsorption of impurity.

Robertson and Shewmon (22), also from measurements on twin boundaries, determined the γ plot for copper in hydrogen. Cusps were found of about 2.6% at (111), 1.6% at (100) and 0.4% at (110). They also studied the effect of different atmospheres and found that a small trace of

oxygen caused faceting but produced no appreciable change in the γ plot. This observation will be discussed later. It suggests that the extrapolation of their measurements to the low index orientations is not altogether reliable and the γ plot may be more deeply cusped.

Table 2 summarizes the available experimental data on the γ plot and gives the values found for the depth of the low index cusps and for the slope of the slope of the γ plot.

Metal	Atmosphere	$\gamma(\text{low index})/\gamma_{\text{max}}$	$\frac{1}{\delta} \frac{\partial \gamma}{\partial \theta}$	Reference
Au	-	-	0.06	(24)
Ni	Vacuum	(111):0.98		(21)
		(100):0.94	0.05-0.25	
Cu	Hydrogen	(111):0.974	0.097 at pole	(22)
		(100):0.984	0.066 "	
		(110):0.996	0.025 "	
Ag	Air	(111):0.84	0.55 at pole	(23)(25)
		(100):0.90	0.42 "	

The spontaneous development of facets on a surface gives another method for investigating the γ plot and is the main topic of this thesis. Moore (23) measured the angles across ridges formed by the growth of low index

Adsorption of impurities on a surface is always

facets on silver specimens heated in air. From his results, discussed more fully in later sections, he found ratios of low index surface energy to the surface energy of high index or complex planes: $\gamma(100)/\gamma_c = 0.90$, $\gamma(111)/\gamma_c = 0.84$.

Table 2 summarises the available experimental data on the γ plot and gives the values found for the depth of the low index cusps and for $\frac{1}{\gamma} \frac{\partial \gamma}{\partial \theta}$ (where $\frac{\partial \gamma}{\partial \theta}$ is the slope of the γ plot). MacKenzie, Moore and Nicholas (26) have made detailed calculations of the density of broken bonds on crystal surfaces. Taking the surface energy as the sum of the energies of individual broken bonds and considering as a first approximation only nearest neighbour bonds, they give theoretical γ plots for f.c.c. and b.c.c. crystals. The theory predicts cusps of 10.6% at (100), 22.5% at (111), based on a maximum at (210), and a saddle point at (110). Comparison with experimental evidence suggests that the simple model is inadequate. However the calculations show that if second nearest neighbour bonds are taken into account the cusps are less pronounced.

1.4 Surface energy and adsorption

Adsorption of impurities on a surface is always

accompanied by a decrease in surface energy. Gibbs (27) showed that surface energy decreases linearly as the chemical potential of the adsorbate increases. Thus for a perfect gas the change in γ may be written:

$$d\gamma = -kT \Gamma \frac{dp}{p} = -kT \Gamma d(\log p) \quad (1.2)$$

where Γ is the surface density of the adsorbed layer and p the gas pressure. Herring (3) has commented on the interpretation of this equation for various adsorption isotherms and has shown that appreciable changes of γ occur only if Γ is comparable with a complete monolayer.

The literature contains few references to measurements of the effect of adsorption on solid surface energies (see references (3) and (8)). Experiments have been done on mica in air, silver in oxygen, gold in oxygen and copper in lead vapour. The silver:oxygen system has been studied more than any other. Buttner, Funk and Udin (17) measured γ for silver in oxygen at partial pressures from 0.2 to 10^{-4} atmospheres and at temperatures just below the melting point. Their results are reproduced in Fig. 2.*

* It is of interest to note that Buttner et al. did not report any faceting on their silver wires; experiments reported here have shown extensive faceting over the same pressure range.

From the observed linear relationship with log (oxygen pressure), given by the equation

$$\gamma = 228 - 188 \log_{10} p \text{ ergs cm}^{-2} \quad (1.3)$$

1.5 Surface energy and thermal etching

where p is in atmospheres, a constant value $\Gamma = 1.98 \times 10^{15}$

Any interface tends to decrease in area in order to lower its total free energy $\Psi_s = \gamma A$. Similarly a two monolayers. Such a high surface density seems implausible and an error of a factor 2 has been pointed out by Herring (3). This is due to a calculation of the minimisation of Ψ_s where the integration of surface energy is taken over all interfaces.

dissolved oxygen and not from the gas phase concentration;

The conditions for equilibrium of three interfaces are illustrated in Fig. 3a. By making virtual displacements of the point of intersection and equating the concentration C of dissolved gas to the gas pressure p: $C = kp^{1/2}$.*

incremental change in Ψ_s to zero it is easily shown that at equilibrium six vectors have to be balanced, two with reference to the use of silver as an oxidation catalyst. He has confirmed some results of Buttner et al. and has measured surface energy as a function of temperature equal to the interfacial energy γ , and another normal to both at constant pressure and at constant dissolved oxygen concentration. At constant pressure (1 atmosphere) the direction of decreasing γ . Physically each surface surface energy was found to increase to about 1000 erg cm^{-2} tends to decrease in area and also to rotate toward when the temperature was lowered to 650°C. Allen gives orientations of low γ . The six vectors are referred to for the heat of adsorption 10.5 kcal per g-atom of oxygen. as 'torque terms' and are important only for solids. However the calculation of the adsorbed oxygen density

* Correction: Buttner's error was an arithmetical one.

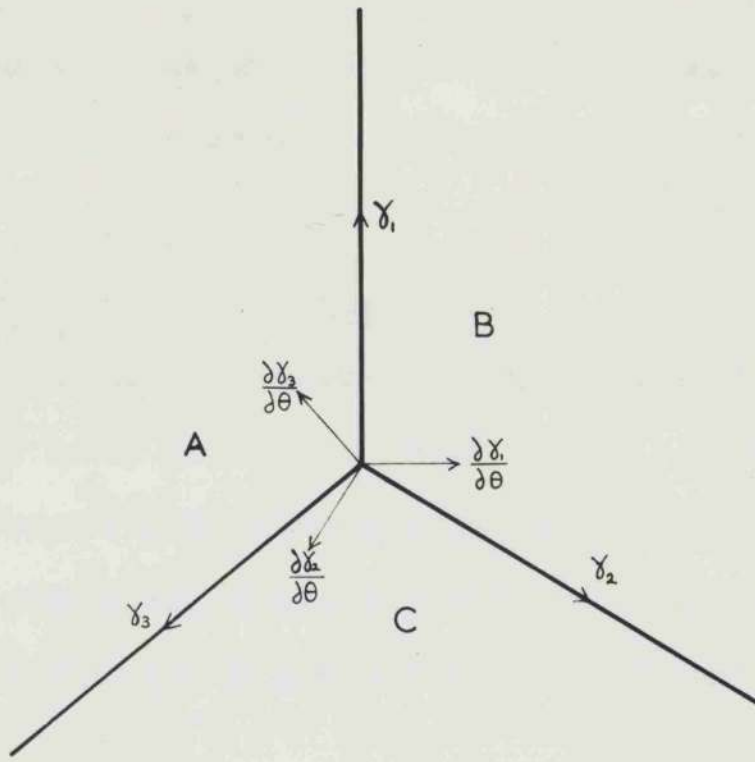
followed the method used by Buttner et al. and his values for Γ should be halved.

1.5 Surface energy and thermal etching

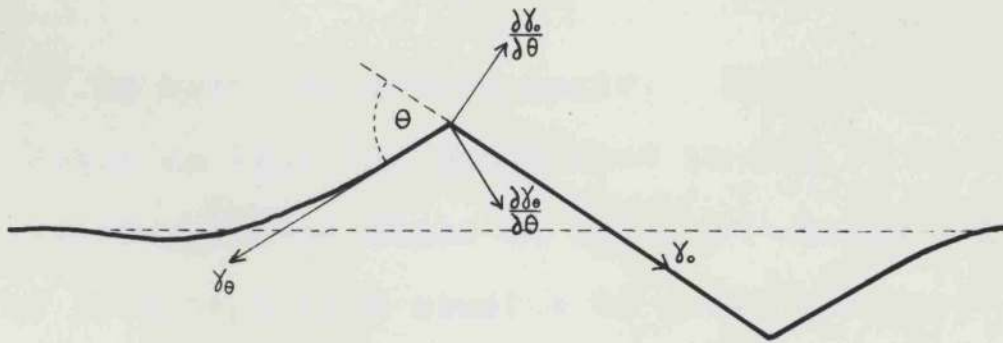
Any interface tends to decrease in area in order to lower its total free energy $\Psi_s = \int \gamma dA$. Similarly a system of interfaces whether internal boundaries or free surfaces reaches an equilibrium configuration by a minimisation of Ψ_s where the integration of surface energy is taken over all interfaces.

The conditions for equilibrium of three interfaces are illustrated in Fig. 3a. By making virtual displacements of the point of intersection and equating the incremental change in Ψ_s to zero it is easily shown that at equilibrium six vectors have to be balanced, two for each surface. (Reference (2)). Effectively two forces are considered to act on a surface: one along the surface, equal to the interfacial energy γ , and another normal to the surface equal to the derivative $\frac{\partial \gamma}{\partial \theta}$ and in the direction of decreasing γ . Physically each surface tends to decrease in area and also to rotate toward orientations of low γ . The $\frac{\partial \gamma}{\partial \theta}$ vectors are referred to as 'torque terms' and are important only for solids.

FIG. 3. EQUILIBRIUM OF INTERSECTING SURFACES.



(a) THREE INTERFACES



(b) HILL AND VALLEY STRUCTURE

FIG. 3. EQUILIBRIUM OF INTERSECTING SURFACES.

Various thermal etching phenomena will now be discussed from the point of view of equilibrium of interfacial energies.

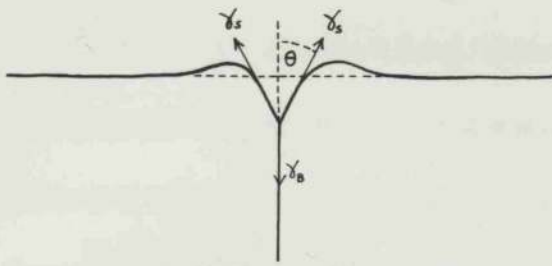
Grain boundary grooving

The formation of grain boundary grooves on metal surfaces has been known for some time. Chalmers, King and Shuttleworth (29) observed grooves on silver heated in various atmospheres and attributed their occurrence to a local equilibrium of grain boundary energy and surface energy.

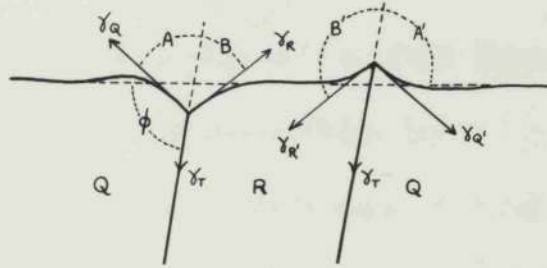
For a symmetrical groove, with the grain boundary normal to the surface, the grain boundary energy γ_B is given approximately by

$$\gamma_B = 2\gamma_s \cos \theta \quad (1.4)$$

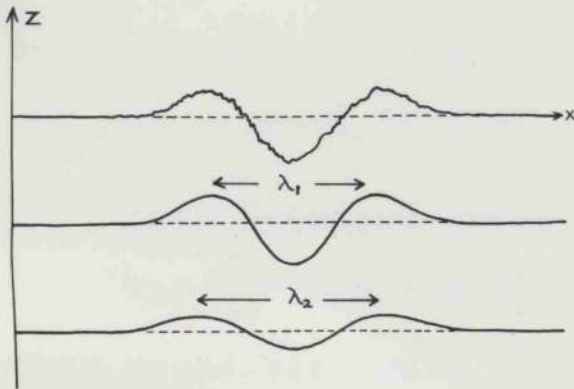
where θ is half the groove angle. This condition is illustrated in Fig. 4a. (Note that in Fig. 4 the vertical scale is exaggerated about 10 times.) Because of the lack of pertinent data studies of grain boundary grooves have mostly ignored the torque terms. Typical values for 2θ , measured by sectioning techniques or by interference microscopy, are about 164° for silver in air (King (30)), 166° for tin (Mykura (31)) the ratio γ_B/γ_s



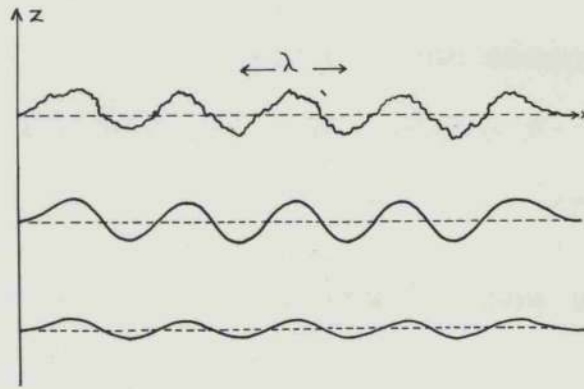
(a) GRAIN BOUNDARY GROOVE.



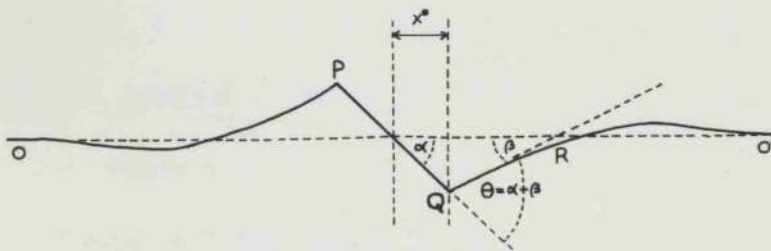
(b) TWIN BOUNDARY GROOVE AND INVERTED GROOVE.



(c) DECAY OF A SINGLE SCRATCH.



(d) DECAY OF MULTIPLE SCRATCHES.



(e) DEVELOPMENT OF A FACET.

FIG. 4. VARIOUS CHANGES IN SURFACE TOPOGRAPHY PRODUCED BY A LOWERING OF TOTAL SURFACE ENERGY.

is usually about 0.3.

After annealing times usually only of a few hours the groove topographies are easily measurable by interference microscopy. Curved surfaces are found to develop above the root of the groove. Recently Inman and Tipler (7) have described techniques for determining groove angles from profiles examined by electron microscopy. Such methods although having disadvantages may give somewhat greater accuracy than interference microscopy and can be used to look more closely at the groove root.

Twin boundary grooving.

The equilibrium conditions at the intersections of twin boundaries with a free surface have been discussed by Mykura (20). Here the torque terms become important since they are comparable with twin boundary energies which are about a hundred times lower than surface energies.

A section normal to a surface and a pair of twin boundaries is shown in Fig. 4b. The torque terms tend to make the surface of crystal R rotate in an anticlockwise direction and Q in a clockwise direction. As a result a groove is formed at one boundary and an inverted groove or hump at the other. The occurrence of inverted twin boundary grooves is perhaps the most dramatic evidence of $\frac{\partial \gamma}{\partial \theta}$ terms. It is analogous to the minimization of

Using the nomenclature of Fig. 4b the equilibrium equations can be written as:

$$\gamma_T = \gamma_Q \cos A + \gamma_R \cos B - \frac{\partial \gamma_Q}{\partial A} \sin A - \frac{\partial \gamma_R}{\partial B} \sin B \quad (1.5)$$

$$\gamma_T = \gamma_{Q'} \cos A' + \gamma_{R'} \cos B' + \frac{\partial \gamma_{Q'}}{\partial A'} \sin A' + \frac{\partial \gamma_{R'}}{\partial B'} \sin B' \quad (1.6)$$

from which may be derived the expressions:

$$\frac{\gamma_T}{\gamma_S} \approx \cos\left(\frac{A+B}{2}\right) + \cos\left(\frac{A'+B'}{2}\right) \quad (1.7)$$

$$\frac{1}{\gamma_S} \left(\frac{\partial \gamma_Q}{\partial A} + \frac{\partial \gamma_R}{\partial B} \right) \approx \cos\left(\frac{A+B}{2}\right) - \cos\left(\frac{A'+B'}{2}\right) \quad (1.8)$$

Blakely and Mykura (33)(16) have reported experiments on the smoothing out of fine scratches drawn on a surface. Equation (1.8) gives values for pairs of orientation derivatives and was used in the measurement of the γ plots of nickel (21) and copper (22). Typical profiles are given in Fig. 4c and Fig. 4d of a single scratch and a set of multiple scratches. Estimates for the ratio of twin boundary energy to surface energy, γ_T/γ_S from recrystallisation occurs during the initial anneal so that equation (1.7) are: Ni: $0.005 \pm .003$, Cu: 0.007. Twin a single crystal can be formed under the scratches. High boundary energies have also been estimated from harmonics in the surface profile quickly disappear and intersections of twin boundaries and grain boundaries the surface rapidly approaches a sinusoidal shape. The (Fullman (32)). The absolute value for the twin boundary subsequent decay of the profile has been used to determine energy in copper has been given as 19 ± 4 ergs cm^{-2} . surface self-diffusion coefficients (Section 1.6.)

Decay of surface undulations

The disappearance of surface roughness on annealing Under the heading 'thermal etching' the most noted is well known and is the simplest example of a surface effect, after grain boundary grooving, is the appearance energy effect. It is analogous to the minimisation of

surface area which accounts for the smooth appearance of liquid surfaces and the formation of spherical drops. However, detectable smoothing off of a solid surface, due to the lowering of total surface energy, occurs only at temperatures high enough for the surface atoms to become mobile. It is evident that since the magnitude of the change in free energy in a process is a measure of the rate of approaching equilibrium that very sharp changes of surface topography will smooth out faster than slowly varying ones.

Blakely and Mykura (33)(16) have reported experiments on the smoothing out of fine scratches drawn on a surface. Typical profiles are given in Fig. 4c and Fig. 4d of a single scratch and a set of multiple scratches.

$$\gamma_e = \gamma_0 \cos \theta - \frac{\partial \gamma_e}{\partial x} \sin \theta \quad (1.9)$$

Recrystallisation occurs during the initial anneal so that a single crystal can be formed under the scratches. High harmonics in the surface profile quickly disappear and the surface rapidly approaches a sinusoidal shape. The subsequent decay of the profile has been used to determine surface self-diffusion coefficients (Section 1.6.)

$$\frac{\partial \gamma_e}{\partial x} > \gamma_0 \sin \theta + \frac{\partial \gamma_e}{\partial x} \cos \theta \quad (1.10)$$

Development of facets.

Under the heading 'thermal etching' the most noted effect, after grain boundary grooving, is the appearance

of planar facets. These occur as striations - strips of low index plane - across crystal surfaces. Fig. 4e represents a section through a faceted surface, taken perpendicular to the striations. The general surface OO' has changed into a hill and valley structure consisting of low index planes PQ with surface energy γ_0 and continuation or complex surfaces QR making an angle θ with the low index planes and with surface energy γ_θ .

The equilibrium conditions for the faceted structure are illustrated in Fig. 3b. Resolving surface energies and torque terms in the direction PQ one arrives at the equation:

$$\gamma_0 = \gamma_\theta \cos \theta - \frac{\partial \gamma_\theta}{\partial \theta} \sin \theta \quad (1.9)$$

The increase in surface energy of the low index plane due to a small tilt away from the low index position is taken to be large enough to prevent any such tilt; i.e. face

$$\frac{\partial \gamma_0}{\partial \theta} > \gamma_\theta \sin \theta + \frac{\partial \gamma_\theta}{\partial \theta} \cos \theta \quad (1.10)$$

The contact angle θ should therefore depend only on the variation of surface energy with crystallographic orientation and be independent of the angle α between the original surface and the low index plane.

Thus the break up of a surface into facets, resulting in an increase of total surface area, is energetically possible if the low index planes have relatively low surface energies, that is if there is a large cusp in the γ plot at the low index orientation. A surface structure in which the angle of contact between low index and continuation surface is given by equation (1.9) is one for which there has been the maximum possible reduction of surface energy by simple faceting; the total surface energy would be greater for a simple hill and valley structure with any other value of θ . It follows that a surface at an angle greater than θ from the low index orientation will not break up into striations which expose that plane.

Spine boundary grooving.

1.6 Mass transfer on surfaces.

Given the energy conditions for changes in surface topography the observation of such changes depends on the kinetics of atomic movement and on the processes of evaporation and condensation, volume diffusion and surface self-diffusion.

In two important papers Herring (34)(2) established the basic equations which relate the rate of flow of atoms

to surface geometry and in particular to the surface (1.11) curvature. Herring developed scaling laws which show (1.12) that for geometrically similar changes, (differing in (1.13) scale by a factor λ , the times taken for the changes are in the ratio λ^n where $n = 2$ for evaporation and condensation, 3 for volume diffusion and 4 for surface diffusion. It follows, from the usual magnitudes of the constants involved, that surface diffusion is dominant over small distances and that either volume diffusion or evaporation and condensation becomes important only for transfer distances above about 100 microns. Similar changes are proportional to $t^{\frac{1}{4}}$, $t^{\frac{1}{3}}$ and $t^{\frac{1}{2}}$ for surface diffusion, volume diffusion and evaporation and condensation respectively.

Grain boundary grooving.

As a consequence of the curved surfaces which form during grain boundary grooving gradients of chemical potential always exist along the groove profile and for that reason material continuously flows out from the groove and causes it to grow progressively deeper and wider.

Mullins (35)(36) has shown that the normalised groove shapes are time independent and that the groove widths (s) increase with time in the following way:

Evaporation and condensation: $S \propto (At)^{\frac{1}{2}}$ (1.11)

Volume diffusion: $S = 5.0(Ct)^{\frac{1}{3}}$ (1.12)

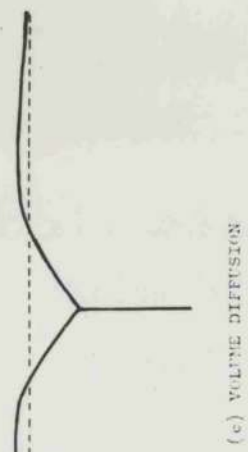
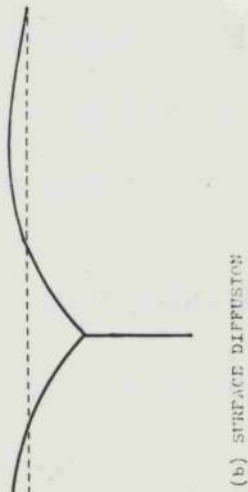
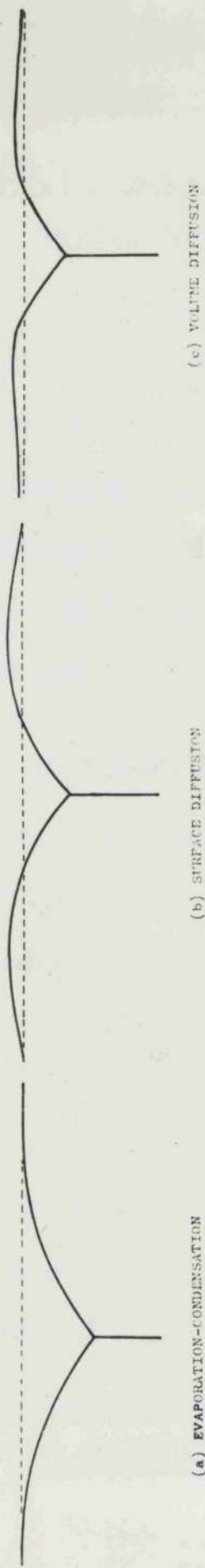
Surface diffusion: $S = 4.6(Bt)^{\frac{1}{2}}$ (1.13)

where $A = p_0 \gamma_s \Omega^2 / (2\pi M)^{\frac{1}{2}} (kT)^{\frac{3}{2}}$, $B = D_s \Omega^2 \nu \gamma_s / kT$ and p_0 is the vapour pressure over a flat surface, γ_s the surface energy, Ω the atomic volume, M the mass of a molecule, ν the surface density of atoms and D_s the surface diffusion coefficient. $C = D_v \gamma_s \Omega / kT$ (P.25)

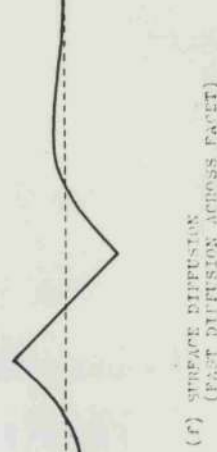
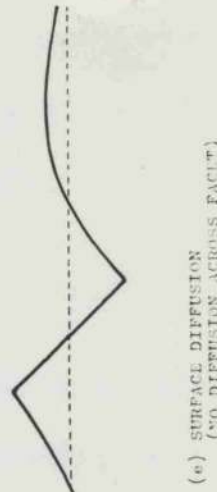
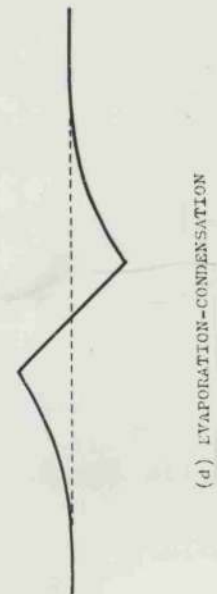
Comparison of the power law for groove widening with the above equations can be used to distinguish between the various kinetic mechanisms which may be operating. In equations (1.12) and (1.13) the widths are taken as the distance between humps which appear on the profiles. Fig. 5 shows how the profile shapes give an indication of the mechanism.

The theory for grain boundary grooving also accounts for the rate of growth of twin boundary grooves and inverted grooves.

Since surface self-diffusion is usually the dominant mechanism up to distances of tens of microns measurement of grain boundary grooving by interference microscopy has been used as a technique for measuring surface diffusion coefficients. Blakely (37) has reviewed work in this



GRAIN BOUNDARY GROOVING



FACETING

FIG. 5. DEPENDENCE OF SURFACE PROFILES ON TRANSPORT MECHANISM.

field up to 1961. (40) for the rate of growth of linear

Surface undulations.

The theory of the flattening of a surface and the decay of scratches has been described by Mullins (38)(39) and by Blakely and Mykura (33)(16). For both single scratches and multiple scratches, which take up a sinusoidal shape, the amplitude of the variation in height decreases exponentially. For single scratches the separation between the humps (Fig. 4c) increases with time and the results are most easily interpreted for sinusoidal profiles:

$$z(x,t) = a \sin \omega x \exp \left[-(B\omega^4 + C\omega^3 + A\omega^2)t \right] \quad (1.14)$$

where z is measured normal to the surface, x along the profile and where $\omega = 2\pi/\lambda$ (Fig. 4d). A and B are defined above and $C = D_v \gamma_s \Omega / kT$ where D_v is the volume self-diffusion coefficient. The last two terms in the exponential are usually negligible so that scratch smoothing gives a measure of surface self-diffusion. A direct check of Herring's scaling laws could be made by comparison of smoothing rates over a range of wavelengths. (Reference (16)).

The theory of facet growth

A theoretical account, based on earlier work, has been

given by Mullins (40) for the rate of growth of linear facets during etching. In anticipation of the experiments reported later some of the results will be quoted.

For the case of evaporation and condensation the half-width of the facet x^* is given by

$$x^* = \omega 2(At)^{\frac{1}{2}} \quad (1.15)$$

where ω is a function of m/n , $m = \tan\beta$, $n = \tan\alpha$ (Fig. 4e).

Shuttleworth (51) pointed out in his review of work on thermal etching up to 1948 that striations are known to facet half-width grows according to a $t^{\frac{1}{4}}$ law:

$$x^* = \omega (Bt)^{\frac{1}{4}} \quad (1.16)$$

where ω is here a different function, also dependent on m/n , but in this case a function of $d = D_s/D_c$ where D_s is the diffusion coefficient for the low index (simple) plane and D_c that for the adjoining continuation (complex) surface.

As in the case of grain boundary grooving it is possible to distinguish between different mechanisms both by the rate of growth and from profile shapes (Fig. 5). Moreover if surface diffusion is the operative mechanism measurements on facets can give interesting information on diffusion across low index, atomically smooth, surfaces.

It is important to note however that Mullins' theory

can only be applied to isolated single facets and not to densely faceted surfaces where the individual profiles impinge on each other. The theory will be discussed in more detail in Chapter 7 where comparison will be made with facets observed on silver in air. planes and that the striations were caused by the development of these

1.7 Previous work on the thermal etching of silver

Shuttleworth (41) pointed out in his review of work on thermal etching up to 1948 that striations are known to appear on a number of metals and in specific atmospheres. Another review of thermal etching has been given by Prasad (42). Reference will be made here to the silver:oxygen system only. Although the earliest recorded observations of thermal etching were made in the late 19th century little progress was made toward understanding the phenomena until 1948.

In 1912 Rosenhain and Ewen (43) reported the formation of striations and grain boundary grooves on silver heated in air and noted that only grain boundary grooves formed surfaces are also low index facets. But the etched in vacuum. Leroux and Raub (44) later showed that structures they discuss show mainly secondary faceting striations appear in oxygen but not in hydrogen. of the type discussed by Moore and faceting of crystals In 1948 Chalmers, King and Shuttleworth (29) completed oriented very near the low index pole and under conditions the first systematic study and ascribed the formation of of net evaporation. (See Chapter 3).

both grain boundary grooves and striations to a lowering of total surface free energy. They showed that striations which formed in oxygen disappeared on heating in nitrogen. It was concluded that the presence of oxygen modified the relative surface energies of different planes and that the striations were caused by the development of those planes with lowest free energy.

King (30) showed that the planes exposed were either $\{100\}$ or $\{111\}$ and made the first measurements of the angles of contact between the low index and continuation surfaces by finding the limiting crystal orientations which became striated.

Moore (23) measured the same angles using an optical goniometer and also from estimates of the relative areas of low index and continuation surfaces.* He then made calculations of relative surface energies γ_0/γ_θ using equation (1.9) but neglecting the $\partial\gamma/\partial\theta$ term.

* Moreau and Benard (45) have claimed that the continuation surfaces are also low index facets. But the etched structures they discuss show mainly secondary faceting of the type discussed by Moore and faceting of crystals oriented very near the low index pole and under conditions of net evaporation. (See Chapter 3).

In 1960 Hondros and Moore (46) reported experiments on the effect of evaporation on thermal etching. They withdrew Moore's earlier conclusions and put forward the view that the thermally etched structure of facets is not determined by relative surface energies and also that in any thermal etching there is a transport of material through the vapour phase. While accepting surface and grain boundary energy as the cause of grooving they supported their statements by two main items of evidence:

- (1) that the rate of faceting initially correlates fairly well with the rate of weight loss for silver freely evaporating in air;

- (2) that faceting is suppressed when weight loss is prevented by enclosing the specimen in a silver container.

In a later paper Hondros and Moore (47) studied the growth of large facets under the influence of an electric field gradient. They suggested that evaporation also played a major part in this effect.

Hondros and Moore's experiments are important since previously the role of evaporation in etching had not been fully investigated. However experiments will be reported here which do not confirm their conclusions and evidence will be presented to show that the development of facets

is a surface energy effect and not primarily caused by evaporation.

1.1 Specimen preparation

1.8 Relevance of the present work.

At the time this work was started there had been no systematic study of the development of facets using interference microscopy. Since such a study would give a more accurate means of examining the surfaces and of measuring contact angles it was decided to repeat Moore's experiments in air and to investigate the effect of adsorption by heating specimens in controlled mixtures of oxygen and nitrogen.

Following the publication of Hondros and Moore's results on evaporation, their experiments were repeated. The method of inhibiting evaporation was then used to study the kinetics of mass transfer during grain boundary grooving and to compare the rate of growth of facets with Mullins' theory which had then recently been published.

wires from a ceramic bead mounted inside the box. In this way net evaporation of the specimens could be reduced to a negligible amount.

CHAPTER 2.

EXPERIMENTAL TECHNIQUES

2.1 Specimen preparation

Polycrystalline specimens of 'specpure' silver were used. The specimens, about 2 sq. cm x 0.2 mm., were prepared from cold-rolled sheet (from Johnson, Matthey & Co., impurities detected spectrographically: Cd, Cu, Fe, Pb and Mn, each less than 1 part per million). To avoid contamination no attempt was made to polish the surfaces; interference microscopy showed that surface irregularities due to rolling were less than 300 Å deep. For some experiments specimens were placed on a Mullite boat so that there was net evaporation from the surface. In other experiments specimens were totally enclosed inside a silver box. The box, about 2" x 1" square, was made from 'specpure' sheet and was loosely constructed so that the surrounding atmosphere had easy access to the enclosure. Specimens were hung by silver wires from a ceramic bead mounted inside the box. In this way net evaporation of the specimens could be reduced to a negligible amount. A controlled flow of oxygen was admitted to the gas stream from a voltaceter in which acidified water was electrolyzed.

2.2 Furnaces

Tube furnaces of Mullite were used for heating specimens in air. The tubes were 1" in diameter and power to the nichrome heating elements was supplied from a stabilising transformer. By setting the power input to the furnaces temperatures at about 900°C could be controlled to within $\pm 5^\circ$. Chromel-alumel thermocouples, calibrated at the melting points of silver and gold, were used for the temperature measurements.

The vacuum furnace, used in one experiment, was of simple design and used a platinum winding and nickel radiation shields. A pressure of less than 10^{-5} torr was obtained by means of a rotary pump and an oil diffusion pump. experiments were made with no oxygen added to the gas flow; at flow rates less than 100 cc/min the reaction

2.3 A continuous flow gas system.

A continuous flow gas system was used for obtaining mixtures of oxygen and nitrogen and of hydrogen and nitrogen. Nitrogen, 99.9% pure, was passed from a cylinder over hot copper turnings to remove oxygen and over potassium hydroxide to remove carbon dioxide. A controlled flow of oxygen was admitted to the gas stream from a voltameter in which acidified water was electrolysed.

The mixture of gases, dried by passing over magnesium perchlorate, went through a cold trap at solid carbon dioxide temperature and into the specimen furnace. The gas mixture finally flowed through a needle valve into the atmosphere and the total flow rate was monitored with a 'Rotameter' flowmeter. The system is shown in Fig. 6.

The pressure in the system was set by means of a manometer in which was incorporated a sintered glass overflow. By carefully controlling the pressure (atmospheric + 21 cm Hg) and the outlet flow of the gas as well as the current through the voltameter, the proportion of oxygen in the mixture could be kept constant to within $\pm 7\%$ for several days. To test the nitrogen purity experiments were made with no oxygen added to the gas flow; at flow rates less than 100 cc/min the reaction with the hot copper was sufficiently fast so that specimens heated in the gas did not become striated.

A careful flushing out procedure was followed before each run. The system was evacuated with a rotary pump, filled with nitrogen, and the process repeated twice - finally filling with the gas passing slowly over the hot copper. Precautions had to be taken to prevent the water in the voltameter from syphoning into the system.

Fig. 6.

Furnace and continuous flow gas system for heating specimens in controlled atmosphere.

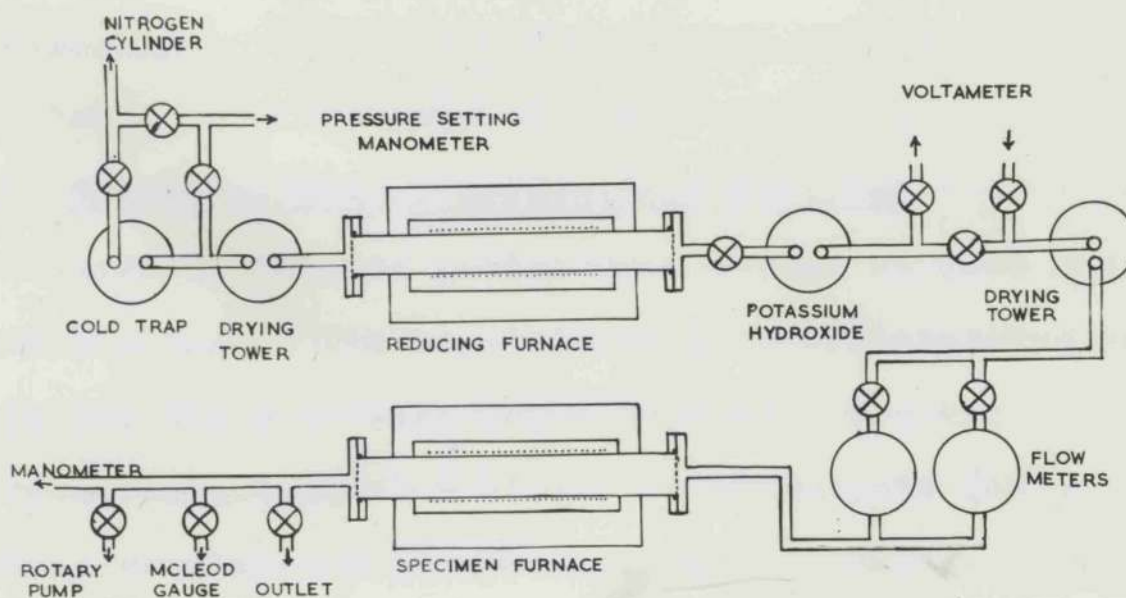
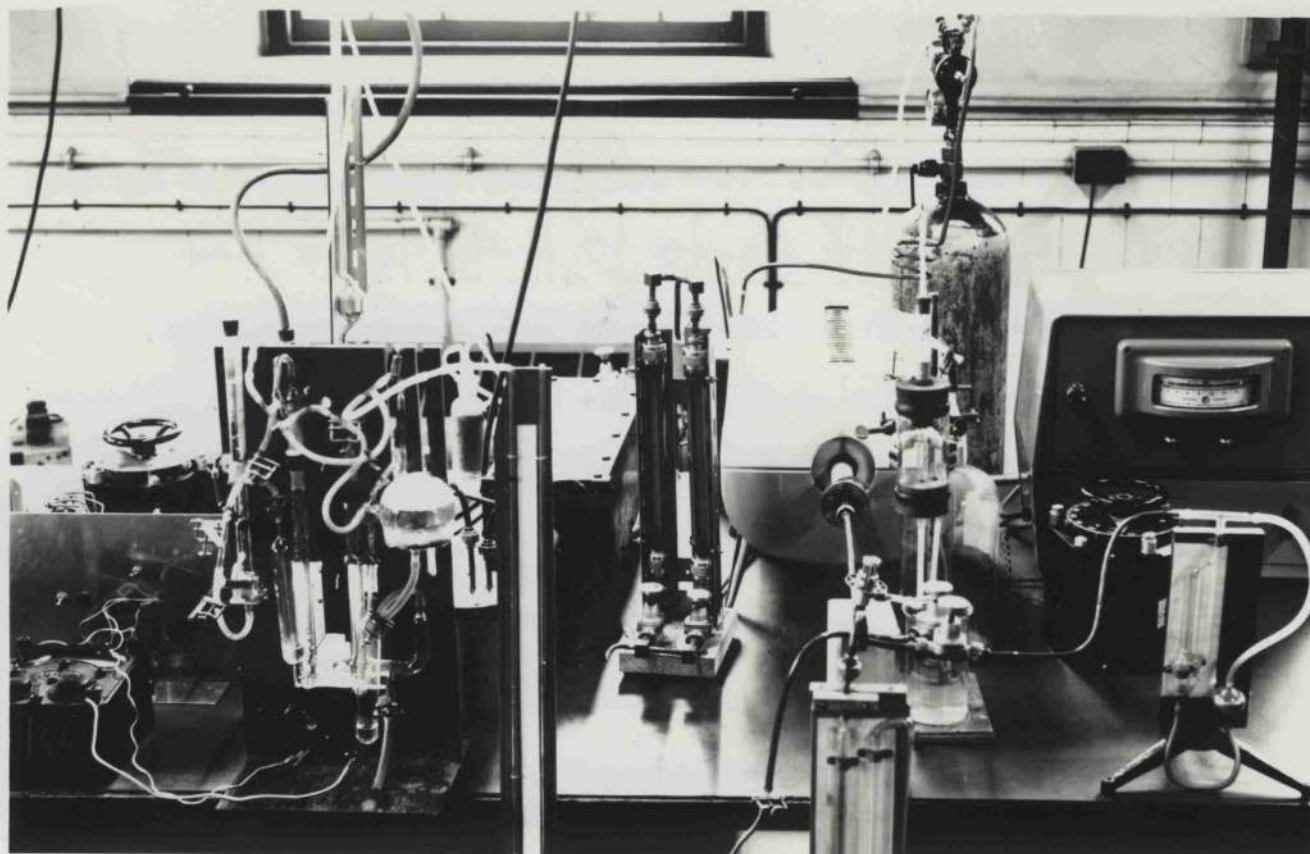


Fig. 6.

Furnace and continuous flow gas system for heating specimens in controlled atmospheres.

Gas from the unused limb of the voltameter was passed into the atmosphere via the pressure setting manometer and in this way the pressure across the voltameter was equalised. This method of gas preparation was satisfactory down to a concentration of 10 parts of oxygen per million but unreliable for concentrations much less than this because of the slow evolution of oxygen and the variation of the nominal purity of the nitrogen from cylinder to cylinder. In the same furnace and gas flow system the specimens were heated in pure nitrogen and (without the hot copper) in pure oxygen. Mixtures of hydrogen and nitrogen were obtained by reversing the polarity of the voltameter.

Use was made too of a method due to Hydrant (49)

2.4 Determination of crystal orientations

Several hundred grains were formed on each specimen on annealing. The crystallographic orientations of selected crystals were found from measurements of the angles between twin traces as described by Barrett (48). This method requires at least three twin traces for one crystal, a condition not always satisfied. Therefore having shown that the directions of the striations were always normal to great circles through either (111) or (100) poles use

was made of this information and of the angles of tilt of the low index facets with the general surface. The method is illustrated in Fig. 7. Here the lines 1, 2 and 3 represent twin traces on crystal A which has a common twinning plane (1) with crystal B. P is parallel to striations on A and Q is parallel to striations on B. Rotation of a standard cubic (111) centred projection by 19° , as measured on a Sigsbee chart, along the line P, brought (111) poles into coincidence with the twin traces and moved a (100) pole onto the line Q. In this way the orientations of both crystals were found.

FROM TWIN TRACES AND STRIATIONS.

The labour involved in finding orientations was considerably reduced by using standard (111) and (100) centred projections with the twinned projection also plotted. Use was made too of a method due to Mykura (49) which is illustrated in Fig. 8. Two twin traces (1)(2) are drawn at a particular angle to each other. By rotating a standard projection with a (111) pole along either of these traces, while constraining a second pole to follow the second twin trace, the positions traced out by the other poles can be easily located. It is found that the other two (111) poles on the projection follow a locus such as PQ P'Q'. If now a third twin

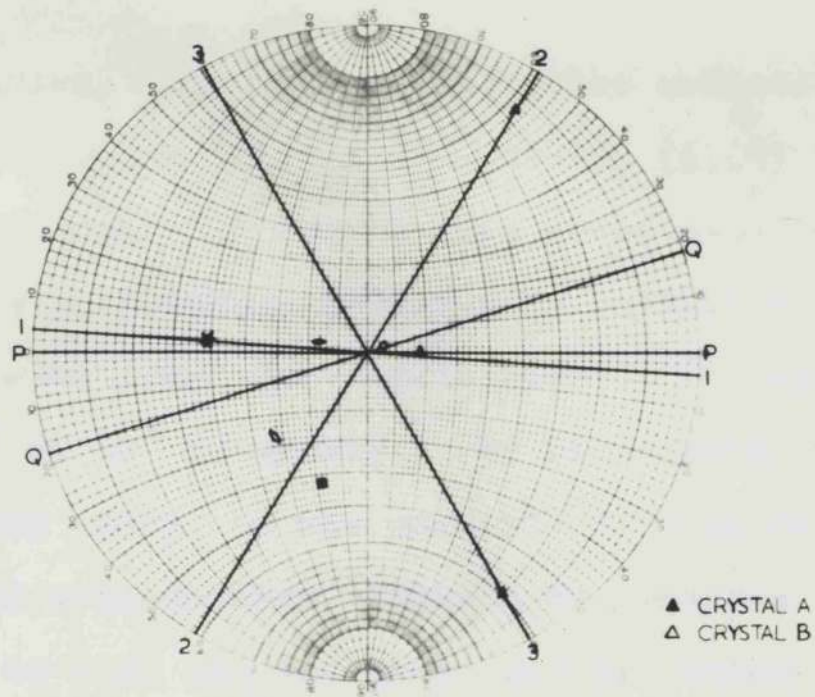


FIG. 7 DETERMINATION OF CRYSTAL ORIENTATIONS FROM TWIN TRACES AND STRIATIONS.

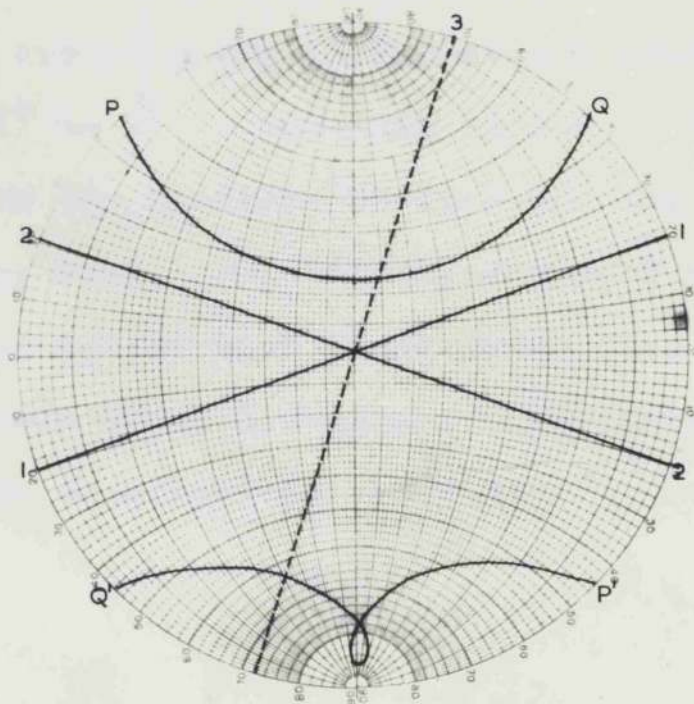


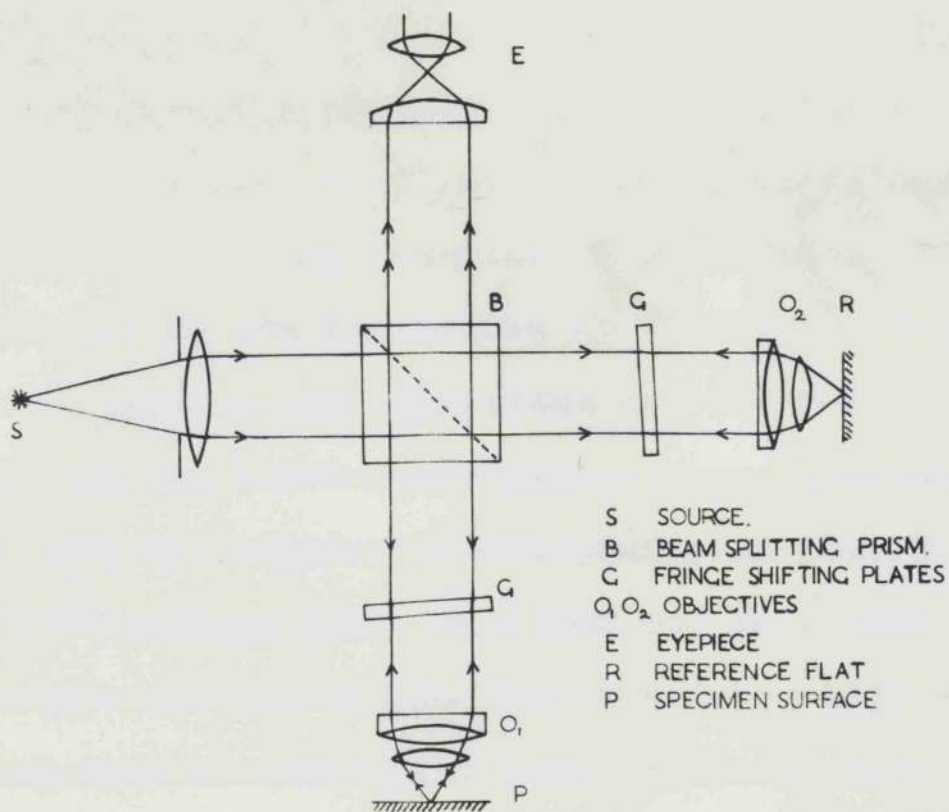
FIG. 8 A CHART FOR DETERMINING ORIENTATIONS.

trace is drawn, e.g. (3), all possible orientations (no more than 4) which fit the twin traces (1)(2) and (3) can be quickly found. A fourth twin trace usually gives an unambiguous solution. Stereograms similar to that shown in Fig. 8 were drawn for angles between (1) and (2) from 10° to 60° in 10° intervals. By using pairs of these, drawn on one chart, it was possible to make interpolations and to find orientations within a few minutes. Errors from $\pm 1^\circ$ to $\pm 2^\circ$ are estimated for the orientations.

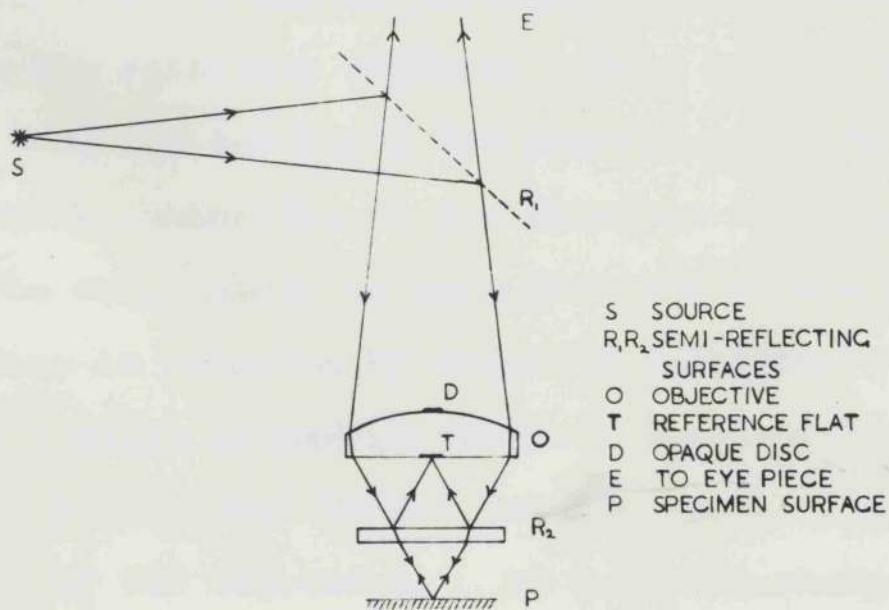
Some crystals were oriented by x-ray diffraction. Back-reflection Laue patterns were obtained using a 3 cm camera and 'white' tungsten radiation from a Hilger micro-focus set operated at 45 kV. The technique, a standard one, is also described by Barrett (48). The orientations found from indexing the diffraction patterns were accurate to within 1° to 2° . The main source of error is in setting both the specimen surface and the film normal to the x-ray beam. Within experimental error the orientations agreed with those found from twin traces and since the twin trace method was more convenient this was used for the experimental analysis.

(b) BAKER

FIG. 9. OPTICAL SYSTEMS FOR INTERFERENCE MICROSCOPY.



(a) LINNICK



(b) BAKER

FIG. 9. OPTICAL SYSTEMS FOR INTERFERENCE MICROSCOPY.

2.5 Interference microscopy plane and the virtual image

The principles of interference microscopy are well known and have been described by Ingelstam (50) who gives references to the literature up to 1959. Two different optical systems are at present available of which the Baker and the Linnick microscopes are representative. These are illustrated schematically in Fig. 9. The Baker microscope which was used for this work has the reference surface inside the objective while the Linnick system uses an additional lens and interchangeable reference surfaces with different reflectivities. There can be no doubt that the Linnick system is the more versatile.

In the Baker microscope an opaque disc prevents light being reflected directly back into the eyepiece from the reference surface. This disc limits the lens aperture and increases the average angle of convergence of the illumination at the specimen surface. Variation of the wedge angle between the reference and the specimen surface is achieved by means of a tilting stage. A disadvantage of having the reference surface inaccessible is that it cannot be set exactly parallel to the focal plane of the objective. As a result sharp fringes are produced only in a small region on either side of the line

of interception of the focal plane and the virtual image of the reference surface.

3.1 The microscope was calibrated directly - fringe spacing against wedge angle. A small optically flat silvered glass splinter was mounted on the goniometer head from an X-ray diffraction camera. Interferograms were then made of the surface for wedge angles up to 25° at 0.5° intervals. It was found that the fringe spacing corresponded to a change in height of $0.289 \pm .003 \mu$, as compared with the half-wavelength of the illumination (Hg. green): 0.273μ . The difference between these two values is discussed in an appendix on errors in interference microscopy. Interferograms were taken on Ilford 35 mm Pan F film and printed at a magnification of 1000. The striations are made up of stripes of smooth flat facets joined by slightly curved surfaces (Fig. 11). It was found from orientations of the grains that the striations are always parallel to the direction of the some axes of low index planes $\{111\}$, $\{100\}$ or $\{110\}$. For $\{111\}$ or $\{100\}$ striations the inclinations of the facets from interferograms verify that the facets are low index planes. The $\{110\}$ striations were often continuous across twin boundaries showing that the facets exposed were in fact

CHAPTER 3.

THERMAL ETCHING OF SILVER IN AIR AND OXYGEN

3.1 General features of etched structures

A great variety of topographical features appeared on silver surfaces annealed in the presence of oxygen. As well as grain and twin boundaries and linear facets (striations) large areas of plane surface, humps, dots and pyramids were found.

The appearance of surfaces etched in oxygen at 900°C, with and without net evaporation, is shown in Fig. 10. Surfaces break up into linear striations in directions which depend on the surface orientation. On specimens where net evaporation was inhibited the striations were much more widely spaced. Interference microscopy showed that the striations are made up of strips of smooth flat facets joined by slightly curved surfaces (Fig. 11). It was found from orientations of the grains that the striations are always parallel to the direction of the zone axes of low index planes $\{111\}$, $\{100\}$ or $\{110\}$. For $\{111\}$ or $\{100\}$ striations the inclinations of the facets from interferograms verify that the facets are low index planes. The $\{110\}$ striations were often continuous across twin boundaries showing that the facets exposed were in fact

Fig. 10. Typically etched surfaces after 10 days in oxygen.

Fig. 11. Interference microscopy.

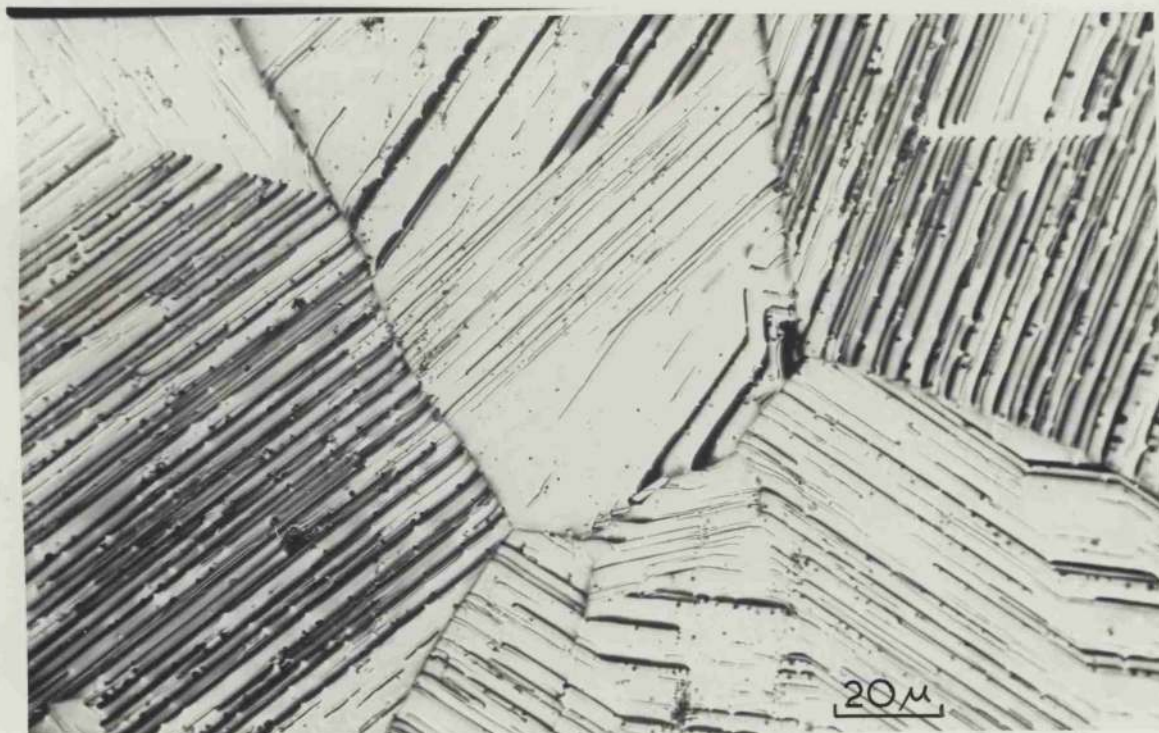
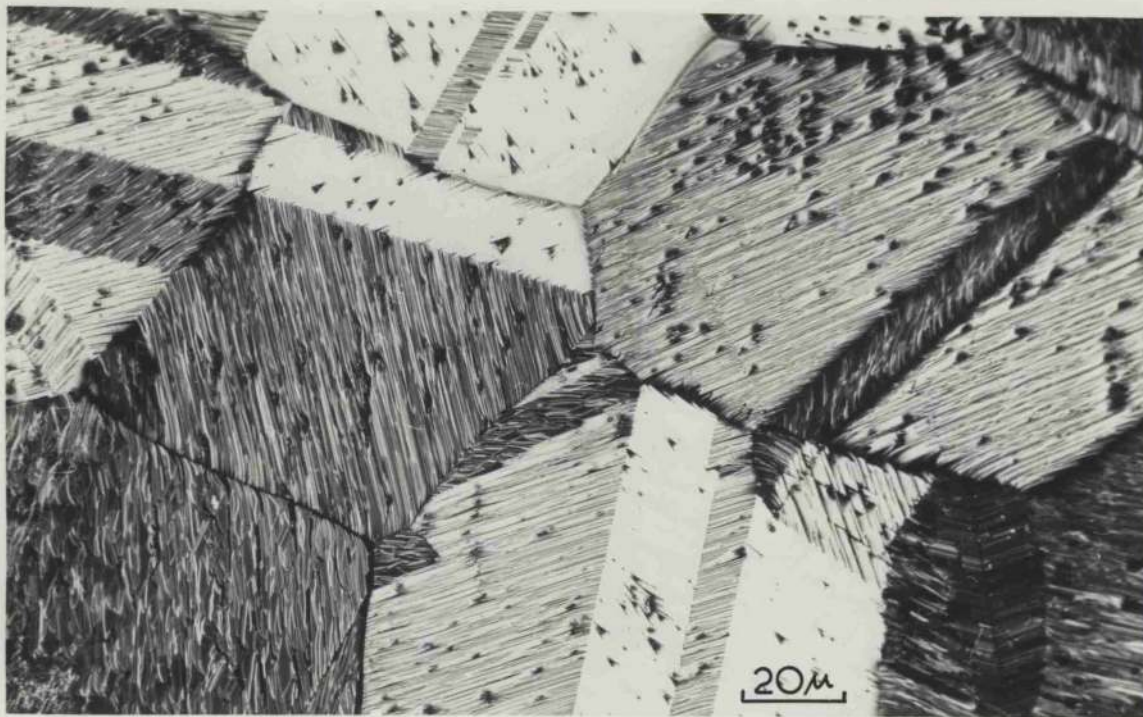


Fig.10. Thermally etched surfaces after 10 days in oxygen.
(a) with evaporation.
(b) evaporation inhibited.



TT': TWIN BOUNDARY. L: LOW INDEX PLANES. C: CONTINUATION SURFACES.

FIG.11. INTERFEROGRAM OF FACETS AFTER 10 DAYS IN OXYGEN.



TT' TWIN BOUNDARY. PP' $\{11\}$ FACETS. SS' $\{110\}$ STRIATIONS.

FIG.12. $\{110\}$ STRIATIONS CONTINUOUS ACROSS TWIN BOUNDARIES.

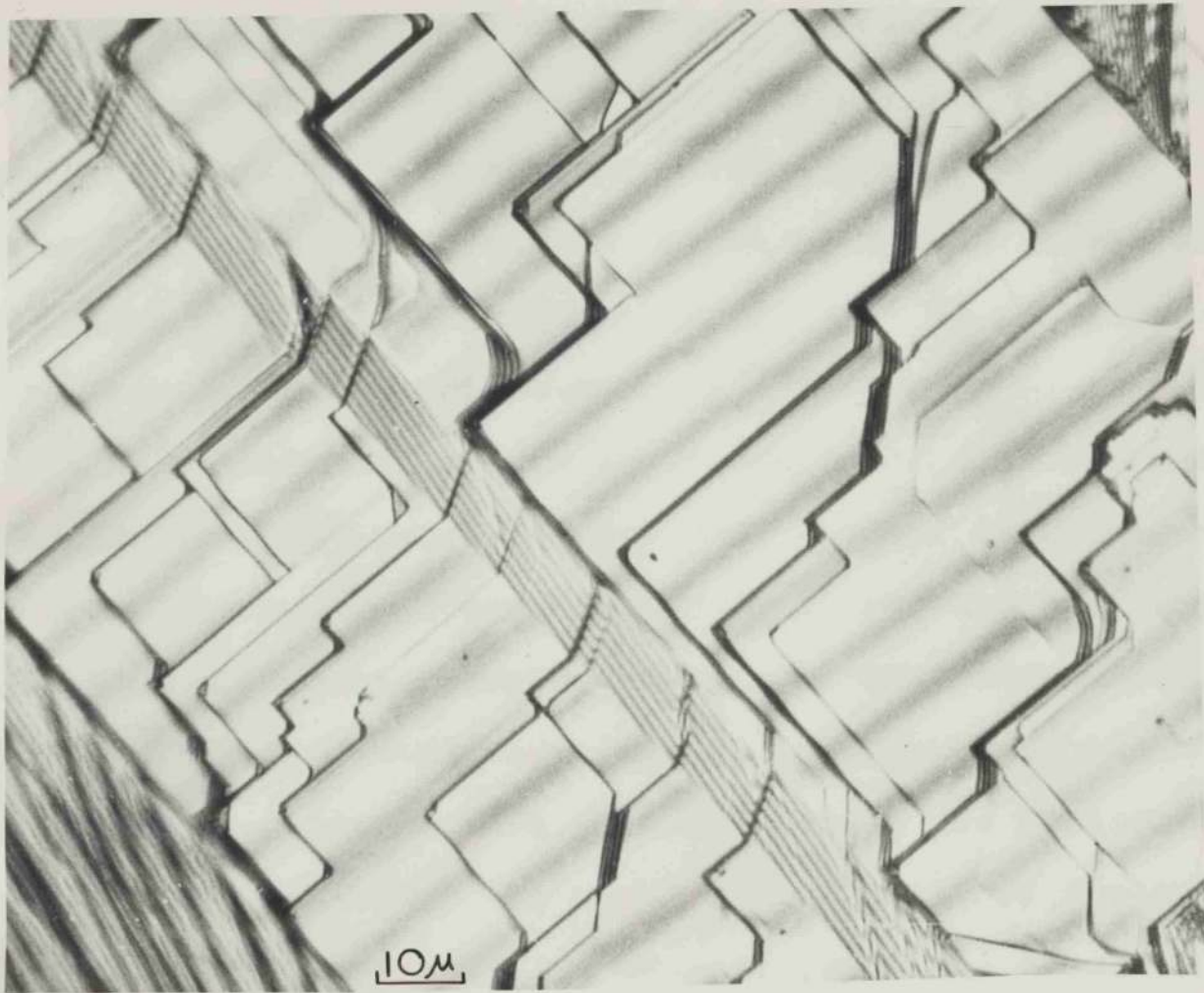


Fig.13.

Interferogram of (100) facets (A) with mainly $\{111\}$ steps after 10 days in oxygen with evaporation. The narrow twin shows (111) facets (B) with $\{100\}$ steps.

ystem for

{110} planes common to both crystals (Fig. 12). On most of the {111} and {100} facets it was not possible to detect any departure from planarity. An upper limit to step heights on these surfaces may therefore be put at about 40 lattice spacings. When the surface of a grain was very near to a {100} or {111} orientation it was sometimes found that striations did not form but instead the surface changed into large areas of low index planes bounded by sharp straight steps. The steps are usually shallow strips of low index facet. In Fig. 13 the surface is mainly (100) planes and the steps {111} planes. This type of etching was frequently found only where there was net evaporation. If low index surfaces have relatively low evaporation rates it would be

number	and container	temp (°C)	unit area (μg/cm ²)	thickness (Å)	Height of general surface (Å)
3.2 Effect of inhibiting evaporation					
1	Wire in	10	46150	440±500	6,000
The higher density of striations where surfaces were allowed to evaporate indicates that nucleation of facets is considerably enhanced by evaporation. Hondros and Moore's (46) claim that faceting does not occur when net evaporation is prevented was investigated by heating a number of specimens inside silver enclosures. In all					
3	Sheet in	10	2790 ± 8	35500 ± 80	20,000

cases faceting was observed to occur. By completely surrounding specimens the evaporation rates were reduced from about $18 \mu\text{g}/\text{cm}^2$ per hr. to $0.18 \mu\text{g}/\text{cm}^2$ per hr. in oxygen and from $10\text{-}20 \mu\text{g}/\text{cm}^2$ per hr. to less than $0.05 \mu\text{g}/\text{cm}^2$ per hr. in air. The effective changes in surface location due to evaporation were therefore less than $10^{-2} \mu$ while the striations were very pronounced and the low index facets projected above the general surface by several microns. This is clear evidence that net evaporation is not essential for the development of striations. Table 3 below summarises the results for a series of experiments.

Table 3.

Specimen number	Type of specimen and container	Heating Period (days at 900°C)	Change in weight per unit area ($\mu\text{g}/\text{cm}^2$)	Corresponding thickness (A°)	Height of facet above general surface (A°)
1	Wire in tube	2	$+46 \pm 50$	$+440 \pm 500$	6,000
2	Wire in tube	5	0 ± 50	0 ± 500	3,000
3	Sheet in box	1	-17 ± 6	-160 ± 60	6,000
4	Sheet in box	5	-5 ± 6	-50 ± 60	8,000
5	Sheet in open air	10	-2790 ± 8	-26500 ± 80	20,000

3.3 Contact angles

Measurements of the angles of contact between low index and continuation surfaces ($\theta = \alpha + \beta$ in Fig. 4e) were made from fringe spacings on the interferograms. The spacings perpendicular to the ridges gave the angles of tilt of both surfaces. As a measure of the tilt of the continuation surfaces the fringe spacing was taken near the top of the ridges where the curvature of the surface was negligible. The measurements were therefore limited to those striations most well developed.

The $\{110\}$ facets occurred only on specimens where there was net evaporation. No interferometric measurements could be made as the facets were too small; they may well have been slightly curved. The contact angle was estimated from the range of orientations on which $\{110\}$ striations formed. On the specimen heated in air the $\{110\}$ facets developed rather erratically, some crystals near (110) not faceting and on others $\{110\}$ facets appearing up to 8° from (110) .

Table 4 summarises the results of measuring the contact angles for specimens heated in air and oxygen and for conditions of both net evaporation and negligible net evaporation. The values obtained are compared with those of previous investigations.

Table 4

Author	Atmosphere	{100} striations (No. of crystals measured in brackets)	Contact angles θ {111} striations {110} striations
King (30)	Specimen Air evaporating	25°	36.5° -
Moore (23)	Specimen Air evaporating	26.2° ± 2.2° (56)	33.3° ± 1.8° (88) -
This work	Specimen Air evaporating	25.4° ± 1.1° (17)	33.8° ± 1.0° (21) 4° ± 4°
This work	No net Air evaporation	19.4° ± 1.0° (8)	30.5° ± 1.0° (24) -
This work	Oxygen Specimen evaporating	26.1° ± 1.3° (12)	34.2° ± 1.0° (27) 14° ± 2° (6)
This work	No net Oxygen evaporation	21.9° ± 0.8° (7)	31.6° ± 1.6° (26) -

Within experimental error the contact angles were independent of α and of the position of the general surface orientation in the unit triangle; i.e. the orientations of the complex surfaces lay on arcs centred at the low index poles (Fig. 14).

It is believed that the errors in the mean values for the angles are due to errors of measurement and not to the existence of a range of contact angles. This view is supported by the appearance of facets on a curved surface. For example on machined grooves, cut by turning a bar of silver in a lathe, facets were formed on curved crystal surfaces up to the limiting orientation and stopped quite sharply. On such curved surfaces the orientations of the complex surfaces were independent of the general surface orientation. The independence of θ on the particular values of α and β was not found in some recent experiments on copper by Stossel (51).

Certain anomalies were found with $\{100\}$ striations. Whereas $\{111\}$ striations usually formed sharp straight ridges $\{100\}$ facets often developed with irregularly shaped edges and the angles of contact, especially during the early stages of etching, were sometimes as low as 15° - 18° . In the later work at lower oxygen concentrations

similar low angle {100} striations were found. Since these angles were not stable they have not been included in the average values quoted. It is believed that the low angles are only an apparent effect due to sharp changes in curvature of the complex surfaces for some facets (for high values of m/n - see Chapter 7). The departure from straightness of the ridges is also visible in Fig. 11. This is probably caused by the interference of dislocations with facet growth.

Table 5.

Atmosphere	γ_{100}/γ_e	γ_{111}/γ_e
Air (specimen evaporating)	0.890 ± .013	0.814 ± .016
Air (no net evaporation)	0.933 ± .010	0.847 ± .016
Oxygen (specimen evaporating)	0.885 ± .015	0.810 ± .016
Oxygen (no net evaporation)	0.917 ± .010	0.836 ± .021

In terms of surface energies the contact angles may be interpreted by means of equation (1.9) and any variations to the mean values for the angles of contact...

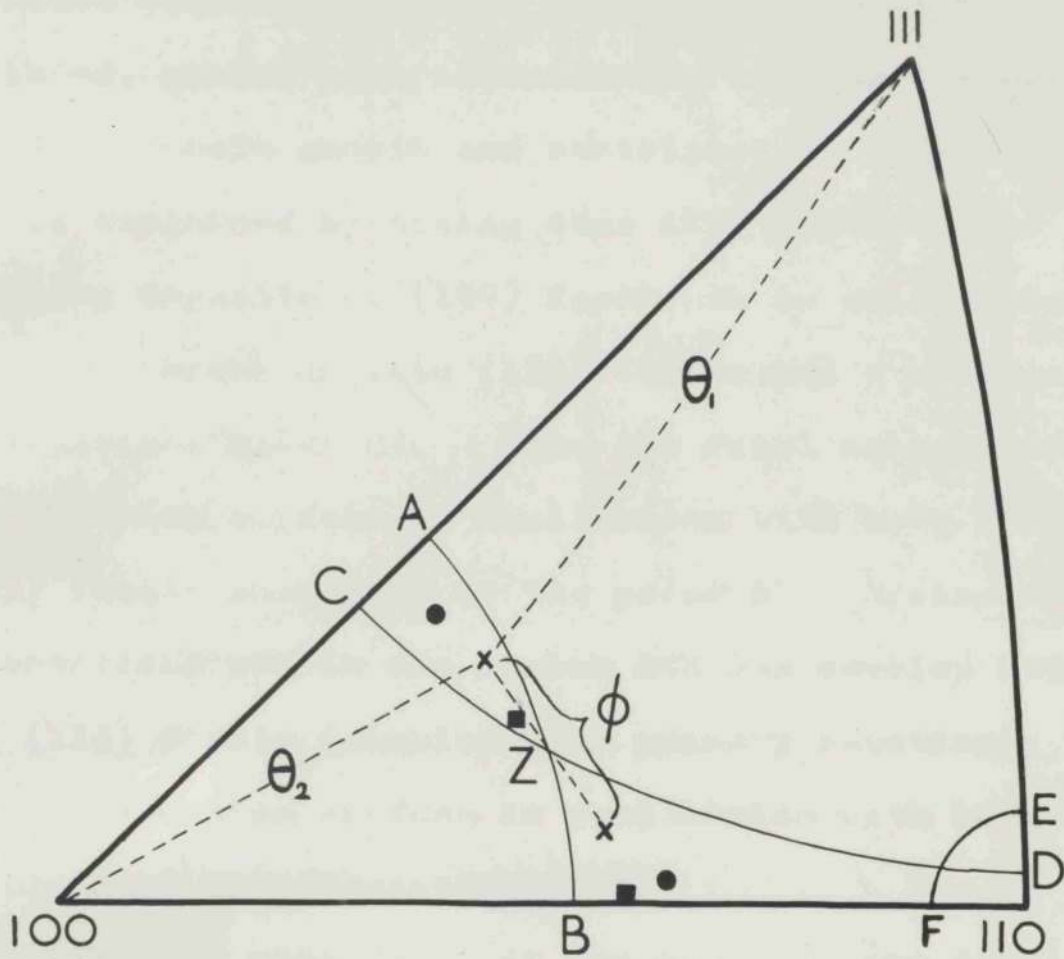


Fig. 14.

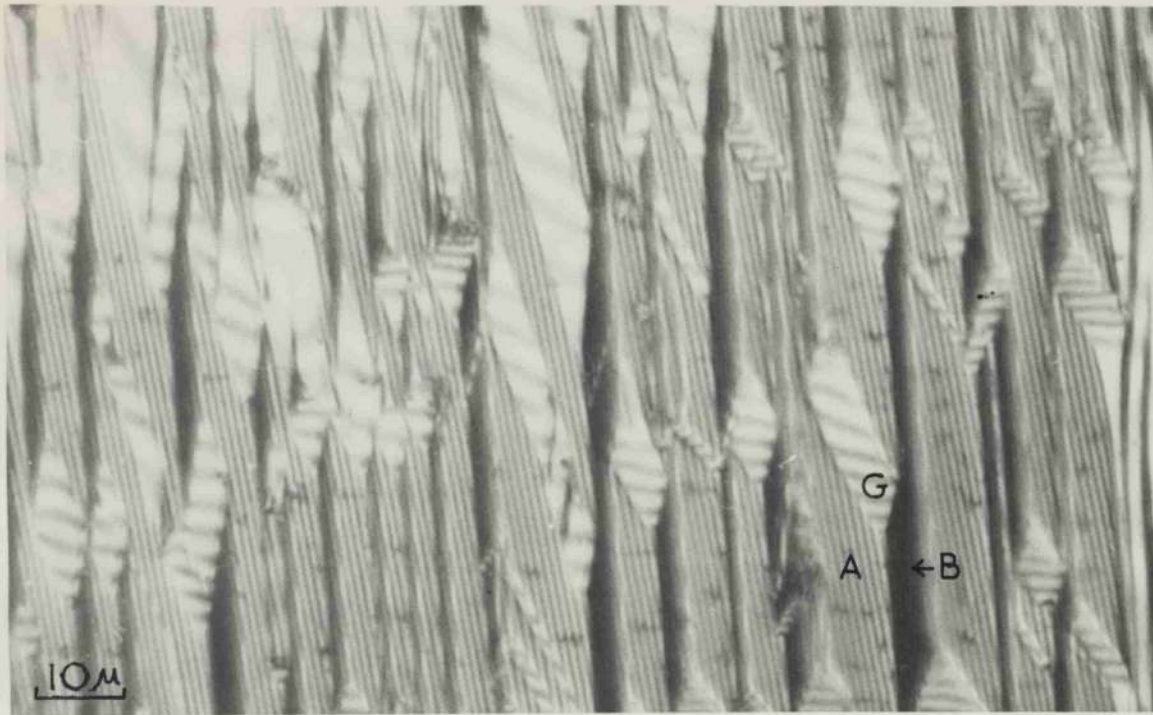
Stereographic triangle illustrating secondary and simultaneous primary faceting.

Points in ACZ: General surface orientations of crystals showing simultaneous primary faceting.

Points in BDZ: Orientations of corresponding 'gable ends'.

surfaces with orientations within these arcs become striated, grains with orientations outside the arcs are found to remain smooth and unstriated. Secondary faceting may be explained by noting that if a continuation surface joining segments of (100) facet has an orientation along AZ it can break up into (111) facets and a surface with an orientation along CZ. Thus the final orientation of a continuation surface in equilibrium with both (100) and (111) facets should be at the point Z. Grains with surface orientations within the region ACZ can develop both (100) and (111) facets (simultaneous primary faceting). Again the continuation surface in equilibrium with both facets should have an orientation at Z.

Examples were found of the simultaneous development of (100) and (111) facets but not of (111) with (110) facets. But measurements show that the above explanation of secondary and simultaneous primary faceting does not predict the observed orientations of the continuation surfaces. The interferogram of Fig. 15 is an example of simultaneous primary faceting in air. The surface has developed into three sets of facets: (100) planes, (111) planes and surfaces at various inclinations and in contact with both sets of low index surfaces. These



15. Interferogram showing simultaneous primary faceting in air after 10 days. A, (100) facet; B, (111) facet; G, 'gable end'.

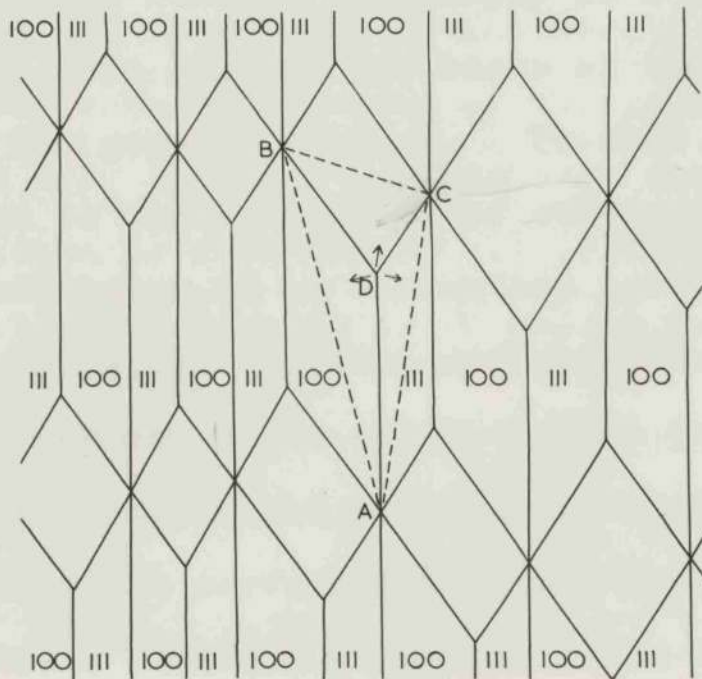


Fig. 16. Schematic representation of Fig. 15.

latter surfaces will be referred to as 'gable ends'. Orientations were determined from fringe spacings and it was found that on each crystal which etched in this way the gable ends have a range of orientations all in the region BZD and not at Z as predicted. (ii) Orientations of original general surfaces and gable ends for three such crystals are plotted in Fig. 14.

To explain this apparently anomalous effect it is necessary to consider the equilibrium of three surfaces taken as a whole rather than the equilibrium between pairs of surfaces. A surface structure similar to that in Fig. 15 is drawn schematically in Fig. 16. This shows where a_{111} , a_{100} and a_g are the fractional areas of the three sets of surfaces, (111), (100) and gable ends. The facets projected onto ABC and θ_1 , θ_2 and ϕ the corresponding angles of inclination to ABC (see Fig. 14), example ABCD. On average the bases of the pyramids are parallel to the general surface. To find the equilibrium configuration of the three sets of surfaces one need only consider equilibrium of an elementary pyramid. Equilibrium will be reached when the total surface energy of the pyramid is a minimum. The total surface energy can change by rotations of the three surfaces bringing about changes in relative surface areas, but the inclinations of the low index facets may be considered fixed

$$\gamma = \frac{\gamma_{111}}{\cos \theta_1} + \frac{\gamma_{100}}{\cos \theta_2} + \frac{\gamma_g}{\cos \phi} \quad (3.1)$$

$$+ \frac{\gamma_g a_g \sin \phi}{\cos^2 \phi} + \frac{a_g \delta \gamma_g}{\cos \phi} = 0 \quad (3.2)$$

crystallographically since they are at sharp minima in the γ plot. Therefore only the gable end may rotate, which it may do (i) by movement of B toward A and C away from A (or vice versa); this changes the relative areas of (111):(100) low index surfaces; (ii) by movement of D along AD, this varies the ratio of low index surface to gable end surface.

The total surface energy $\Psi = \int \gamma dA$ for the pyramid

may be written:

$$\Psi = \frac{\gamma_{111} a_{111}}{\cos \theta_1} + \frac{\gamma_{100} a_{100}}{\cos \theta_2} + \frac{\gamma_G a_G}{\cos \phi} \quad (3.1)$$

where a_{111} , a_{100} and a_G are the fractional areas of the facets projected onto ABC and θ_1 , θ_2 and ϕ the corresponding angles of inclination to ABC (see Fig. 14).

For the equilibrium orientation of the gable end rotations of type (ii) are considered; the minimum energy condition is obtained by differentiation of

equation (3.1) with respect to ϕ and by putting

$$\frac{\partial \Psi}{\partial \phi} = 0 :$$

$$\frac{\gamma_{111} \frac{\partial a_{111}}{\partial \phi}}{\cos \theta_1} + \frac{\gamma_{100} \frac{\partial a_{100}}{\partial \phi}}{\cos \theta_2} + \frac{\gamma_G \frac{\partial a_G}{\partial \phi}}{\cos \phi} + \frac{\gamma_G a_G \sin \phi}{\cos^2 \phi} + \frac{a_G \frac{\partial \gamma_G}{\partial \phi}}{\cos \phi} = 0 \quad (3.2)$$

The following relationships can be shown from geometry:

$$\frac{\partial a_{111}}{\partial \phi} \approx -\frac{\partial a_G}{\partial \phi} \frac{\sin \chi_1}{\sin \chi_1 + \sin \chi_2} \quad (3.3)$$

$$\frac{\partial a_{100}}{\partial \phi} \approx -\frac{\partial a_G}{\partial \phi} \frac{\sin \chi_1}{\sin \chi_1 + \sin \chi_2} \quad (3.4)$$

$$\frac{1}{a_G} \frac{\partial a_G}{\partial \phi} \approx -\cot \phi \quad (3.5)$$

where $\chi_1 = \angle DAC$ and $\chi_2 = \angle DAB$, the projected angles in the plane ABC of Fig. 16. On substitution of these relationships in equation (3.2) the equilibrium condition becomes:

$$\frac{\gamma_{111} \sin \chi_1}{\gamma_G \cos \theta_1 (\sin \chi_1 + \sin \chi_2)} + \frac{\gamma_{100} \sin \chi_2}{\gamma_G \cos \theta_2 (\sin \chi_1 + \sin \chi_2)} = 2 \sec \phi - \sec^3 \phi - \frac{1}{\gamma_G} \frac{\partial \gamma_G}{\partial \phi} \frac{\sin \phi}{\cos^2 \phi} \quad (3.6)$$

A reasonable approximation can be made by assuming the symmetrical case $\chi_1 = \chi_2$ and by neglecting $\frac{\partial \gamma}{\partial \theta}$ and $\frac{\partial \gamma}{\partial \phi}$ terms. Substitution of the approximate values $\gamma_{111}/\gamma_G = \cos 34^\circ$ and $\gamma_{100}/\gamma_G = \cos 25^\circ$ together with typical values $\theta_1 = 32\frac{1}{2}^\circ$ and $\theta_2 = 24^\circ$ then gives $\phi \approx 10^\circ$ which

puts the orientation of the gable end in the region BZD
and not at the point Z. The orientations of the gable ends can be explained
therefore if it is assumed that the three surfaces are in
equilibrium simultaneously as a unit. It was found that on a given crystal the smaller gable ends are tilted
most from the general surface. This is presumably because
equilibrium between the three surfaces occurs most
rapidly across small areas of facet. The same explanation
would account for the shape of a continuation surface
where it crosses a twin boundary and is in contact with
two low index facets and for the shape of the continuation
surface on pyramids found during enhanced evaporation;
in both these cases the surfaces become steeper in the
region near the point of contact of the three surfaces.

3.5 Temperature dependence of the contact angles.

Table 6 below gives the mean values for contact
angles on specimens etched for 10 days at temperatures
from 940°C to 850°C in conditions of free evaporation.

Below 850°C no satisfactory measurements could be
made as the specimens, though densely striated, did not
have large enough facets for accurate determination of

surfaces and the complex surfaces. But Allen's results (28) show that T/γ decreases by about 30% between 900°C and 800°C. The temperature dependence of the contact angles must therefore be ascribed to a general increase in the concentration of adsorbed oxygen at lower temperatures and hence to an increase in the variation of adsorbed density with orientation.

3.6 Effect of enhanced evaporation

The net loss of material by evaporation from the specimens heated in air was limited by the rate of diffusion of vapour through the air in the sealed furnace tube. To find out how thermal etching was affected by a faster evaporation rate specimens were heated in a steady flow of air and as a result a quite different form of etching was found on many crystals. After a few hours dots appeared on the surface; these were apparently small hillocks and had a density of about $2 \times 10^6 \text{ cm}^{-2}$. They may be the sites of screw dislocations. The dots became the nucleation sites for the formation of facets which grew into striations by extending sideways (Fig. 17). Under these conditions of fast evaporation the final structure after 20 days consisted mainly of large pyramids with exact low index

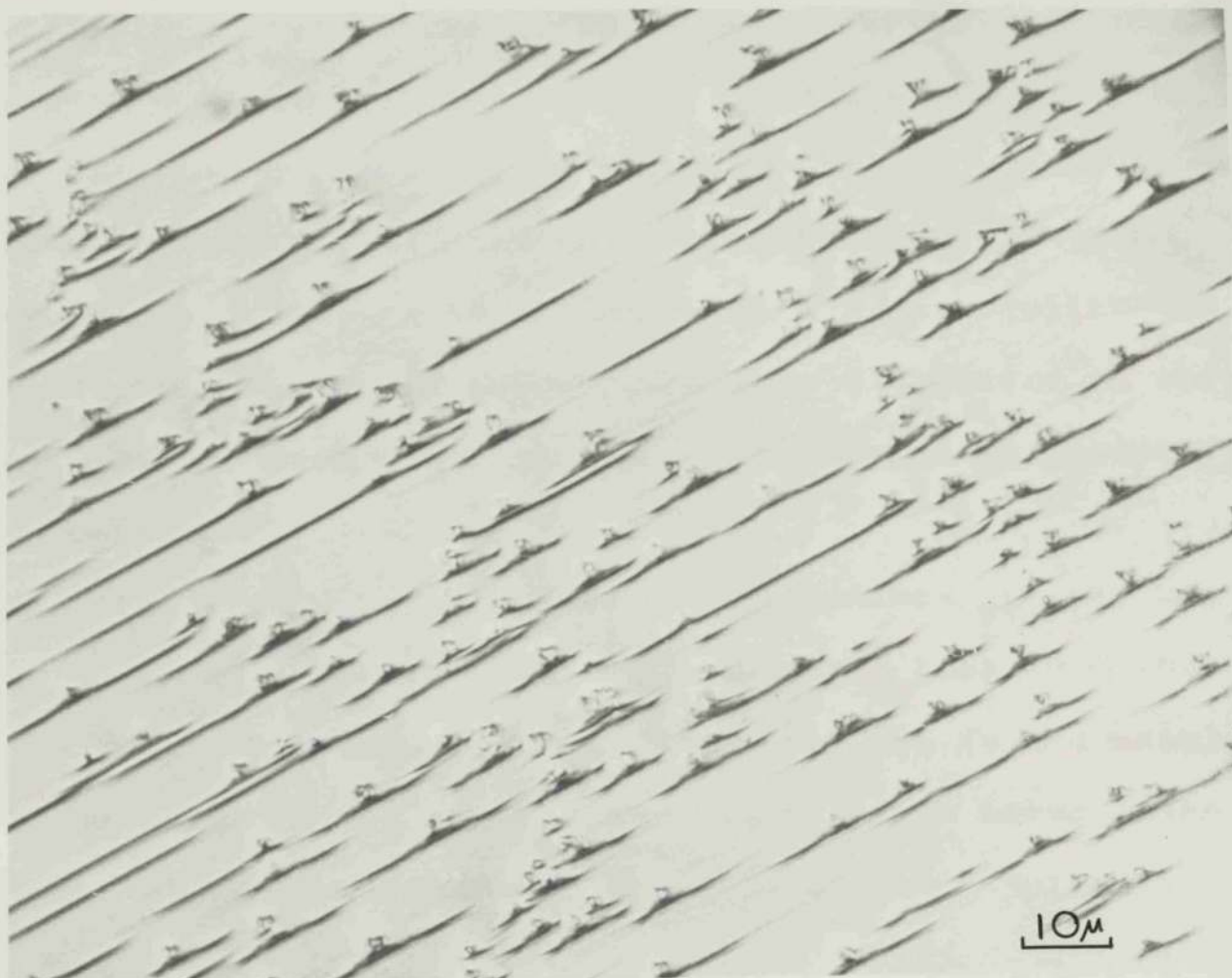


Fig.17. The formation of facets during enhanced evaporation. After 2 days in air.

sides (Fig. 18). The sides of the pyramids were often inclined to the general surface at angles greater than the equilibrium contact angles given in Table 4 - this is not however in conflict with the theory which accounts for spontaneous changes of a flat surface under equilibrium conditions. The interferograms show that close to the base of the pyramids a shallow groove forms to preserve the correct contact angles.

The heights of the pyramids - sometimes greater than 10μ - when compared with the net weight loss from the surface, 14 mg/cm^2 , indicate that they are formed mainly by evaporation of the general surface and that evaporation from low index surfaces is appreciably lower than the average evaporation rate. Additional information on this point comes from the variation of evaporation rate with time which occurs during etching as the proportion of surface made up of low index facets progressively increases.

Fig. 15. Interferogram of pyramids formed by enhanced evaporation. After 20 days in air. The height of the pyramids is greater than the depth of facets of the microstructure.

A typical specimen was heated in air in a sealed furnace tube and the weight of the specimen found at 20 hour intervals up to 300 hours. The tube had previously been used for several thousand hours for heating silver so that it may be assumed that the silver vapour near the specimen was in dynamic equilibrium and the vapour pressure



Fig.18. Interferogram of pyramids formed by enhanced evaporation. After 20 days in air. The height of the pyramids is greater than the depth of focus of the microscope.

constant during the experiment. As the fraction of the surface made up of visible low index facet changed from zero at the beginning to not more than 40 per cent after 300 hours the weight loss changed from about $20 \mu\text{g}/\text{cm}^2$ per hour to $12 \mu\text{g}/\text{cm}^2$ per hour. Part of the change in evaporation rate may be due to an increase in surface impurity concentration by diffusion from the interior of the specimen, but if it is ascribed mainly to a lower evaporation rate from low index surfaces then these surfaces evaporate at least ten times more slowly than the average. Similar conclusions can be drawn from observations on specimens heated in atmospheres of low oxygen content (Chapter 4). Grain surfaces were frequently found, made almost entirely of smooth low index facets similar to those shown in Fig. 13, standing higher than the surrounding grains by several microns.

by the presence of impurities which are removed by oxygen.

Evaporation roughening was observed on specimens heated and allowed to evaporate in vacuum ($<10^{-5}$ mm Hg). Evaporation exposed large areas of plane facet (Fig. 20). But on specimens heated in vacuum and completely enclosed in a silver box to inhibit evaporation no evaporation roughening occurred and the surfaces were similar to



Fig.19. Surface after 5 days heating in nitrogen. Shallow grain boundaries and inverted twin boundaries (T). The horizontal markings are rolling marks.



Fig.20. Evaporation roughening with the development of facets after $\frac{1}{2}$ hour in vacuum.(Interferogram).

those heated in nitrogen and the nitrogen plus hydrogen mixture. In Fig. 21a and a typical area of the specimen

The observation that striations do not always occur even when there are finite cusps in the γ plot does not conflict with the view that thermal etching is driven by a lowering of total surface energy. For values of γ/γ_0 near unity the contact angles will be necessarily small and $\delta\gamma/\gamma_0$ may be too large for equation (1.9) to be satisfied for any real value of θ . This point has been discussed by Blakely and Mykura (52). The mean contact

4.2 Etching in oxygen:nitrogen mixtures.

Specimens were heated for periods of 10 days in atmospheres with nominal oxygen concentrations, parts by weight: 10^{-5} , 3×10^{-5} , 10^{-4} , 3×10^{-4} , 10^{-3} and 10^{-2} .

In 10 p.p.m. of oxygen only about half the grains became striated and considerably more grains were unstriated than on the air-etched specimens. There was also some evaporation roughening but not as much as occurred in vacuum. Some 46 grains, striated and unstriated, were oriented and from interferograms the orientations of the continuation surfaces for both $\{100\}$ and $\{111\}$ facets were found by measurement of the fringe

spacings. The results are plotted in a unit stereographic triangle in Fig. 21a and a typical area of the specimen is shown in Fig. 22. The mean contact angles were: $\{100\}$, $17.6^\circ \pm 2.0^\circ$; $\{111\}$, $24.9^\circ \pm 2.0^\circ$; these angles are appreciably lower than the angles for air-etched specimens.

Comparable results for an oxygen concentration of about 100 p.p.m. are shown in Fig. 21b. At this concentration however the contact angles were several degrees higher than those for 10 p.p.m. The mean contact angles for all concentrations are shown in Table 7 and the variation of the cosine of the contact angle with the logarithm of oxygen partial pressure is plotted in Fig. 23. The table summarizes all the measurements on specimens which were allowed to evaporate.

The increase in the experimental error in the contact angles at low oxygen concentrations and especially at 10 p.p.m. is due to a much wider scatter in the measurements at these concentrations. This scatter is the result of variations in the surface condition of the specimens. It was found that those crystals furthest upstream in the gas flow striated much more than those downstream. It is possible that a higher concentration

X striated grains.

(a) Oxygen concentration 10^{-3} .

(b) Oxygen concentration 10^{-4} .

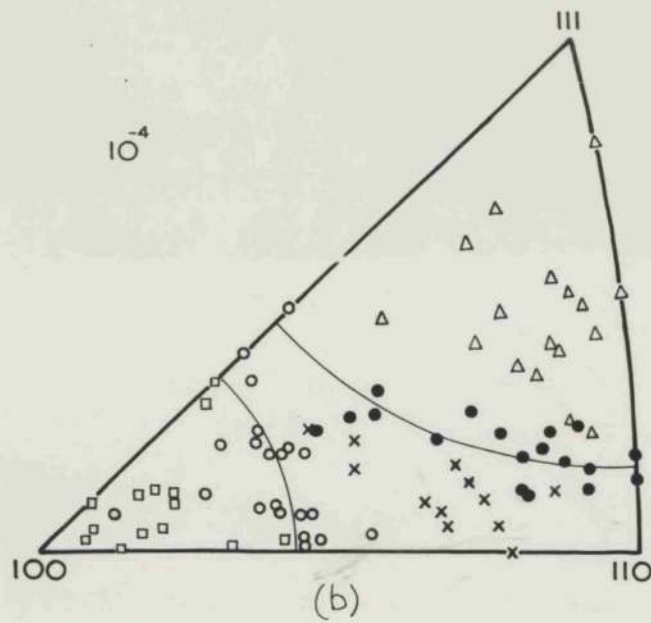
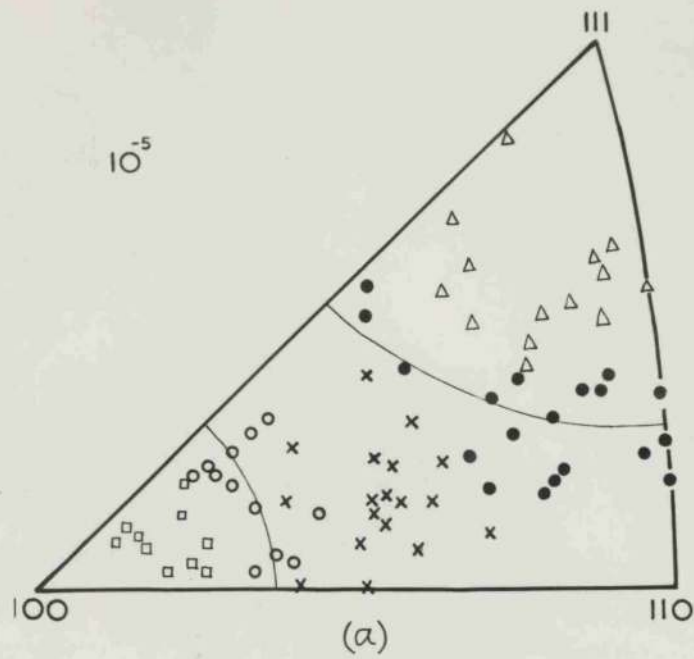


Fig. 21. Stereographic projections showing orientations of:

- grains which formed striations with (100) facets.
- △ " " " " " (111) " .
- continuation surfaces in equilibrium with (100) facets.
- " " " " " (111) facets.
- × unstriated grains.

(a) Oxygen concentration 10^{-5} .

(b) Oxygen concentration 10^{-4} .

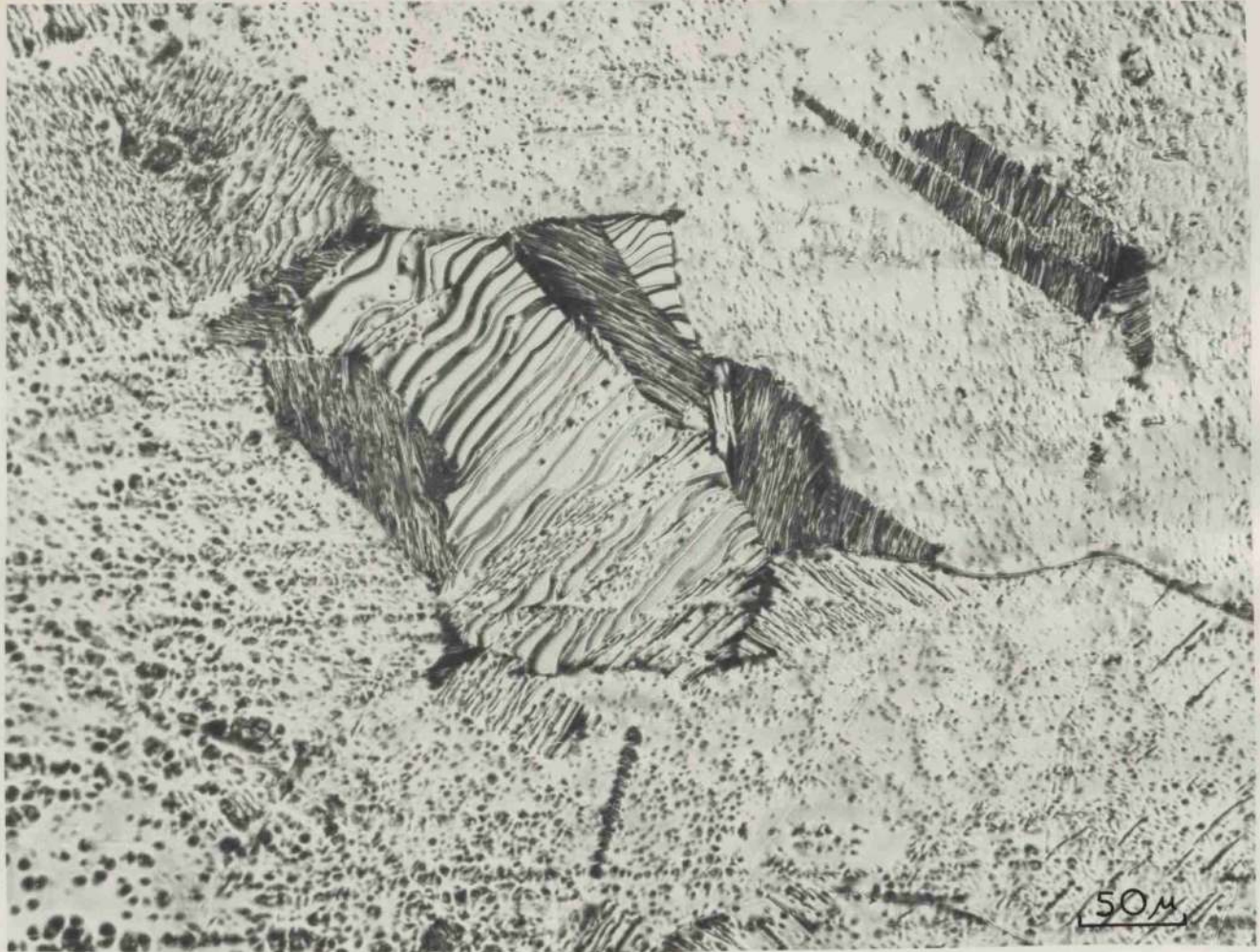


Fig.22. Typical area of surface heated for 10 days in 10^{-5} parts oxygen.

Table 7. Contact angles at different oxygen concentrations

Nominal concentration	Relative concentration parts O ₂ by weight	Partial pressure O ₂ mm. Hg.	{100} Striations (No. of crystals measured in brackets)	Contact angles θ
Oxygen	1.00	970	26.0° ± 1.3° (12)	34.2° ± 1.0° (27)
Air	2.04 × 10 ⁻¹	155	25.4° ± 1.1° (17)	33.8° ± 1.0° (21)
10 ⁻²	0.92 ± .05 × 10 ⁻²	9.05	27.2° ± 1.6° (22)	32.0° ± 1.4° (18)
10 ⁻³	1.23 ± .06 × 10 ⁻³	1.21	23.5° ± 1.5° (17)	28.6° ± 1.2° (27)
3 × 10 ⁻⁴	2.46 ± .14 × 10 ⁻⁴	2.41 × 10 ⁻¹	21.9° ± 1.8° (16)	29.8° ± 1.0° (25)
10 ⁻⁴	0.90 ± .05 × 10 ⁻⁴	0.88 × 10 ⁻¹	20.0° ± 1.7° (17)	29.4° ± 1.7° (17)
3 × 10 ⁻⁵	3.70 ± .22 × 10 ⁻⁵	3.63 × 10 ⁻²	21.6° ± 2.0° (26)	29.2° ± 1.4° (41)
10 ⁻⁵	1.23 ± .06 × 10 ⁻⁵	1.21 × 10 ⁻²	17.6° ± 2.0° (13)	24.9° ± 2.0° (19)

of silver vapour downstream would clean off some of the adsorbed oxygen. At low concentrations the etched topography is complicated by the surface roughness caused by evaporation. Few areas of smooth surface were found and on many grains facets formed on the sides of hillocks and troughs where the surface was tilted by several degrees from the general orientation. Occasional {110} facets were found on the underneath surfaces of specimens heated in 10^{-2} and 10^{-3} parts of oxygen; this is possibly due to contact with Mullite. A few small areas of plane facet with orientations near the (110) pole developed on the specimens heated in 10^{-4} parts of oxygen.

It appears that reducing the oxygen concentration produces a marked decrease in the contact angles. The orientations of unstriated grains were always found in the region of the stereographic triangle outside the arcs drawn at the orientations of the continuation surfaces. For concentrations where the arcs do not intersect no examples of simultaneous primary faceting were found.

The data on evaporation is completed in Table 8 which gives evaporation rates in various atmospheres. For similar specimens heated in the same atmosphere there were differences in weight losses of as much as threefold. The values quoted are typical ones. Weight losses in nitrogen were as much as a quarter those in air.

Table 8. Net evaporation rates of silver in various atmospheres at 900°C.

Atmosphere	Evaporation rate in $\mu\text{g}/\text{cm}^2/\text{hour}$
Oxygen	~ 18
Oxygen Evaporation inhibited	~ 0.18
Air	10-20
Air Evaporation inhibited	< 0.05
Air Fast stream	25-35
Nitrogen plus 10^{-3} parts oxygen	5-16
Nitrogen plus 10^{-5} parts oxygen	5-7
Nitrogen	3-5
Nitrogen + 10^{-3} parts hydrogen	4-10
* Vacuum	~ 10600
* Vacuum Evaporation inhibited	~ 80

* The figure for evaporation in vacuum is for a period of $\frac{1}{2}$ hour and for vacuum with evaporation inhibited, 10 hours. All the other rates are mean values over 5-10 days.

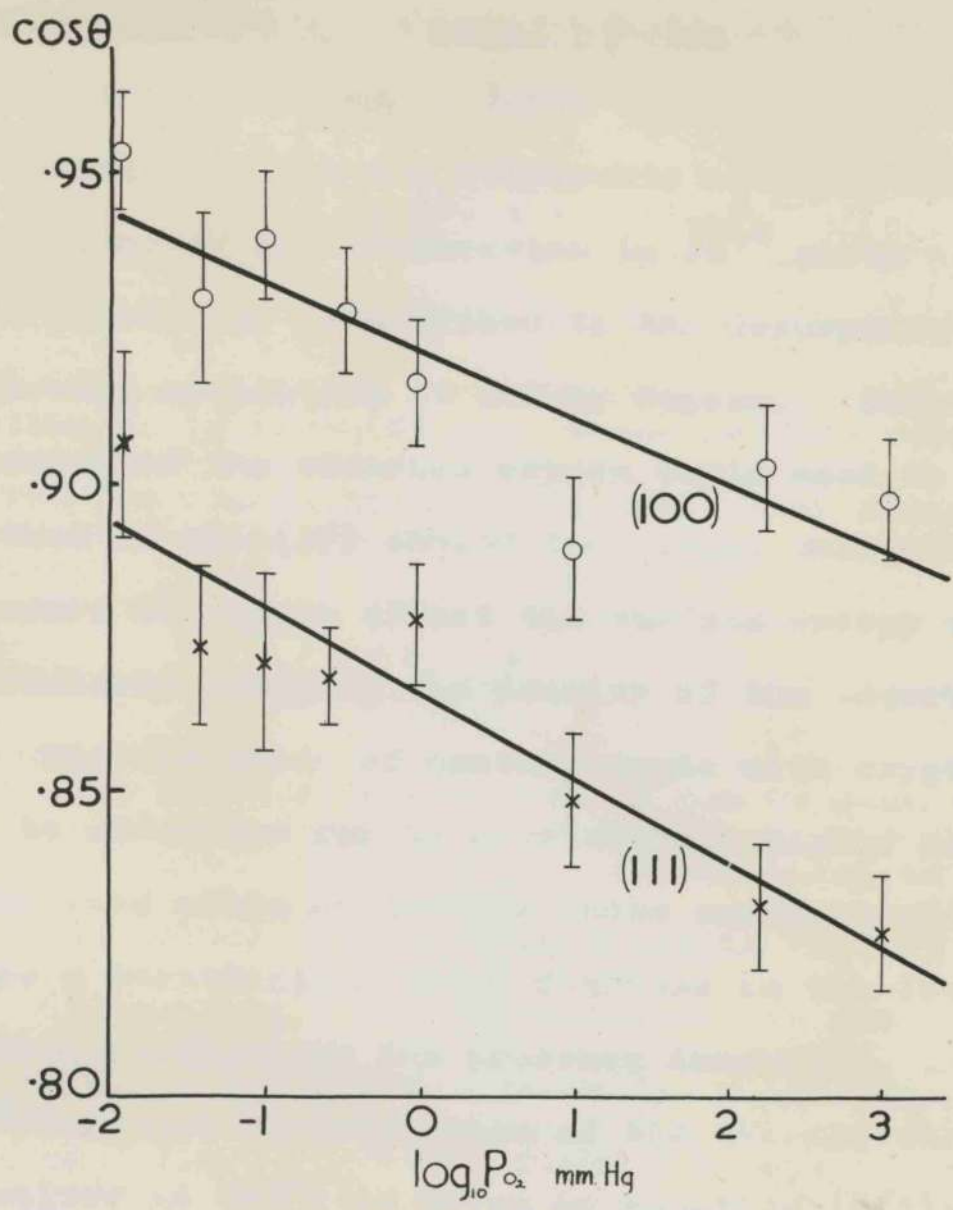


Fig.23. Variation of the cosine of the contact angles with logarithm of partial pressure of oxygen. 'Least squares' straight lines.

4.3 Adsorption and thermal etching

The contact angles found for conditions of negligible evaporation in air are comparable with the angles for conditions of net evaporation in 10^{-4} parts of oxygen.

$$\gamma_L(p) = \gamma_L(0) - K_L \log_{10} p \quad (4.1)$$

This effect may be ascribed to the desorption of oxygen

following adsorption of silver vapour. Only a small fraction of the adsorbed oxygen would need to be removed. Buttner et al. (17) showed that large changes in the partial pressure of oxygen affect the surface energy without appreciably changing the density of the adsorbed layer.

The variation of contact angle with oxygen pressure may be accounted for by a relatively higher density of adsorption sites on the low index surfaces which would cause a relatively greater decrease in the low index surface energies as the pressure increased. It is recalled that the variation of the average surface energy of silver at 900°C is given by equation (1.3):

$$\gamma = 228 - 188 \log_{10} p \text{ ergs cm}^{-2}$$

From the Gibbs adsorption equation (1.2) the coefficient of $\log_{10} p$, \bar{K} , is proportional to the density of adsorbed oxygen atoms. A refinement to the above calculation would take into account the variation of γ with pressure. If this is done energies of both the low index surfaces γ_L and continuation

surfaces γ_θ vary with oxygen pressure in the same way as the average surface energy then

$$\gamma_L(p) = \gamma_L(0) - K_L \log_{10} p \quad (4.1)$$

$$\gamma_\theta(p) = \gamma_\theta(0) - K_\theta \log_{10} p \quad (4.2)$$

There is a difference of only 3% between putting $\gamma_L(0) = \gamma_\theta(0)$ i.e. assuming that cusps in the γ plot are caused mostly by differential adsorption one layer (presumably a monolayer) would fit onto the silver lattice with very little mismatch. Since {111} and {100} surfaces differ by only 14% differences of the same order are expected between these surfaces and the

As a first approximation it can be assumed that

$$\frac{\gamma_L}{\gamma_\theta} = \cos \theta \quad \text{and} \quad \frac{K_L - K_\theta}{\gamma_\theta(p)} \quad \text{can be taken as a constant.}$$

From the slopes of the lines drawn in Fig. 23 and putting $\gamma_\theta = 600 \text{ ergs cm}^{-2}$ the following values are found:

$$K_{111} - K_\theta = 8.3 \pm 1.6 \text{ ergs cm}^{-2}; \quad K_{100} - K_\theta = 6.4 \pm 1.4 \text{ ergs cm}^{-2} \text{ i.e. } \frac{K_{111} - K_\theta}{\bar{K}} = 0.044 \pm 0.009;$$

$$\frac{K_{100} - K_\theta}{\bar{K}} = 0.034 \pm 0.007. \quad \text{Since } K_\theta \approx \bar{K} \text{ and } K \text{ is}$$

proportional to Γ it may be concluded that about 4% more oxygen atoms per unit area are adsorbed onto low index surfaces than onto surfaces with other orientations.

A refinement to the above calculation would take into account the variation of γ with pressure. If this is done

and values for γ_r/γ_θ calculated using values for $\frac{1}{\gamma} \frac{\partial \gamma}{\partial \theta}$ from 0.03 up to 0.06 for lower contact angles then the best estimate for the differences in surface densities of adsorbed atoms is $4 \pm 2\%$.

A 4% difference in the adsorbed layers is not unreasonable. There is a difference of only 3% between the atomic diameters of silver and oxygen and the oxygen layer (presumably a monolayer) would fit onto the silver lattice with very little mismatch. Since {111} and {100} surfaces differ in density by about 14% differences of the same order are expected between these surfaces and the high index continuation surfaces.

3.1 Twin boundaries in nitrogen.

Specimens were annealed for periods up to 10 days in an atmosphere of nitrogen with 0.1% hydrogen. Some of the coherent twin boundaries were extremely faint and could only be located by the adjoining sections of incoherent boundary. Where observable grooves had formed these appeared, surprisingly, smaller in width than the grain boundary grooves. The best pairs of twin boundary grooves were photographed but of these only three sets could be

CHAPTER 5

TWIN BOUNDARY GROOVES

Annealing twins occur very readily in silver; the abundance of twin boundaries on all specimens greatly facilitated the orientation determinations. Pairs of twin boundaries, one with a groove, the other an inverted groove, were found to occur independently of the annealing atmosphere. As mentioned in the last chapter this indicates a definite variation of surface energy with orientation even in atmospheres where facets did not develop. It was of some interest therefore to make some measurements on twin boundary grooves and to estimate the torque terms $\frac{\partial \gamma}{\partial \theta}$.

5.1 Twin boundaries in nitrogen.

Specimens were annealed for periods up to 10 days in an atmosphere of nitrogen with 0.1% hydrogen. Some of the coherent twin boundaries were extremely faint and could only be located by the adjoining sections of incoherent boundary. Where observable grooves had formed these appeared, surprisingly, smaller in width than the grain boundary grooves. The best pairs of twin boundary grooves were photographed but of these only three sets could be

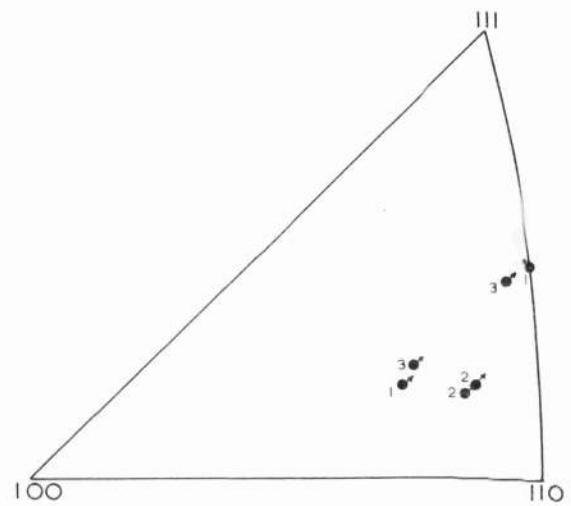
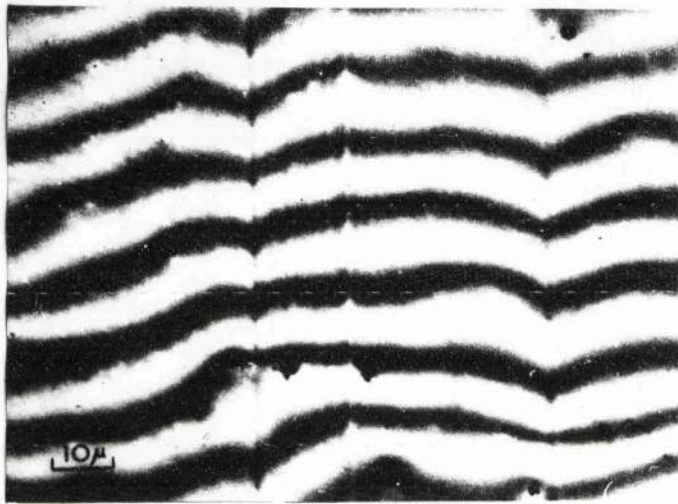
measured with any accuracy; one is shown in Fig. 24a. Measurements from the interferograms are summarised in Table 9. The angles A, B, A' and B' are those referred to in Fig. 4b. Values for the ratio twin boundary to surface energy, γ_T/γ_S , and for the sum of pairs of orientation derivatives were obtained using equations (1.7) and (1.8).

Table 9. Twin boundaries in nitrogen

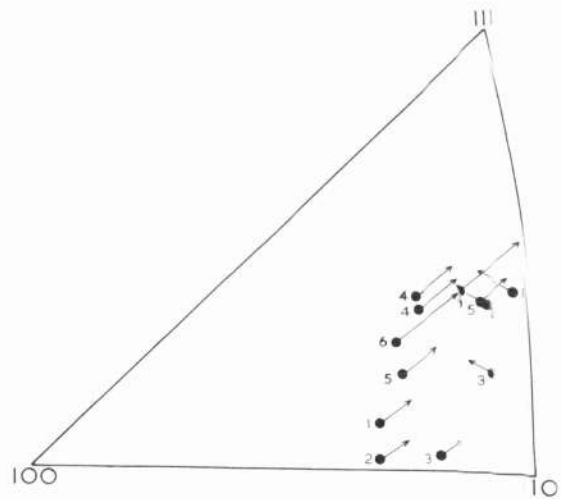
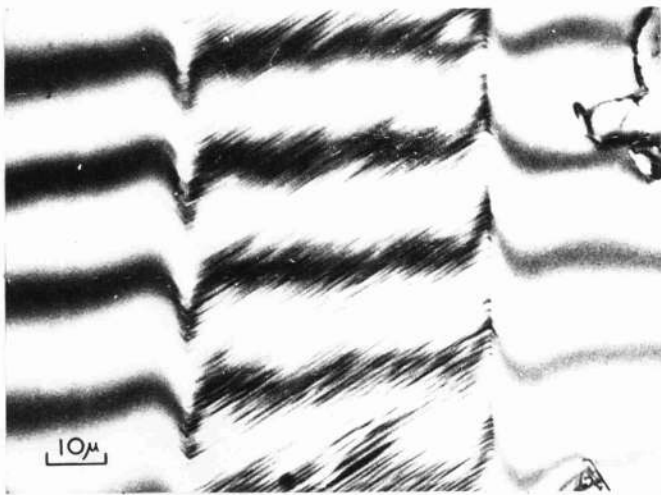
Twin pair	A + B	A' + B'	γ_T/γ_S	$\frac{1}{\gamma_S} \left(\frac{\partial \gamma_Q}{\partial A} + \frac{\partial \gamma_R}{\partial B} \right)$
1	178°47' ± 6'	180°40' ± 8'	0.0047 ± 0.0021	0.0163 ± 0.0021
2	178°46' ± 8'	181° ± 7'	0.0021 ± 0.0024	0.0195 ± 0.0024
3	178°52' ± 7'	180°48' ± 6'	0.0029 ± 0.0018	0.0169 ± 0.0018

From the above figures the best value for γ_T/γ_S is $0.0033 \pm .0012$. Taking $1140 \text{ ergs cm}^{-2}$ as the surface energy in nitrogen, this gives for the twin boundary energy $3.8 \pm 1.4 \text{ ergs cm}^{-2}$

The pairs of crystals were oriented from twin traces. All the orientations were within about 15° of the (110)



(a) NITROGEN



(b) AIR

FIG.24, TWIN BOUNDARY GROOVES IN NITROGEN AND IN AIR; ORIENTATIONS OF $\frac{1}{\gamma} \frac{\partial \gamma}{\partial \theta}$ VALUES

pole (Fig. 24). Normally it is not possible to distinguish by the twin trace method between a surface orientation and its mirror image so that it would not be possible to find the direction of $\frac{\partial \gamma}{\partial \theta}$. However, a particular twin boundary used for one orientation showed a slight curvature at the intersection with a grain boundary groove. From this it was possible to find the direction of tilt of this twin boundary and hence the direction of the torque terms (decrease of γ). Arrows on the stereographic projections indicate the direction of decreasing γ and the relative magnitudes of $\frac{1}{\gamma} \frac{\partial \gamma}{\partial \theta}$, taking for this quantity half the value given in the last column of the tables.

There is evidence of the cusp in the γ plot toward the (111) pole. The mean resolved value for $\frac{1}{\gamma} \frac{\partial \gamma}{\partial \theta}$ in the direction of the (111) pole is $0.0060 \pm .0005$ at about 28° from the pole. This very low value is comparable with the measurements of Robertson and Shemon (22) for copper in hydrogen.

5.2 Twin boundaries in air.

Before the possibility of inverted twin boundaries had been fully appreciated King (53) observed these boundaries on air-etched silver specimens. He found

that striations showed slight curvatures at twin boundaries and at a pair of twin boundaries the curvatures were in opposite directions - indicating that one twin boundary was projecting above the general surface. This feature of the etch pattern was frequently observed but it is difficult to estimate the groove angles directly from the striations.

For measurement of the groove angles in air interferograms were made of specimens which had been heated for only about 6 hours (with evaporation inhibited). By that time the striations had not developed well enough to obscure the twin boundary profiles (Fig. 24b). Some six pairs of twins were oriented. The groove angles are given in Table 10 and the orientations and directions of decreasing γ are plotted in the stereogram of Fig. 24b. It was possible to find the correct sense of the orientations from directions of tilt of small areas of low index facet.

The orientation derivatives are from 4 to 10 times larger in air than in nitrogen and $\frac{1}{\gamma} \frac{\partial \gamma}{\partial \theta}$ is as high as 0.03 at about 35° from the (111) pole. No reliable estimate of the twin boundary energy could be made from grooving in air since the $\frac{\partial \gamma}{\partial \theta}$ terms have more effect than γ_r on the groove angles.

Table 10. Twin boundaries in air

Twin pair	A + B	A' + B'	γ_T/γ_S	$\frac{1}{\gamma_S} \left(\frac{\partial \gamma_Q}{\partial A} + \frac{\partial \gamma_R}{\partial B} \right)$
1	176° ± 20'	183°57' ± 20'	.0005 ±.0060	.0693 ±.0060
2	176°25' ± 22'	183°16' ± 22'	.0026 ±.0066	.0596 ±.0066
3	177° ± 20'	182°41' ± 10'	.0029 ±.0060	.0495 ±.0060
4	174° ± 35'	186°15' ± 40'	-.0024 ±.0109	.1070 ±.0109
5	175°30' ± 27'	185°34' ± 33'	-.0092 ±.0087	.0878 ±.0087
6	170°34' ± 58'	188°40' ± 52'	.0066 ±.0160	.1578 ±.0160

5.3 Conclusions

The limited number of twin boundary measurements confirm the evidence from faceting for cusps in the γ plot. Although suitable crystals were not oriented similar values for $\frac{1}{\gamma} \frac{\partial \gamma}{\partial \theta}$ are expected in the direction of the (100) pole. If a large number of crystals were studied

it would be possible to map out the complete γ plot but for accurate measurements on silver in nitrogen it would be necessary to use very long annealing times - of the order 1 year - to obtain boundaries comparable in width with those found in air after a few hours.

Reference has already been made to the effect of the value of $\frac{\partial \gamma_0}{\partial \theta}$ on facet contact angles. Some other consequences of $\frac{\partial \gamma}{\partial \theta}$ terms are worth mentioning. Fig. 25 shows an interferogram of two twinned crystals which have faceted in air. It is seen that the complex surface in contact with the low index facets is continuous across the twin boundary with no evidence of a groove. In this case however the components of $\frac{\partial \gamma}{\partial \theta}$ act in directions almost normal to the maximum variation of γ , assumed to be toward the low index pole. The $\frac{\partial \gamma}{\partial \theta}$ terms are therefore very small and the twin boundary energy alone is insufficient to produce a detectable groove. A rather different situation is illustrated in Fig. 26. Here a boundary has produced a groove in strips of complex surface but not in low index facets. The boundary is evidently a low angle grain boundary for facets could not be continuous across a twin boundary. The groove angle gives a boundary energy equal to $0.24 \gamma_s$ and the energy condition

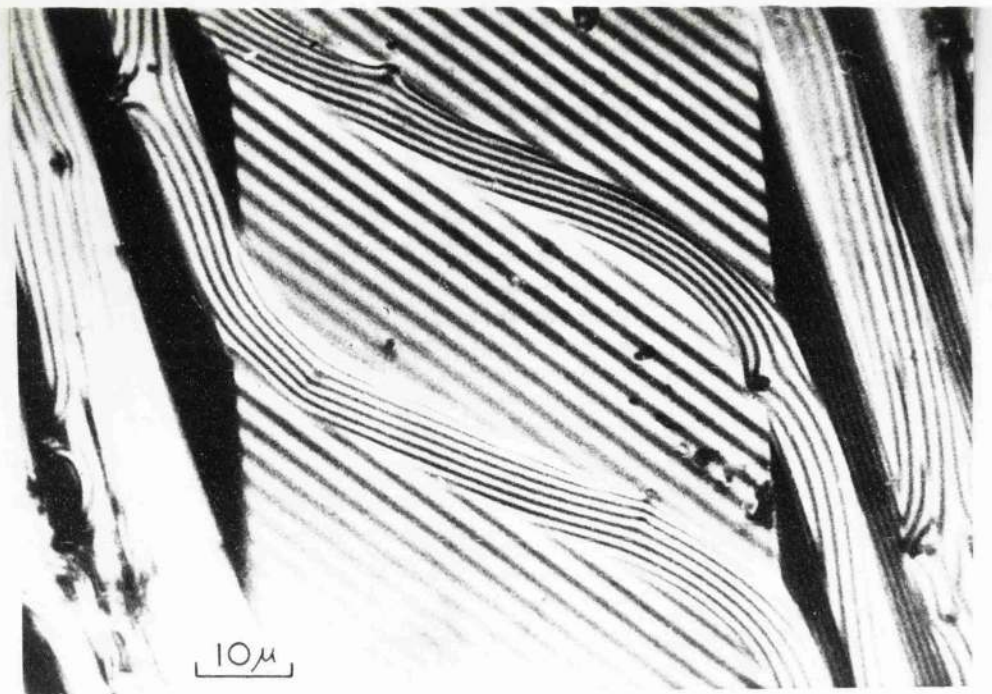


FIG.25. ABSENCE OF TWIN BOUNDARY GROOVES ON COMPLEX SURFACES.

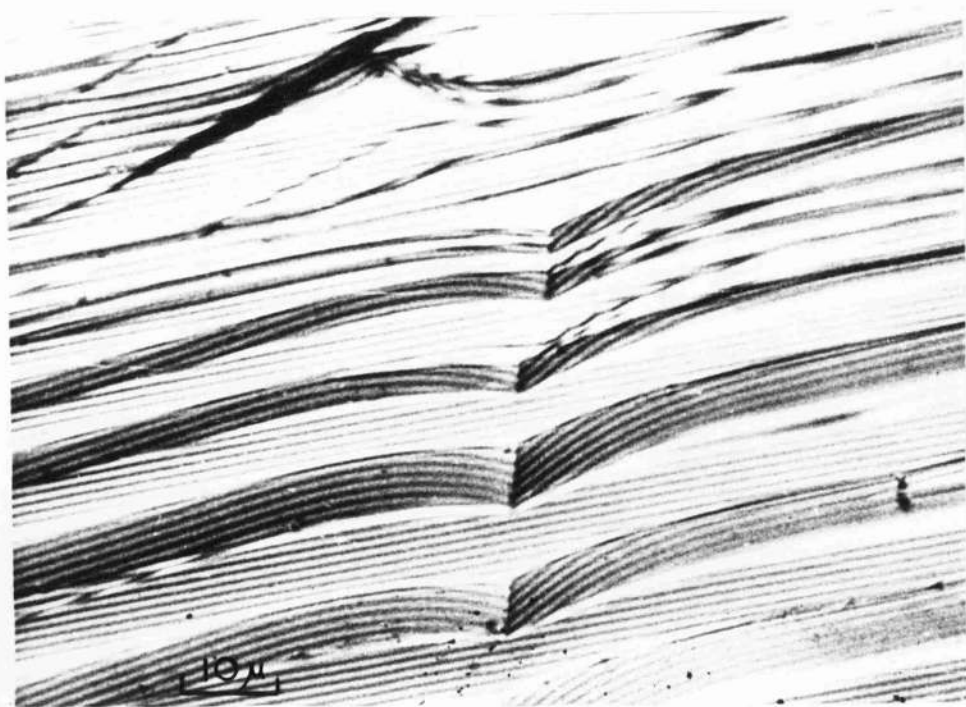


FIG.26. LOW ANGLE GRAIN BOUNDARY AND CONTINUOUS FACETS.

for no groove to form in the low index facet is $\frac{\partial \gamma_0}{\partial \theta} > \frac{\gamma_B}{2}$
i.e. $\frac{\partial \gamma_0}{\partial \theta} > 0.12 \gamma_s$. This condition is clearly satisfied
since equation (1.10) and the observed contact angles
give the inequality $\frac{\partial \gamma_0}{\partial \theta} > 0.5 \gamma_s$.

CHAPTER 6

GRAIN BOUNDARY GROOVES AND SURFACE SELF-DIFFUSION ON SILVER

A number of investigations were made on the kinetics of mass transport on silver surfaces. In the first of these transport on unstriated regions was studied from measurements on the growth of grain boundary grooves and the rate of decay of scratches.

6.1 Rate of grain boundary grooving

Specimens were mounted inside silver boxes and annealed at 900°C for periods up to 4 days. Interferograms of selected grain boundary grooves were made at regular intervals. It was difficult to follow the rate of growth of individual grooves on account of grain boundary migration during the early stages and also because of the development of facets. Faceting was particularly troublesome in these experiments. It was necessary to choose boundaries between relatively unstriated grains where the profiles were unobscured by facets; grooves with facets would be expected to develop in an anomalous way because of different diffusion rates across low index surfaces and they were avoided on this account too.

This criterion for the choice of grooves set a limit on the orientations of the crystals examined. For faceting not to occur the orientations of both grains have to be within the region equivalent to BZD in Fig. 14.

After annealing for 30 minutes humps were distinctly visible (cf. Fig. 5) and the groove widths - hump to hump - were about 7 microns. After 4 days the groove widths were as much as 30 microns (Fig. 29) but because of faceting very few suitable boundaries could be found. The average width (s) as a function of time (t) is plotted on a logarithmic scale in Fig. 27. Each point represents an average of about 20 boundaries. A 'least squares' straight line through the points has a slope $0.265 \pm .008$ which indicates that surface self-diffusion is the dominant transport mechanism up to at least 30 microns. There is the possibility of a small contribution from volume diffusion or evaporation and condensation. A graph of s^4 against t gives a straight line from which the diffusion constant (equation 1.13) $B = D_s \gamma \Omega^2 \nu / kT = 3.99 \pm 0.36 \times 10^{-19} \text{ cm}^4 \text{ sec}^{-1}$. Putting $\gamma = 360 \text{ ergs cm}^{-2}$, $\Omega = 17.05 \times 10^{-24} \text{ cm}^3$ and $\nu = 1.3 \times 10^{15} \text{ cm}^{-2}$, the value for the surface self-diffusion coefficient D_s is $4.75 \times 10^{-4} \text{ cm}^2 \text{ sec}^{-1}$.

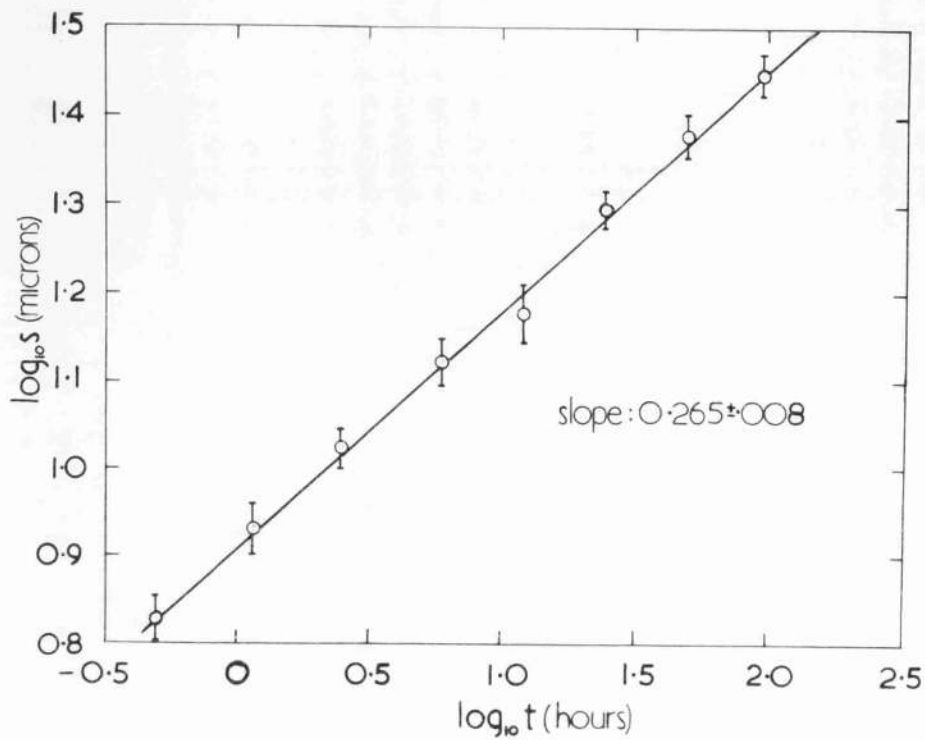


FIG. 27. GRAIN BOUNDARY GROOVE WIDTH (s) AS A FUNCTION OF TIME (t). SILVER IN AIR AT 900°C.

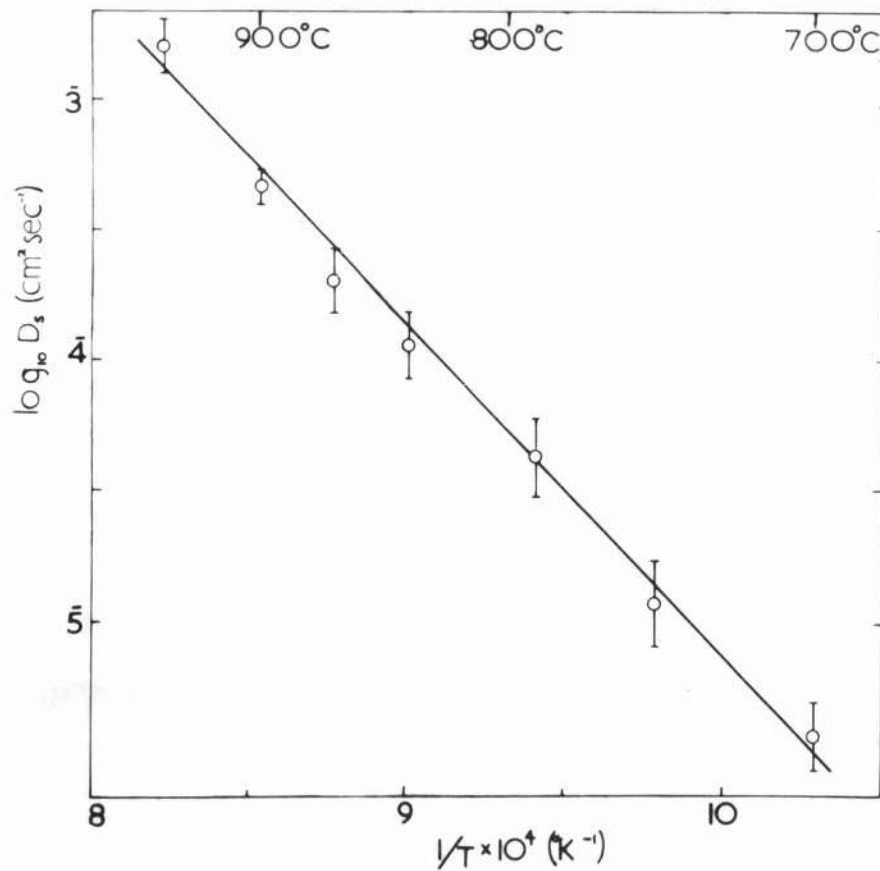


FIG. 28. TEMPERATURE DEPENDENCE OF SURFACE SELF-DIFFUSION ON SILVER IN AIR.

If surface diffusion is dominant at 900°C then the same mechanism will also be dominant at lower temperatures. Therefore for measurements of diffusion rates at lower temperatures grain boundary groove widths were measured after only one period of annealing, 25 hours. This was considered the optimum time to use; for longer periods the increased accuracy from the measurement of larger groove widths is not very significant and extensive faceting at lower temperatures limits the number of suitable grain boundaries available. Table 11 and Fig. 28 give the results for measurements of B and D_s for the range 945°C to 700°C . In calculating values for D_s allowance has been made for the variation of surface energy with temperature by assuming a linear dependence with a temperature coefficient equal to that given for silver in oxygen at 1 atmosphere (Allen (28)).

Table 11. Surface self-diffusion data for silver in air

Temperature $^{\circ}\text{C}$	$B \text{ cm}^4 \text{ sec}^{-1} \times 10^{19}$	$D_s \text{ cm}^2 \text{ sec}^{-1} \times 10^4$
945	9.86	16.3
900	3.99	4.75
870	2.12	2.10
840	1.36	1.15
790	0.662	0.441
750	0.200	0.115
700	0.072	0.034

The results may be represented by an Arrhenius equation $D_s = D_0 \exp(-Q_s/kT)$ where $D_0 \approx 10^6 \text{ cm}^2 \text{ sec}^{-1}$ and $Q_s = 2.48 \pm 0.12 \text{ ev}$. The very high values of both D_0 and Q_s are not typical of a self-diffusion process on a pure surface for which D_0 is expected to be about 10^{-2} to $10^{-3} \text{ cm}^2 \text{ sec}^{-1}$ and the activation energy of the order 1 ev. At lower temperatures (650°C to 250°C) Drew and Pye (54) have measured surface diffusion on silver by a radioactive tracer technique and have found $D_0 = 1.5 \times 10^{-5} \text{ cm}^2 \text{ sec}^{-1}$ and $Q_s = 0.35 \text{ ev}$; the experiments were in an atmosphere of pure hydrogen. The much higher activation energy for silver in air may be attributed to a transport process involving both the migration of silver and the desorption of oxygen atoms. Similar high values for D_0 and Q_s have been reported for copper in hydrogen (Choi and Shewmon (55)) and for iron in vacuum (Blakely (37)).

For comparison with the relatively fast diffusion in air an estimate of surface diffusion in nitrogen (plus 0.1% hydrogen) can be made from grain boundary groove widths after 10 days at 900°C . The observed mean width for 20 boundaries, $25.9 \pm 2.3 \text{ microns}$, gives $B = 1.17 \pm 0.44 \text{ cm}^4 \text{ sec}^{-1}$ and $D_s = 4.4 \pm 1.9 \times 10^{-5} \text{ cm}^2 \text{ sec}^{-1}$ - an order

of magnitude lower than the diffusion coefficient in air at the same temperature.

6.2 Grain boundary groove profiles

The grain boundary groove profiles had the humped shape characteristic of development by surface diffusion (Fig. 29) Mullins (35) showed that for a symmetrical groove the ratio of width s , to depth d , satisfies the relationship: $s/d = 4.73/m$ where $m (= \tan^{-1}\theta)$ is the slope of the surface at the root of the groove (Fig. 4a). From measurements on 12 grooves etched in air at 900°C and showing little asymmetry the mean value for s/d is 42.8 ± 3.6 while that for $4.73/m$ is 43.4 ± 6.8 . Taking as a mean value $m = 0.110 \pm 0.01$ and $\theta = 6.3 \pm 0.6^{\circ}$ one finds for the ratio grain boundary to surface energy $\gamma_B/\gamma_s = 0.22 \pm 0.02$ and putting $\gamma_s = 360 \text{ ergs cm}^{-2}$, $\gamma_B = 80 \pm 8 \text{ ergs cm}^{-2}$. It is interesting to compare this result with King's (30): $\theta = 8^{\circ}26'$ for silver in nitrogen which gives $\gamma_B = 320 \text{ ergs cm}^{-2}$ (assuming, as before, that the surface energy in nitrogen is the same as that measured in helium). For grooves etched in the nitrogen and hydrogen mixture θ was found to be $5.1^{\circ} \pm 1.0^{\circ}$ which is still rather high and gives a grain boundary

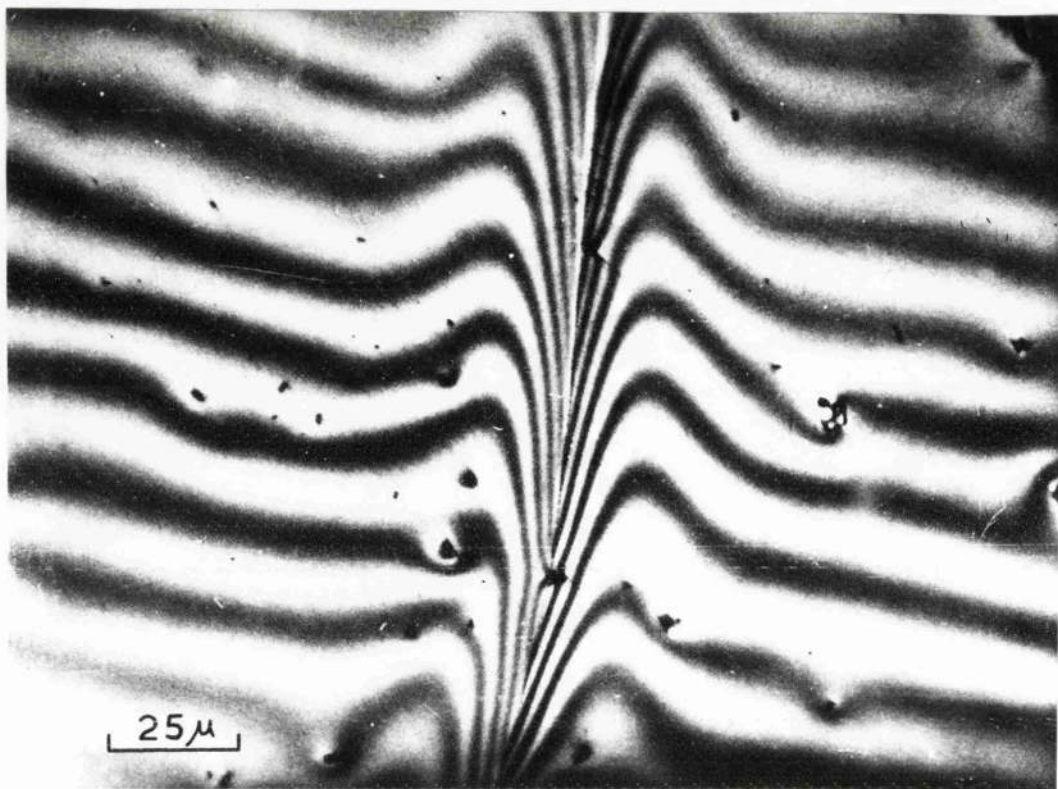


FIG. 29. A GRAIN BOUNDARY GROOVE AFTER 4 DAYS IN AIR.

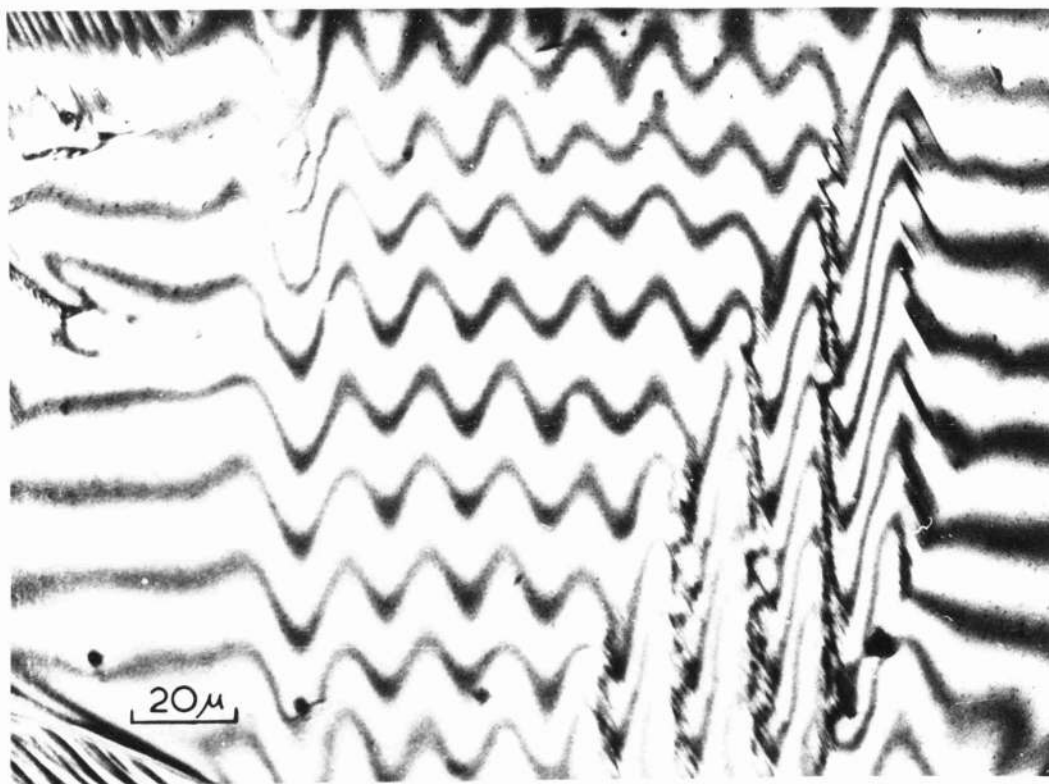


FIG. 30. MULTIPLE SCRATCHES AFTER 5 HOURS IN AIR.

energy 200 ± 40 ergs cm^{-2} . It is possible that solution of oxygen into the bulk material lowers the grain boundary energy.

6.3 Scratch smoothing experiments.

An approximate value for the diffusivity in air at 900°C , obtained from scratch smoothing experiments, confirmed the result from grain boundary grooving. Sets of scratches about 1 micron deep and with 15 micron spacings were ruled with a diamond mounted on a ruling engine. Interferograms (e.g. Fig. 30) were made of scratch profiles over periods of a few hours and an analysis making use of equation (1.14) yielded a mean value $B = 3.8 \pm 0.7 \times 10^{-19} \text{ cm}^4 \text{ sec}^{-1}$. Since a detailed investigation using this technique was not carried out the measurements from grain boundaries are considered more reliable. The observed continuity of scratches from crystal to crystal suggests that there is little variation of diffusion coefficient with crystallographic orientation - in contrast with results for nickel and platinum (Blakely (37)) which exhibit variations of one or two orders of magnitude.

Fig. 30 shows scratch profiles after 5 hours; the

onset of faceting seriously distorts the normal sinusoidal shape and limits the useful duration of scratch smoothing experiments. It will be shown in the next chapter that diffusion across the low index facets is considerably faster than on atomically rough high index surfaces.

CHAPTER 7

THE KINETICS OF FACET FORMATION

During the course of the work on the variation of contact angle with oxygen pressure Mullins (40) published his theoretical account of the growth of linear facets. The theory gives a number of interesting predictions which suggested that a systematic study of the kinetics would be worthwhile. Some observations on the effect of evaporation on the nucleation and growth of facets have already been reported. In this chapter experimental investigations of facet growth for conditions of negligible net evaporation will be described.

7.1 Comparison with growth by evaporation and condensation.

Facets on specimens heated in a silver enclosure were found to have grown higher than the original general surface by as much as a micron - considerably higher than the possible change in depth due to net evaporation (Table 3, p.41). This evidence alone is sufficient to support the conclusion that the spontaneous development of low index facets on silver is not primarily due to net evaporation although undoubtedly where there is net evaporation it does contribute to both the nucleation and

development of facets.

For some initial experiments on 'evaporation-inhibited' specimens heating periods up to 5 days were used*. On a few crystals there were a number of isolated facets with widths up to 10 microns and separated from adjacent facets by as much as 80 microns. These isolated facets seemed very suitable for comparison with Mullins' theory but the shape of the continuation surfaces showed very indistinct humps; the profiles were similar to those predicted for evaporation-condensation (Fig. 5). Although the measurements on grain boundary grooving showed fairly conclusively that surface self-diffusion is the dominant mechanism for mass transport up to about 30 microns, it was felt necessary in view of the claims of Hondros and Moore (46)(56) to examine the possibility of facet growth by evaporation-condensation.

It is observed from interferograms that the facet profiles are symmetrical about the centre of the facet. The facets are produced by removal of a certain volume of material from below the original surface on one side of

* The temperature for all the experiments on kinetics of facet growth was 900°C.

the facet and the deposition of the same quantity above the surface on the other side. From fringe profiles measurements were made of the volumes of material transferred in building up the facets. The theory predicts that the cross-sectional area A of material transported by evaporation-condensation in time t is given by

$$A(t) = -mat \quad (7.1)$$

where $A = p_0 \Omega^2 \gamma_s / (2\pi M)^{1/2} (kT)^{3/2}$ as defined in Chapter 1 and where $m (= \tan\beta)$ is the slope of the complex surface at the point of contact with the facet. For twelve separate crystals, giving a range of m from 0.1 to 0.25, a mean value $A = (7.7 \pm 1.1) \times 10^{-13} \text{ cm}^2 \text{ sec}^{-1}$ was calculated from the above equation. This value is a lower limit because t , taken as the total time of anneal, is an overestimate; it is supposed that the observed facets did not begin to develop until some time had elapsed for grain growth. The value for A is however extremely high; from vapour pressure data given by Dushman (57) and 360 ergs cm^{-2} for the surface energy, the calculated value for A is $4.3 \times 10^{-14} \text{ cm}^2 \text{ sec}^{-1}$. Effectively A would be even less than this as the silver vapour has to diffuse through air with a mean free path

of 0.4μ which thus reduces the effective vapour pressure. It is not possible therefore to account for the observed facet widths by a mechanism of vapour transfer.

7.2 Investigations on the rate of growth of facets.

The most direct method of investigating the contribution of various mechanisms to facet growth would be to determine the rate of growth as a function of time. Facet widths should increase as $t^{\frac{1}{2}}$ by evaporation-condensation, $t^{\frac{1}{3}}$ by volume diffusion and $t^{\frac{1}{4}}$ by surface diffusion. For various reasons it was not possible to make such a systematic study.

Grain boundary migration prevented any measurement of striations during the early stages of etching. Striations photographed after 30 minutes disappeared after 1 hour - the particular grain having been replaced by another with a different orientation. A stable grain size, about 200 microns diameter, was not reached until after 6-8 hours. After that some grains had reasonably well isolated striations with widths of the order 1 micron. However on returning the specimens to the furnace after photography, the facets showed very erratic development; extra facets were quickly nucleated close to the facet

under observation and facets were frequently found to diminish in width and even to disappear completely.

Nucleation of facets occurs very readily. The proportion of crystals with well isolated striations was quite small (less than 5%) and decreased with time. After longer heating periods, about 16 hours, facets were observed with widths up to 4 microns (Fig. 31). Distinct humps appeared on the complex surface with profiles similar to those predicted by Mullins for surface diffusion. But at the same time additional nucleation of facets produced faint striations - just visible in Fig. 31 - parallel to the main facet axis. From the displacement of the fringes the faint facets have depths of about 0.1 micron while the main facet has a depth of 1 micron. Assuming that surface diffusion is the dominant mechanism and applying Herring's scaling laws these figures suggest that the faint striations were formed within a period 10^{-4} of the time to form the main facet, that is within about 1 second. The faint striations must have appeared as the specimen was cooled down to room temperature.

The subsequent development of a large facet on returning a specimen to the furnace is shown in Fig. 32. After a further hour the facet had become slightly

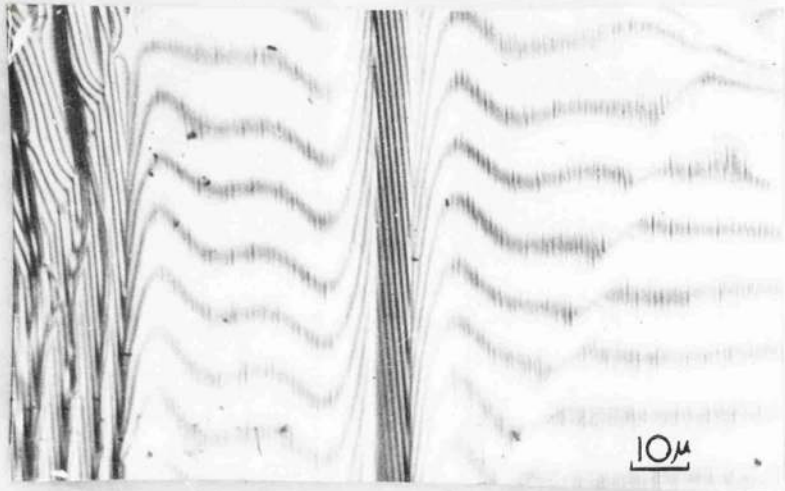


FIG.31. AN ISOLATED $\{111\}$ FACET AFTER 16 HOURS. FAINT STRIATIONS HAVE DEVELOPED DURING COOLING.

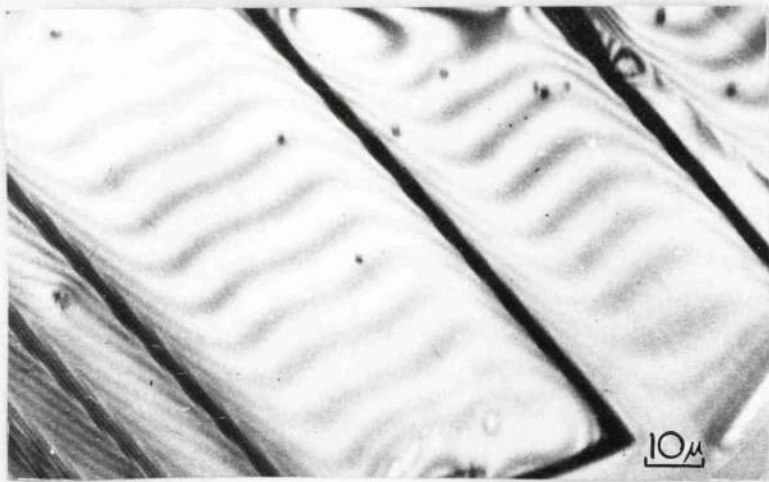
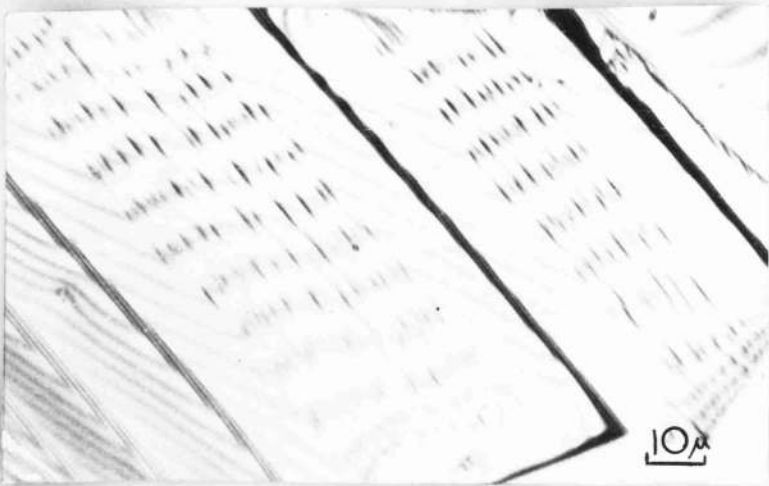


FIG.32. DISCONTINUOUS DEVELOPMENT OF A FACET WITH NUCLEATION OF ADDITIONAL FACETS.

(a) AFTER 20 HOURS.



(b) AFTER 21 HOURS.

narrower. Extra facets were nucleated up to a few microns from the main facet and the bordering complex surfaces had smoothed off to become flat. (Additional faceting cannot occur on the complex surface close to the main facet because there the complex surface is at the limiting orientation for faceting). Additional nucleation of striations occurred near each facet studied, the faint striations developing either on cooling or after a further short period of heating. The effect appeared to be independent of the rate of cooling or reheating and made impossible all attempts to measure the rate of growth of facets. Other experiments show that the nucleation rate increases as the temperature decreases which suggests that the additional facets grow while the specimen is at lower temperatures and that they are due to a sudden increase in the density of adsorbed oxygen.

The spacing between adjacent facets ultimately determines the maximum size. When the crystal surfaces are densely striated the complex surfaces become quite flat. After this stage has been reached no more facets can be nucleated and since there are no gradients of surface curvature no further mass transport can occur. The 'saw-tooth' surface profile will then be metastable

and changes can only occur by net evaporation.

7.3 Measurements on single facets.

Mullins shows that for surface diffusion the half width of a facet X^* is given by:

$$X^* = \omega (Bt)^{\frac{1}{2}} \quad (7.2)$$

where ω is a function of m/n - the ratio of the slope of the complex surface to the slope of the facet. ω also depends on a parameter equal to the ratio of the surface diffusion coefficient for the (simple) low index facet to that for the complex surface, $d = D_s/D_c$. Mullins considers two extreme possibilities:

(1) No diffusion across the facet ($d = 0$). This might possibly be the case if for example the adsorbed oxygen on the low index plane prevented diffusion.

(2) Very fast diffusion across the facet ($d = \infty$). This would be possible if atoms could migrate across the facet in one jump.

The function $\omega(m/n)$ is plotted for the two limiting cases in Fig. 33. There is only a factor of 3 between the facet widths for the two cases and the growth rate is mainly determined by the diffusion coefficient for the

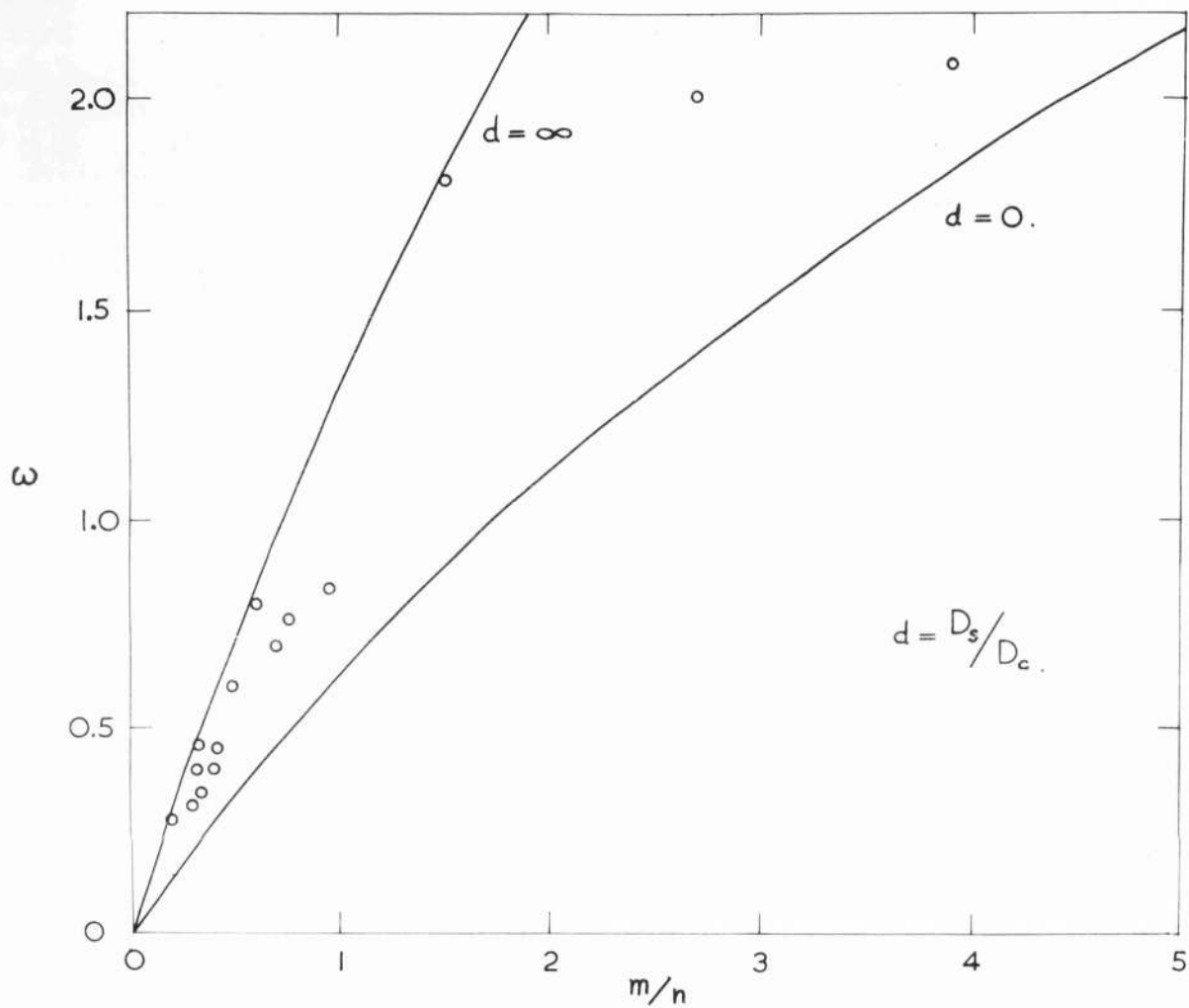


FIG.33. PLOT OF $\omega - \chi^*/(bt)^{1/2}$ FOR THE TWO LIMITING CASES OF SURFACE DIFFUSION. EXPERIMENTAL POINTS REPRESENT LOWER LIMITS FOR ω .

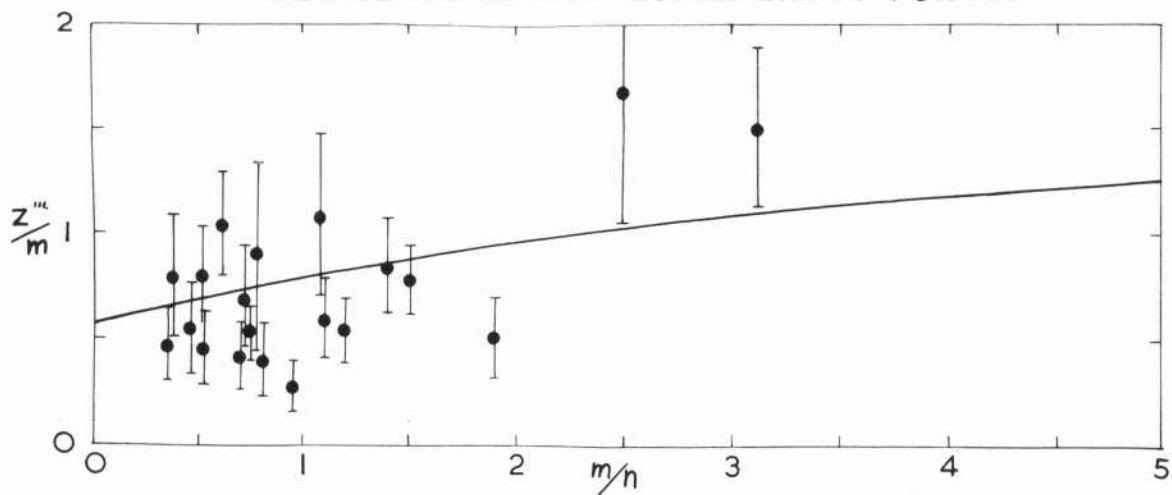


FIG.36. PLOT OF $-Z'''/m = -A/2m(bt)^{1/2}$ FOR $d = \infty$. EXPERIMENTAL POINTS FOR ISOLATED FACETS.

complex surface via the constant B in equation (7.2). Facet widths should be greatest for high values of m/n , that is for low inclinations of the facet to the general surface. This was indeed observed; the only large facets during the early stages of etching were inclined at low angles and this would explain why low index facets nearly parallel to the surface can completely cover a grain (Fig. 13).

Although it was not possible to follow the history of an isolated facet throughout its development some conclusions about the kinetic processes can be made from measurements on facets after one period of annealing. 16 hours was found convenient; after longer times there were very few isolated facets. From about 40 thousand grains on several dozen specimens only about 30 measurable isolated facets were observed. Interferograms were made from which the facet profiles were traced and values of m/n calculated to within 5 to 10%. From the measured facet widths values of ω were calculated from equation (7.2) using the value of B found from grain boundary grooving and taking for t the total time of annealing. The results, ω plotted as a function of m/n , are shown in Fig. 33. Errors in ω are between 5 and 10% and the

calculated values represent lower limits since the total time of facet growth will be somewhat less than the total annealing time. The uncertainty in time explains the scatter of the results. Points are plotted for both $\{111\}$ and $\{100\}$ facets; no significant difference could be found. The fact that all the experimental points lie below the $d = \infty$ curve for a wide range of facet widths supports the conclusion that surface self-diffusion is the transport mechanism. Within experimental error values of ω are as high as those predicted for $d = \infty$.

It is of interest to note that quite frequently the facet growth was observed to have been impeded by point imperfections, possibly dislocations. In such cases the junction between the complex and low index surfaces was not a straight edge but showed localised kinks about a micron wide - particularly noticeable on facets at a low angle to the surface.

Apart from evidence from facet widths, the $d = 0$ case may be ruled out on account of the facet profiles. Fig. 34 shows Mullins' theoretical results for the two limiting cases $d = 0$ and $d = \infty$. Because of symmetry only one half of the profiles are plotted. These standardized profiles, drawn for unit facet slope and a

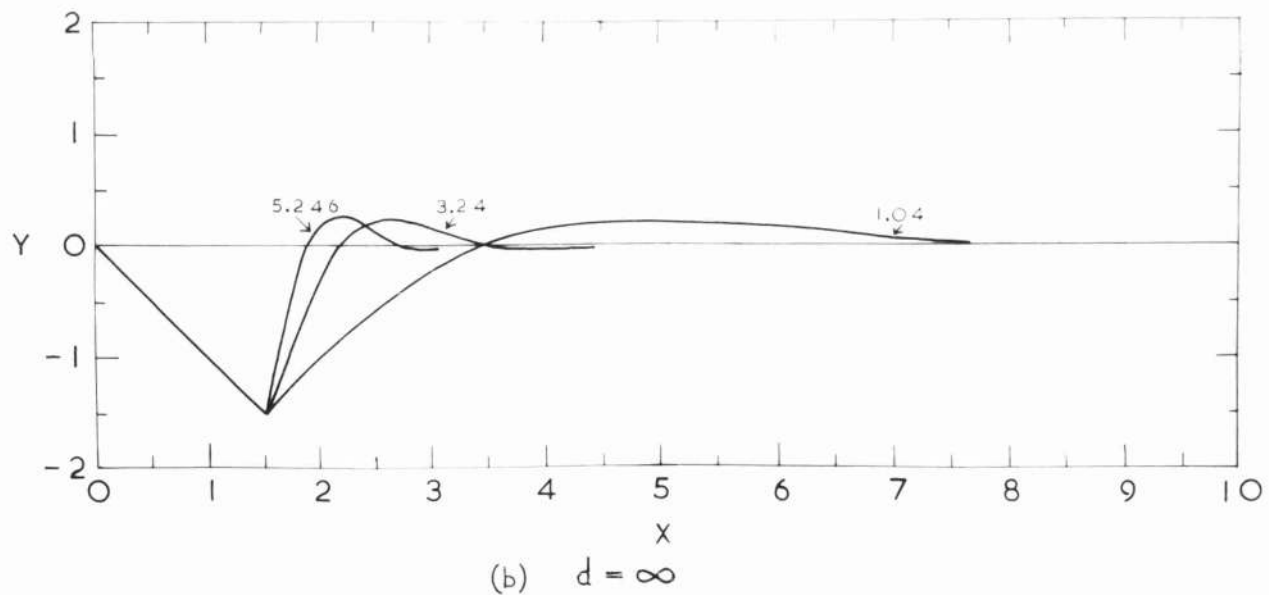
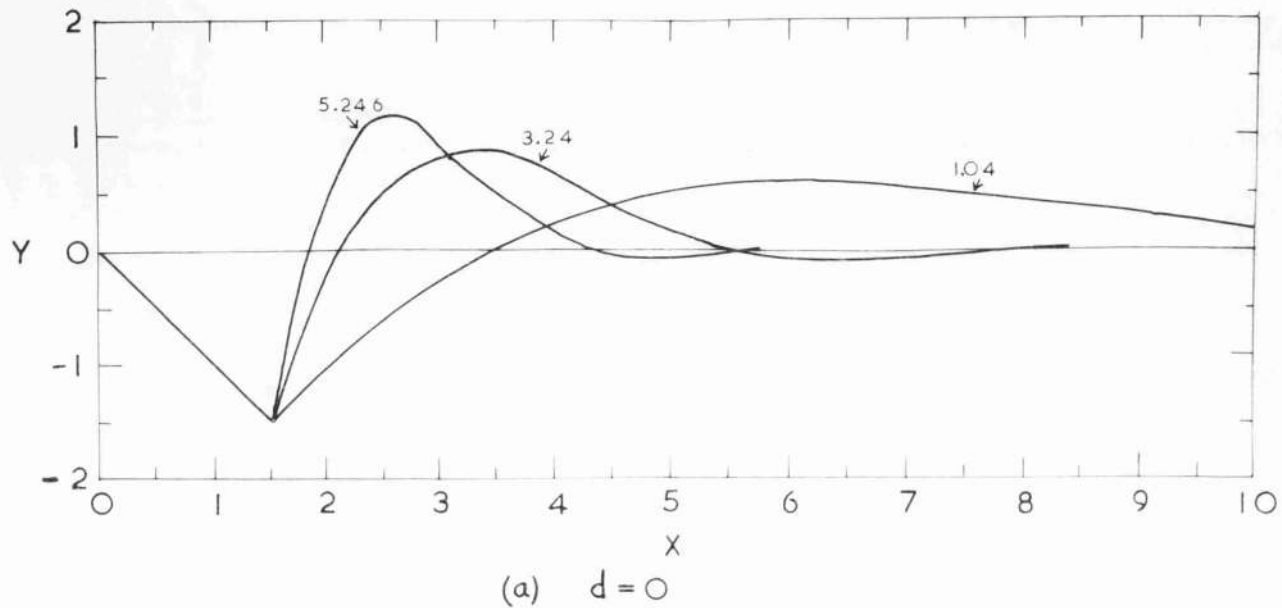


FIG.34. THEORETICAL STANDARDIZED FACET PROFILES FOR THE TWO LIMITING CASES; ATTACHED NUMBERS GIVE VALUES OF $\frac{M}{N}$.

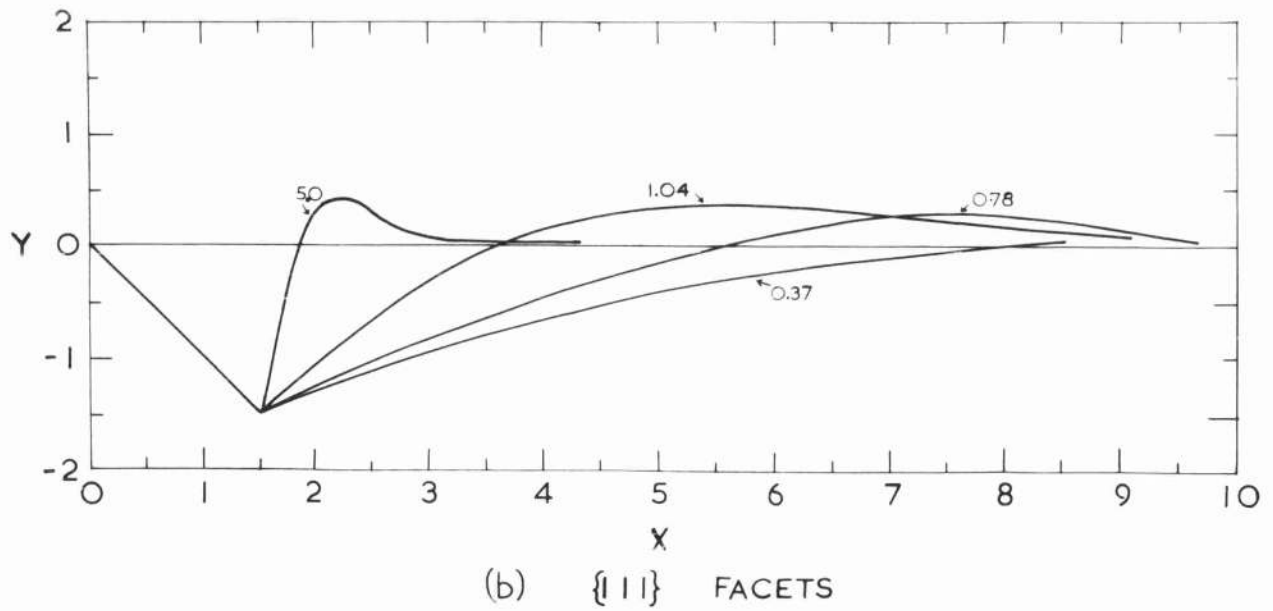
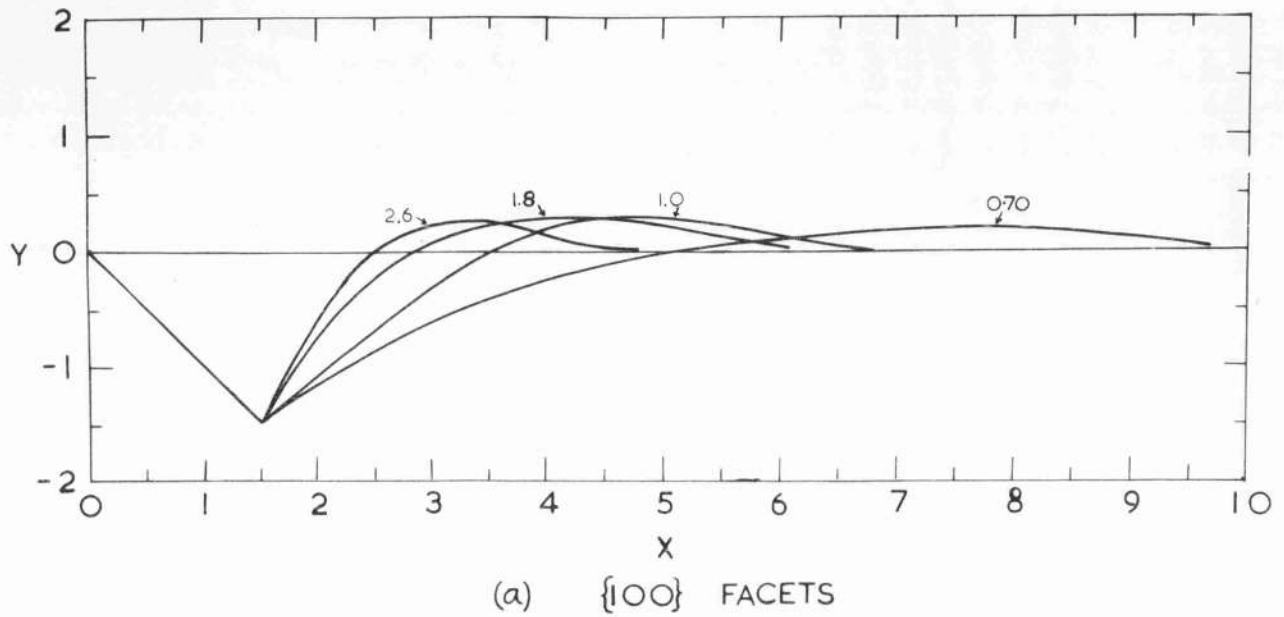


FIG.35. STANDARDIZED FACET PROFILES FROM MEASUREMENTS OF INTERFEROGRAMS; ATTACHED NUMBERS GIVE VALUES OF M/N .

total width of 3 units, should be time independent. The shape of the complex surface depends on m/n and d . If no diffusion occurs across the facet then the total area between the profile and the original surface must be zero and as a result a hump on the complex surface up to one unit high would occur. If on the other hand there is fast diffusion across the facet, the area under the curve, representing the quantity of material transported across the facet, is negative and the humps are much less pronounced. Some twenty facet profiles were traced and redrawn on the standardized scale. They all showed small humps (mean height $0.25 \pm .05$ units) and the areas under the profiles were negative (a greater area below the original surface than above). Some experimentally determined standardized profiles are shown in Fig. 35 for various values of m/n . Little significant difference could be detected between the experimental profiles and those predicted for $d = \infty$. The area above the general surface may be slightly higher for the experimental curves. Again no difference was found between $\{111\}$ and $\{100\}$ facets.

The humps on the complex surfaces are less pronounced and farther away from the facet for low values of m/n - this suggests an explanation for the profiles observed

in the earlier experiments which had very indistinct humps and suggested the possibility of evaporation-condensation. All those facets had very low values of m/n , that is the facets were inclined at high angles to the original surface. The development of such facets results in a relatively small lowering of total surface free energy. They would therefore begin to develop at a late stage in the etching and after 5 days would be the only isolated facets remaining when grains near low index orientations had become densely striated.

Measurements of the areas under the facet profiles gave an additional check of the transport mechanism. For the case of infinitely fast diffusion across the facet the area A increases according to a $t^{\frac{1}{2}}$ law:

$$A = 2mZ'''(Bt^{\frac{1}{2}}) \quad (7.3)$$

where Z''' is a slowly varying function of m/n with values between 0.6 and 1.3 for the range of m/n from 0 to 5. This function is plotted as the full curve in Fig. 36. In attempting an experimental check of equation (7.3) the same difficulty occurs as for the measurement of facet widths: the duration of growth of a facet is unknown. However a check can be made by calculating

the time from the facet width assuming the theoretical values of ω for $d = \infty$. Combination of equations (7.3) and (7.2) yields:

$$Z''' = A / 2m \left(\frac{x^*}{\omega} \right)^2 \quad (7.4)$$

From measurements of facet areas and widths and calculations of ω from the slopes of the surfaces the values of Z''' plotted in Fig. 36 were obtained. On account of the small size of the facets (cross-sectional areas about 1 micron², facet widths a few microns) the experimental accuracy is quite low. There are inevitably uncertainties in drawing the profiles since the individual fringes are up to 3 mm wide on the prints. The calculated values of Z''' , with errors up to 40%, are however in accord with the theoretical predictions: there is a somewhat better than order of magnitude agreement. All the evidence points toward very fast diffusion across the low index surfaces.

7.4 Nucleation of facets.

The presence of isolated facets shows that there must be a 'nucleation barrier' for faceting. Nucleation evidently depends on a number of factors. From the

relative reductions in total surface energy for different values of α (Fig. 4e) it is to be expected that facets inclined at low angles to the general surface will be nucleated more readily. Facets at high inclinations did occur only at later stages.

It has been mentioned that with free evaporation from the surface facets started to grow from small humps - dots - presumably dislocation sites (Fig. 17). For negligible net evaporation facets usually appeared at random on the flat crystal surfaces but often facets started where the surfaces were slightly curved - at grain boundaries and on small humps.

It is interesting to note that on any particular grain the facets were usually all the same size indicating that they all started at the same time. Frequently pairs of facets were found indicating that one facet had been nucleated on the curved complex surface produced during the development of the other facet. Facets on adjacent crystals were often contiguous at grain boundaries and twin boundaries.

The early stages of facet growth were studied by hot stage microscopy. A simple assembly was made for mounting a specimen in the form of a thin strip under the

microscope and for passing through it an alternating current of about 10A. At temperatures near 800°C very rapid smoothing off of surface roughness was observed. Both grain boundaries and striations could be seen after only about 20 seconds. Striations appeared in dense patches, often near grain boundaries. The rate of development along the facet axis was so rapid that lengths of striations up to 40 microns seemed to appear simultaneously.

CHAPTER 8.

GENERAL DISCUSSION

8.1 Low index facets.

Few previous experimental studies have been made on the properties of exact low index surfaces. Gomer (58), using field emission microscopy, observed fast migration on atomically smooth surfaces of nickel. Blakely (37) also found evidence for fast migration from the development of large flats on grain boundary grooves on platinum and nickel.

It is probable that the facets developed during thermal etching are atomically smooth over distances of at least several microns although additional experimental confirmation is needed on this point. Burton, Cabrera and Frank (59) and Mullins (60) have discussed the roughening of atomically smooth low index planes and have shown that for most metals no large scale disordering (surface melting) of low index planes will occur even near the melting point.

It would seem that many surface properties, varying with crystallographic orientation, may have quite marked singularities at low index orientations.

Evidence from the thermal etching of silver shows that

the low index surfaces have appreciably lower surface energies, extremely low evaporation rates and provide effective short circuit paths for surface diffusion. These special features of exact low index surfaces are not generally appreciated and the literature contains reports of measurements on 'low index' surfaces which were in fact several degrees away from the low index orientation.

8.2 Adsorption and the γ plot.

Information on the γ plot would be useful in setting up detailed atomistic models of solid surfaces. However it is unlikely that the intrinsic γ plot, that is the γ plot of a pure surface without an adsorbed layer, could ever be measured directly and it is of some interest to have data on the effect of adsorption.

While this thesis was 'in the press' Gjostein (61) completed two theoretical papers on adsorption and surface energy dealing in particular with the effect of adsorption on the γ plot and on thermal etching. He has developed theories based on a model of adsorption of gaseous atoms at three different types of adsorption site - surface, single ledge and double ledge sites - each characterized by different adsorption energies. It appears from

Gjostein's analysis that adsorption energies can be determined by measuring the critical pressure for faceting as a function of temperature. Experimental work following the lines suggested by Gjostein might yield interesting results on surface models for adsorption.

Some care is necessary in extrapolating measurements of $\frac{\partial \gamma}{\partial \theta}$ terms to low index orientations. Robertson and Shewmon (22) drew a straight line through values of $\frac{1}{\gamma} \frac{\partial \gamma}{\partial \theta}$ for copper in an $H_2:H_2O$ atmosphere and estimated that $\frac{1}{\gamma} \frac{\partial \gamma}{\partial \theta}$ is about 0.10 at the (111) pole. However in the same atmosphere they observed faceting and it is not possible to fit to their data a finite contact angle satisfying equation (1.9). Their suggestion that stability of facets depends on $\frac{\partial^2 \gamma}{\partial \theta^2}$ and not on $\frac{\partial \gamma}{\partial \theta}$ does not appear well founded and it is more likely that faceting is the result of a deeper cusp in the γ plot than their extrapolation indicates.

8.3 Diffusion on surfaces with adsorbed layers.

Most measurements of surface diffusivity of metals have been for surfaces in inert atmospheres or in vacuum and it is usually supposed that the measurements give

information about the pure solid surface - the effect of atmosphere is often ignored. In the experiments reported here on silver in air there is no doubt about the presence of an adsorbed gaseous layer and the high activation energy almost certainly implies a 'two step' process for diffusion: a combination of desorption of oxygen and migration of silver. The high value of the pre-exponential factor D_0 must be due to a high increase in entropy for migrating atoms. Choi and Shewmon's (55) high values for the activation energy and D_0 for copper in hydrogen are suspiciously close to the values found for silver in air and it is probable that some impurity was adsorbed on the copper. Recently Brandon and Bradshaw (62) have studied diffusion on copper in vacuum and have found much lower activation energies of the order 1 ev.

8.4 Future work.

In view of the growing interest in solid surfaces at high temperatures and the practical difficulties of obtaining pure surfaces experimental studies are needed of the effects of adsorption on various properties. The data on adsorption isotherms at high temperature is very meagre. No measurements have yet been made of diffusivity as a function of adsorbed surface coverage.

The measurements reported here could be extended to

other metals in different atmospheres. Faceting would probably occur on most metals in suitable conditions, for example at high pressures. An interesting point which has never been investigated is that from the Gibbs adsorption equation negative surface energies are possible at high enough gas pressures and surfaces would be unstable. The available data suggests that this would happen for silver at an oxygen pressure of about 20 atmospheres.

APPENDIX.

ERRORS IN INTERFERENCE MICROSCOPY

Interferograms are frequently interpreted by assuming that one fringe spacing corresponds to a change in height of one half-wavelength of the illumination and that the wedge angle α , between the reference and specimen surfaces, is given by $\tan^{-1} (\lambda/2d)$ where d is the fringe spacing. However this expression is valid only for low wedge angles and for parallel illumination.

The illumination from the objective of the interference microscope falls on the surface in a convergent cone with angles of incidence up to 40° for high power objectives. If the illumination were only at one angle of incidence θ then each fringe spacing would correspond to a change in height of $\frac{\lambda}{2 \cos \theta}$. It follows that the effective half-wavelength for the cone of light is $\lambda/2$ multiplied by the mean value of $\sec \theta$ for all incident beams and it is easily shown (63) that for uniform illumination by a cone of half angle ϕ the fringe spacing corresponds to an effective half-wavelength

$$\frac{\lambda'}{2} = \frac{\lambda}{2} \frac{\log_e \cos \phi}{\cos \phi - 1} \quad (\text{A.1})$$

which for a high power objective can be as much as 6% higher than $\lambda/2$.

At high wedge angles there is a second source of error due to fringes being localised in the focal plane and not at the specimen surface (Mykura (64)). As a result a fringe shift occurs and the wedge angle is given by a sine and not a tangent formula:

$$\alpha = \sin^{-1} (\lambda'/2d) \quad (\text{A.2})$$

Computation of λ' for a particular microscope is not easy since generally the illumination will not be spread uniformly over the whole illuminating cone. A further complication arises because at high wedge angles a large part of the illumination is reflected outside the acceptance aperture of the objective. Tolmon and Wood (65) measured λ' from interferograms of steps of known height prepared by evaporating two successive layers of metal onto a flat surface. A simpler method has been adopted here which has the advantage that it gives a direct calibration of the microscope up to very high wedge angles. A small splinter of optically flat silvered glass was mounted on a goniometer head from an X-ray diffraction camera. Interferograms of a small area of

the splinter were made over a range of wedge angles at 0.5° intervals. With the x60 objective on the Linnick microscope fringes could be observed for wedge angles up to 30° . Plots of sine (wedge angle) against the reciprocal of the fringe spacing gave straight lines from which the effective wavelengths were calculated. (The tangent formula is valid within experimental errors up to 15°). Table 12 summarizes the results for the Linnick and the Baker microscopes.

Table 12.

Objective	Aperture setting	<u>Effective wavelength</u> Actual wavelength
<u>Linnick</u>		
x60	3.3	1.03 \pm .01
x60	2.0	1.03 \pm .01
x60	1.0	1.03 \pm .01
x25	3.0	1.01 \pm .01
<u>Baker</u>		
x40	2.0	1.06 \pm .01

An additional effect occurs if the surface under examination is not flat but gives a rapidly changing

wedge angle. It has been shown (64) that the fringe spacing is then given by the expression:

$$d = \frac{\lambda'}{2 \sin \alpha} + \frac{n \lambda'}{2} \frac{d}{dn} (\sin \alpha) \quad (\text{A.3})$$

where the second term is a derivative with respect to fringe order n . Arising from this second term distortions of the fringe pattern can occur at sharp changes of wedge angle. Inglestam (50) discusses another type of distortion due to 'three-wave interferences' which produce the effect of overlapping fringes - these are often visible on the ridges at the edges of facets and at the roots of grain boundary grooves.

REFERENCES

- (1) Smith, C.S. Trans A.I.M.E. 175, 15 (1948).
- (2) Herring, C. 'Physics of Powder Metallurgy' edited by W.E. Kingston (New York: McGraw-Hill) (1951).
- (3) Herring, C. 'Structure and Properties of Solid Surfaces' edited by R. Gomer and C.S. Smith (Chicago: University of Chicago Press) (1953).
- (4) Tolansky, S. 'Multiple-beam Interferometry of Surfaces and Films' Oxford. (1948).
- (5) Shuttleworth, R. Proc. Phys. Soc. A62, 167 (1949).
- (6) Shuttleworth, R. Proc. Phys. Soc. A63, 444 (1950).
- (7) Inman, M.C. and Tipler, H.R. To be published in Metallurgia.
- (8) Udin, H. 'Metal Interfaces' (Cleveland: A.S.M.)(1952).
- (9) Fisher, J.C. and Dunn, C.G. 'Imperfections in Nearly Perfect Crystals' (New York: Wiley)(1952).
- (10) Benson, G.C. Schreiber, H.P. and van Zeggeren, F. Can. J. Chem. 34, 1553 (1956).
- (11) Obreimov, J.W. Proc. Roy. Soc. (London) A127, 290 (1930).
- (12) Gilman, J.J. J. App. Phys. 31, 2208 (1960).
- (13) Udin, H. Shaler, A.J. and Wulff, J. Trans A.I.M.E. 185, 186 (1949).

- (14) Shuttleworth, R. 'Imperfections in Nearly Perfect Crystals' (New York: Wiley) (1952).
- (15) Barbour, J.P., Charbonnier, F.M., Dolan, W.W., Dyke, W.P., Martin, E.E. and Trolan, J.K. Phys. Rev. 117, 1452 (1960).
- (16) Blakely, J.N. and Mykura, H. Acta Met. 10, 565 (1962).
- (17) Buttner, F.H., Funk, E.R. and Udin, H. J. Phys. Chem. 56, 657 (1952).
- (18) Greenhill, F.B. and McDonald, S.R., Nature 171, 37 (1953).
- (19) Hayward, E.R. and Greenough, A.P. J. Inst. Metals, 88, 217 (1960).
- (20) Mykura, H. Acta Met. 5, 346 (1957).
- (21) Mykura, H. Acta Met. 9, 570 (1961).
- (22) Robertson, W.M. and Shewmon, P.G. Trans. A.I.M.E. (to be published).
- (23) Moore, A.J.W. Acta Met. 6, 293 (1958).
- (24) Buttner, F.H., Udin H. and Wulff, J. Trans. A.I.M.E. 197, 313 (1953).
- (25) Gjostein, N.A. Acta Met. 7, 812 (1959).
- (26) MacKenzie, J.K., Moore, A.J.W. and Nicholas, J.F. J. Phys. Chem. Solids 23, 185 (1962).
- (27) Gibbs. J.W. Collected Works. 55-353, (1928).

- (28) Allen, J.A. Austr. J. Chem. 13, 210 (1960).
- (29) Chalmers, B., King, R. and Shuttleworth, R.
Proc. Roy. Soc. A193, 465 (1948).
- (30) King, R. Ph.D. Thesis. London University (1955).
- (31) Mykura, H. Acta Met. 3, 436 (1955).
- (32) Fullman, R.L. 'Imperfections in nearly perfect
crystals' (New York: Wiley) 33, (1952).
- (33) Blakely, J.M. and Mykura, H. Acta Met. 9, 23 (1961).
- (34) Herring, C. J. App. Phys. 21, 301 (1950).
- (35) Mullins, W.W. J. App. Phys. 28, 333 (1957).
- (36) Mullins, W.W. Trans. A.I.M.E. 218, 354 (1960).
- (37) Blakely, J.M. Ph.D. Thesis, Glasgow University (1961).
- (38) Mullins, W.W. J. App. Phys. 30, 77 (1959).
- (39) King, R.T. and Mullins, W.W. Acta Met. 10, 601,
(1962).
- (40) Mullins, W.W. Phil. Mag. 71, 1313 (1961).
- (41) Shuttleworth, R. Metallurgia 38, 125 (1948).
- (42) Prasad, R. Dissertation, Cambridge University (1954).
- (43) Rosenhain, W. and Ewen, D. J. Inst. Metals 8, 149
(1912).
- (44) Leroux, J.A.A. and Raub, E. Z. Anorg. Chem. 188,
205 (1930).

- (45) Moreau, J. and Benard, J. C.R. Acad. Sci. Paris, 248, 1658 (1959).
- (46) Hondros, E.D. and Moore, A.J.W. Acta Met. 8, 647 (1960).
- (47) Hondros, E.D. and Moore, A.J.W. Acta Met. 8, 751 (1960).
- (48) Barrett, C.S. 'Structure of Metals' 2nd edn. p.41 (McGraw-Hill, New York and London) (1952).
- (49) Mykura, H. Bull. Inst. Metals 4, 102 (1958).
- (50) Ingelstan, E. 'Interferometry' N.P.L. Symposium. H.M. Stationery Office (1960).
- (51) Stössel, W. Z. Naturforschg. 17a, 165 (1962).
- (52) Blakely, J.M. and Mykura, H. Acta Met. 9, 595, (1961).
- (53) King, R. Private communication.
- (54) Drew, J.B. and Pye, J.J. Trans. A.I.M.E. (to be published).
- (55) Choi, J.Y. and Shewmon, P.G. Trans. A.I.M.E. (to be published).
- (56) Moore, A.J.W. Acta Met. 10, 579 (1962).
- (57) Dushman, S. 'Vacuum Technique' Wiley, New York, (1949).

- (58) Gomer, R. 'Structure and Properties of Solid Surfaces' edited by R. Gomer and C.S. Smith (Chicago: University of Chicago Press) p.75 (1953).
- (59) Burton, W.K., Cabrera, N. and Frank, F.C. Phil Trans. Roy. Soc. London 243A, 299 (1951).
- (60) Mullins, W.W. Acta Met. 7, 746 (1959).
- (61) Gjostein, N.A. Acta Met. (to be published).
- (62) Brandon, R.H. and Bradshaw, F.J. Private communication.
- (63) Gates, J.W. J. sci. Instrum. 33, 507 (1956).
- (64) Mykura, H. Proc. Phys. Soc. B67, 281 (1954).
- (65) Tolmon, F.R. and Wood, J.G. J. sci. Instrum. 33, 236 (1956).